Print ISSN: 0975-5861
Online ISSN: 2249-4596

Global Journal of Researches In Engineering: A Mechanical & Mechanics Engineering

DISCOVERING THOUGHTS AND INVENTING FUTURE

December 2011

Highlights...

- Neurofuzzy Implementation
- Hydrodynamic Lubrication
- Classical Plate Theory
- The Turbines Tested

Volume 11
Issue 7
version 1.0

ENG

Global Journal of Research in Engineering :A
Mechanical And Mechanics Engineering

Global Journal of Research in Engineering : A
Mechanical And Mechanics Engineering
Volume 11 Issue 7 (Ver. 1.0)

Open Association of Research Society

Incorporation No.: 0423089
License No.: 42125/022010/1186
Registration No.: 430374
Import-Export Code: 1109007027
Employer Identification Number (EIN):
USA Tax ID: 98-0673427

Global Journals Inc.

*(A Delaware USA Incorporation with "Good Standing"; **Reg. Number: 0423089**)*

Sponsors: Open Association of Research Society
Open Scientific Standards

Publisher's Headquarters office

Global Journals Inc., Headquarters Corporate Office, Cambridge Office Center, II Canal Park, Floor No. 5th, ***Cambridge (Massachusetts)***, Pin: MA 02141 United States
USA Toll Free: +001-888-839-7392
USA Toll Free Fax: +001-888-839-7392

Offset Typesetting

Open Association of Research Society, Marsh Road, Rainham, Essex, London RM13 8EU
United Kingdom.

Packaging & Continental Dispatching

Global Journals, India

Find a correspondence nodal officer near you

To find nodal officer of your country, please email us at *local@globaljournals.org*

eContacts

Press Inquiries: *press@globaljournals.org*
Investor Inquiries: *investers@globaljournals.org*
Technical Support: *technology@globaljournals.org*
Media & Releases: *media@globaljournals.org*

Pricing (Including by Air Parcel Charges):

For Authors:
22 USD (B/W) & 50 USD (Color)
Yearly Subscription (Personal & Institutional):
200 USD (B/W) & 250 USD (Color)

Editorial Board Members (HON.)

Dr. Bart Lambrecht
Director of Research in Accounting and FinanceProfessor of Finance
Lancaster University Management School
BA (Antwerp); MPhil, MA, PhD (Cambridge)

Dr. Carlos García Pont
Associate Professor of Marketing
IESE Business School, University of Navarra
Doctor of Philosophy (Management), Massachusetts Institute of Technology (MIT)
Master in Business Administration, IESE, University of Navarra
Degree in Industrial Engineering, Universitat Politècnica de Catalunya

Dr. Fotini Labropulu
Mathematics - Luther College
University of ReginaPh.D., M.Sc. in Mathematics
B.A. (Honors) in Mathematics
University of Windso

Dr. Lynn Lim
Reader in Business and Marketing
Roehampton University, London
BCom, PGDip, MBA (Distinction), PhD, FHEA

Dr. Mihaly Mezei
ASSOCIATE PROFESSOR
Department of Structural and Chemical Biology, Mount Sinai School of Medical Center
Ph.D., Etvs Lornd University
Postdoctoral Training,
New York University

Dr. Söhnke M. Bartram
Department of Accounting and FinanceLancaster University Management SchoolPh.D. (WHU Koblenz)
MBA/BBA (University of Saarbrücken)

Dr. Miguel Angel Ariño
Professor of Decision Sciences
IESE Business School
Barcelona, Spain (Universidad de Navarra)
CEIBS (China Europe International Business School).
Beijing, Shanghai and Shenzhen
Ph.D. in Mathematics
University of Barcelona
BA in Mathematics (Licenciatura)
University of Barcelona

Philip G. Moscoso
Technology and Operations Management
IESE Business School, University of Navarra
Ph.D in Industrial Engineering and Management, ETH Zurich
M.Sc. in Chemical Engineering, ETH Zurich

Dr. Sanjay Dixit, M.D.
Director, EP Laboratories, Philadelphia VA Medical Center
Cardiovascular Medicine - Cardiac Arrhythmia
Univ of Penn School of Medicine

Dr. Han-Xiang Deng
MD., Ph.D
Associate Professor and Research
Department Division of Neuromuscular Medicine
Davee Department of Neurology and Clinical NeuroscienceNorthwestern University
Feinberg School of Medicine

Dr. Pina C. Sanelli
Associate Professor of Public Health
Weill Cornell Medical College
Associate Attending Radiologist
NewYork-Presbyterian Hospital
MRI, MRA, CT, and CTA
Neuroradiology and Diagnostic Radiology
M.D., State University of New York at Buffalo,School of Medicine and Biomedical Sciences

Dr. Roberto Sanchez
Associate Professor
Department of Structural and Chemical Biology
Mount Sinai School of Medicine
Ph.D., The Rockefeller University

Dr. Wen-Yih Sun
Professor of Earth and Atmospheric SciencesPurdue University Director
National Center for Typhoon and Flooding Research, Taiwan
University Chair Professor
Department of Atmospheric Sciences, National Central University, Chung-Li, TaiwanUniversity Chair Professor
Institute of Environmental Engineering, National Chiao Tung University, Hsin-chu, Taiwan.Ph.D., MS The University of Chicago, Geophysical Sciences
BS National Taiwan University, Atmospheric Sciences
Associate Professor of Radiology

Dr. Michael R. Rudnick
M.D., FACP
Associate Professor of Medicine
Chief, Renal Electrolyte and Hypertension Division (PMC)
Penn Medicine, University of Pennsylvania
Presbyterian Medical Center, Philadelphia
Nephrology and Internal Medicine
Certified by the American Board of Internal Medicine

Dr. Bassey Benjamin Esu
B.Sc. Marketing; MBA Marketing; Ph.D Marketing
Lecturer, Department of Marketing, University of Calabar
Tourism Consultant, Cross River State Tourism Development Department
Co-ordinator , Sustainable Tourism Initiative, Calabar, Nigeria

Dr. Aziz M. Barbar, Ph.D.
IEEE Senior Member
Chairperson, Department of Computer Science
AUST - American University of Science & Technology
Alfred Naccash Avenue – Ashrafieh

Contents of the Volume

Global Journal of researches in engineering
Mechanical and mechanics engineering
Volume 11 Issue 7 Version 1.0 December 2011
Type: Double Blind Peer Reviewed International Research Journal
Publisher: Global Journals Inc. (USA)
Online ISSN: 2249-4596 Print ISSN:0975-5861

Neurofuzzy Implementation in Smart Toolpost to Improve Performance

By Maki K. Rashid
Mechanical and Industrial Engineering Sultan Qaboos University.

Abstract - Machining is a complex process that requires a high degree of precision with tight geometrical tolerance and surface finish. Those are confronted by the existence of vibration in the turning machine tool. Overcoming a micro level vibration of a cutting tool using smart materials can save old machines and enhance flexibility in designing new generations of machine tools. Using smart materials to resolve such problems represent one of the challenges in this area. In this work the transient solution for tool tip displacement, the pulse width modulation (PWM) technique is implemented for smart material activation to compensate for the radial disturbing cutting forces. A Neurofuzzy algorithm is developed to control the actuator voltage level to improve dynamic performance. The deployment of the finite element method in this work as a dynamic model is to investigate the ability of the in intelligent techniques in improving cutting tool accuracies. The influence of minimum number of PWM cycles with each disturbing force cycle is investigated in controlling the tool error growth. Toolpost structural force excitation due to the PWM cycles was not given adequate attention in previous publications. A methodology is developed to utilize toolpost static force-displacement diagram to obtain required activation voltage to shrink error under different dynamic operating conditions using neurofuzzy.

Keywords : *Tool vibration, Smart Material, Vibration suppression, Cutting tool, Neurofuzzy*

GJRE-A Classification: *FOR Code: 091304*

Strictly as per the compliance and regulations of:

Neurofuzzy Implementation in Smart Toolpost to Improve Performance

Maki K. Rashid

Abstract - Machining is a complex process that requires a high degree of precision with tight geometrical tolerance and surface finish. Those are confronted by the existence of vibration in the turning machine tool. Overcoming a micro level vibration of a cutting tool using smart materials can save old machines and enhance flexibility in designing new generations of machine tools. Using smart materials to resolve such problems represent one of the challenges in this area. In this work the transient solution for tool tip displacement, the pulse width modulation (PWM) technique is implemented for smart material activation to compensate for the radial disturbing cutting forces. A Neurofuzzy algorithm is developed to control the actuator voltage level to improve dynamic performance. The deployment of the finite element method in this work as a dynamic model is to investigate the ability of the in intelligent techniques in improving cutting tool accuracies. The influence of minimum number of PWM cycles with each disturbing force cycle is investigated in controlling the tool error growth. Toolpost structural force excitation due to the PWM cycles was not given adequate attention in previous publications. A methodology is developed to utilize toolpost static force-displacement diagram to obtain required activation voltage to shrink error under different dynamic operating conditions using neurofuzzy.

Keywords : Tool vibration, Smart Material, Vibration suppression, Cutting tool, Neurofuzzy

I. Introduction

Improving quality of surface finish and geometrical accuracies during machining using active material was under intensive investigation (Park, et al. 2007). Raw material conversion to new product requires material removal processes using machine tool. Demand for higher productivity in automated manufacturing brought attention for controlling machine tool dynamics for better machining accuracy. Both economic and ecological factors encouraged old conventional machines to continue in service by overcoming tool vibration problems. Various factors might affect the machining process, some of them are non-measurable and others might change in real-time. However, the wider use and the availability of cost effective microcontrollers encouraged the implementation of intelligent control schemes to overcome such time dependent machining problems (Krzysztof, et al. 2011). The tiny unfavorable relative motion between the cutting tool and the working piece that associated with high excitation forces encouraged the use of smart material actuators to counteract such motion errors (Radecki, et al. 2010). The rigid fixture is a good choice for minimizing displacements of cutting tools from its nominal position during machining. Unfortunately, such option is not available in all applications. The reconfigurable manufacturing era prefers fixtures consumes less space with minimum weight (Gopalakrishnan, et al. 2002; Moon and Kota 2002).

When the control system, and real time microprocessor implementation were examined no details were given for the design and selection of actuator, tool holder, and tool bit stiffness, and, actuator switching. Also in the case of future geometrical changes, the validity of using lumped masses in system modeling is questionable. Information is required regarding the nature and type of signals controlling smart material and how might affect toolpost dynamic response. Recently a tool adaptor is used with built-in active vibration damping device to dynamically stabilize the turning process (Harms, et al. 2004). The vibration compensation system is based on a multilayer piezo-actuator in collocation with a piezoelectric force sensor. An analogue controller based on integral force feedback method is used for active damping. Latest dynamic modeling of smart toolpost (Rashid, 2005) is based on continuous elastic structural toolpost overcoming previous limitations of lumped mass modeling without further steps toward the development of a generalized scheme for tool error attenuation. Such models are then implemented for designing an adaptive controller using fuzzy controller (Rashid, 2006).

This work is implementing the finite element method (FEM) to model flexible smart tool post incorporating PZT actuator, tool holder, supporting fixture, and tool bit, and, discusses the effect of structural properties on the critical frequencies as compared to lumped mass modeling. Also investigate the effectiveness of the developed Neurofuzzy algorithm in controlling error attenuation under different excitation cutting force frequencies. The tool radial motion that causes dimensional variation in the work-piece is emphasized. The smart toolpost static force-displacement analysis under different voltage input is integrated with the development the Neurofuzzy scheme

Author : Mechanical and Industrial Engineering Sultan Qaboos University. P. O. Box: 33 Al-Khod Postal Code No.123 Muscat, Sultanate of Oman. E-mail : maki@squ.edu.om

to predict the activation voltage in dynamic error attenuation. A special attention is given for the model to be a robust for large variations in design parameters. Such a finite element model offers a methodology for micro-vibration attenuation in smart toolpost using smart materials and intelligent schemes like Neurofuzzy.

II. The Toolpost Fem Model

In this work Lead Zirconate Titanate (PZT), is employed as a smart material actuator. This is encouraged by a well-developed theoretical analysis of this material. Also it is the most common used piezoelectric materials. The Toolpost model incorporates actuator, tool carrier (holder), supporting diaphragm, and tool bit (spring buffer between the tool carrier and the net actuating force at tool tip) as shown in Figure 1.

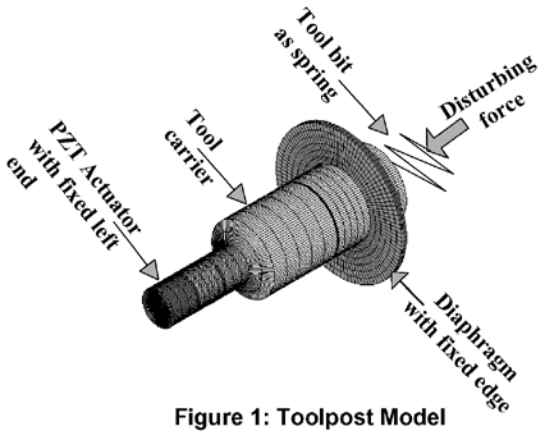

Figure 1: Toolpost Model

a) Model Governing Equations

The model consists of a conventional stacked PZT actuator contains polarized ferroelectric ceramic in the direction of actuation,

$$\{T\} = [c^E]\{S\} - [e]^T\{E\}$$
$$\{D\} = [e]\{S\} + [\varepsilon^S]\{E\} \quad (1)$$

adhesive, supporting structure, and electrically wired electrodes as shown in Figure 2.

The finite element modeling of the PZT actuator and toolpost is developed (Piefort 2001) by using the general constitutive equations of linear piezoelectricity and equations of mechanical and electrical balance.

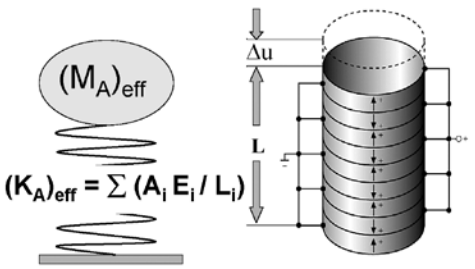

Figure 2: PZT Stacked Actuator

The momentum balance equation is

$$\rho\{\ddot{u}\} = \nabla.\{T\} \quad (2)$$

And the electric balance equation is

$$\nabla.\{D\} = 0 \quad (3)$$

Knowing, $\{S\} = \nabla^S.\{u\}$, $\{E\} = -\nabla\phi$

Where $\{T\}$ represents the stress vector, $\{S\}$, the strain vector, $\{E\}$, the electric field, $\{D\}$, the electric displacement, $[c^E]$, the elastic coefficients at constant $\{E\}$, $[\varepsilon^S]$, the dielectric coefficients at constant $\{S\}$, and $[e]$, the piezoelectric coupling coefficients. As well $\{u\}$ is the mechanical displacement vector and $\{\ddot{u}\} = \partial^2\{u\}/\partial t^2$ is the acceleration. In addition ϕ is the electric potential (voltage). The boundary conditions are shown in Figure 1, as represented by the fixed end conditions for both, actuator left side and, diaphragm outer edge. The model description is completed by specifying the applied voltage at actuator electrodes' using the PWM technique weighted by a factor worked out from the developed fuzzy algorithm and based on the inputs from the calculated toolpost dynamic response.

b) Building The Finite Element Equations

The finite element model of this work is built by using the piecewise application of classical variational methods on smaller and simpler sub-domains connected to each other by a finite number of nodes. A 8-node isoparametric solid element is used for domain discretization. The unknowns are the displacements vector u_i and the electric potential values ϕ_i at node i. The formulation of the dynamic equations of a piezoelectric continuum is discussed thoroughly in the literature (Allik and Hughes 1970; Lerch 1990). Taking into account the constitutive equations (1) and by introducing the Lagrangian and virtual work formulation into the Hamilton's principle we that satisfies the arbitrary deviation of the displacements $\{u_i\}$ and the electrical potentials $\{\phi_i\}$ and their compatibilities with the compatibilities with the associated boundary conditions,

$$[m_{uu}]\{\ddot{u}_i\} + [c_{uu}]\{\dot{u}_i\} + [k_{uu}]\{u_i\} + [k_{u\phi}]\{\phi_i\} = \{f_i\}$$
$$[k_{u\phi}]^T\{u_i\} + [k_{\phi\phi}]\{\phi_i\} = \{q_i\} \quad (4)$$

$[m_{uu}]$ $[k_{uu}]$ and, $[c_{uu}]$ are the mechanical mass, stiffness, and, $[k_{\phi\phi}]$ damping matrices, respectively. $[k_{u\phi}]$ is the piezoelectric coupling matrix and, $[k_{\phi\phi}]$ is the dielectric stiffness matrix. $\{f_i\}$ and $\{q_i\}$ are the nodal mechanical force and electric charge vectors, respectively. and, are the nodal displacement and potential vectors, respectively. For the sake of brevity,

the scheme by which the elemental contributions are assembled to form the global system matrices are discussed in (Zienkiewicz and, Taylor 2000a, b).

III. Natural Frequency Comparison Between Lumped and Fem Modeling

The lumped mass modeling of the PZT actuator and tool carrier generate a simple closed form solution that is of interest to designers and modelers. However using such model in different applications requires more alertness. Most applications require a precise displacement sensing and accurate prediction for natural frequency to ensure the effective control for smart material actuator.

a) Comparative Results for PZT Actuator

Mode shapes and the resonant frequencies for undamped system are obtained by using Eigenvalue analysis. Free vibration implies that $\{f_i\} = 0$ and $\{q_i\} = 0$ in equation (4). Modal analysis is based on the orthogonality principle of natural modes and expansion theorem (Zienkiewicz and Taylor 2000 b).

The fundamental angular undamped natural frequency of a beam of fixed –free end condition is represented by:

$$\omega_n = \frac{\pi}{2L}\sqrt{\frac{E}{\rho}} \tag{5}$$

Usually the actuator is composed of several PZT layers, electrodes, adhesive, and supporting structure as shown in Figure 2. To compare between simple calculations and the FEM solutions the actuator effective stiffness assumed to be the stiffness sum in the series for all individual layers neglecting all piezoelectric effects.

$$KA = \Sigma\left(\frac{A_i E_i}{L_i}\right) \tag{6}$$

Actuator effective lumped mass is estimated to be a 20 or 30% of the summed layers masses as indicated in Figure 3.

$$(M_A)_{eff} = (0.2 \quad or \quad 0.3)\Sigma(A_i \rho_i L_i) \tag{7}$$

Then,

$$\omega_{Lumped} = \sqrt{\frac{K_A}{(M_A)_{eff}}} \tag{8}$$

The FEM solutions for the actuator first natural frequency under short circuit (zero piezo effect) and open circuit conditions (maximum piezo effect) compare to the estimated lumped mass natural frequency as given in Eq. (8) and their ratios plotted in Figure 3. Present calculations are based on PZT8 property from (Berlincourt and Krueger 2000).

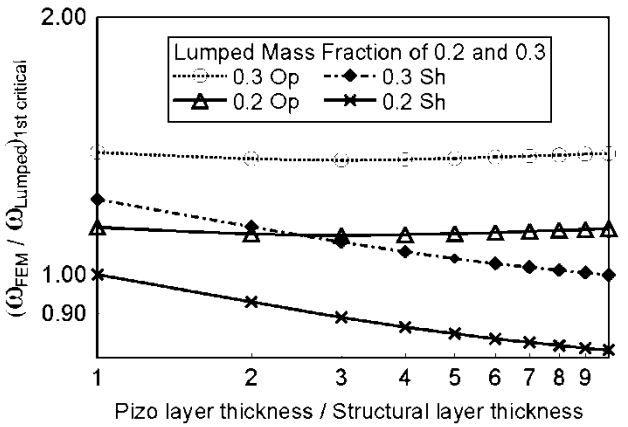

Figure 3: First critical frequency ratio (FEM / Lumped) versus layers thickness ratios for short circuit (Sh) and open circuit (Op)

Plotted results in Figure 3 neglected any stiffness variation that might result from actuator fabrication. The short circuit actuator (Sh) gave lower value for natural frequency indicating a lower stiffness in the absence of piezo effect. Such data is offering the designers a rapid tool for estimating natural frequencies in the early stages of design. The short (Sh) and open circuit (Op) conditions map the extremes of natural frequency values. The deviation in natural frequencies between the FEM and lumped mass solutions are different between open and short circuit conditions.

b) Comparative Results for Integrated Toolpost

Incorporating the tool carrier and the supporting diaphragm to the PZT actuator model introduces the multi-degree of freedom system. In this work the effective mass at the actuator end $(M_{AE})_{eff}$ in Fig. 4 represent 30% of the combined actuator and tool carrier masses. While the effective mass near to the diaphragm end $(M_{CE})_{eff}$ is 30% of the combined tool carrier and diaphragm masses. Higher mass percentages resulted in a higher deviation from the FEM solutions. Solutions for the two-degree of freedom system incorporating piezoelectric coupling effects are investigated by (Frankpitt 1995; Abboud, et al. 1998), However, the significant deviation between the FEM and the lumped mass solution and its range of applicability has not investigated. KA is calculated as in Eq. (6) which is shown in Fig. 4 as a coupling stiffness joining $(M_{AE})_{eff}$ and the ground. The tool carrier stiffness KC is calculated accordingly from the relation (A_C E_C/L_C). The tool carrier stiffness KC is calculated accordingly from the relation (A_C E_C/L_C).

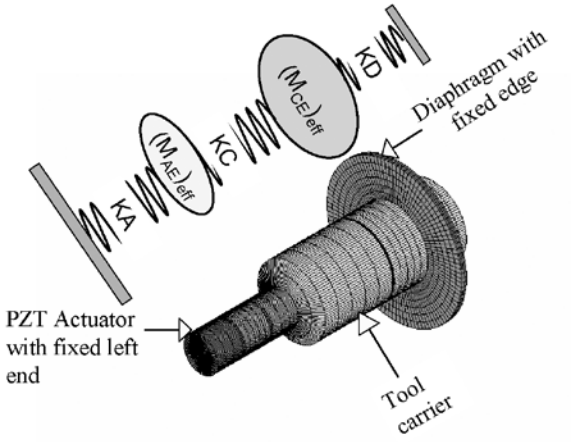

Figure 4: Tool Carrier and Actuator with Diaphragm

Diaphragm stiffness (KD) is based on plate theory with fixed central hole at both inner and outer edges, (Roark and Young 1975). Then the stiffness matrix of this 2-degree of freedom system shown in Figure 4 is:

$$[K]=\begin{bmatrix} KA+KC & -KC \\ -KC & KC+KD \end{bmatrix} \qquad (9)$$

Modal shapes and frequencies that resulted from the FEM model compare to the lumped mass model in Figure 4 by considering three different frequency ratios, namely $(\omega_{FEM})_{1st}/(\omega_{Lumped})_{1st}$ for 1st critical, $(\omega_{FEM})_{2nd}/(\omega_{Lumped})_{2nd}$ for 2nd critical, $(\omega_{FEM})_{3rd}/(\omega_{Lumped})_{2nd}$ and for 3rd critical. Structural stiffness contributions to these frequency ratios are presented in Figures 5-7 including tool carrier to actuator stiffness (KC/KA) and diaphragm to actuator stiffness (KD/KA) under both open and closed circuit conditions.

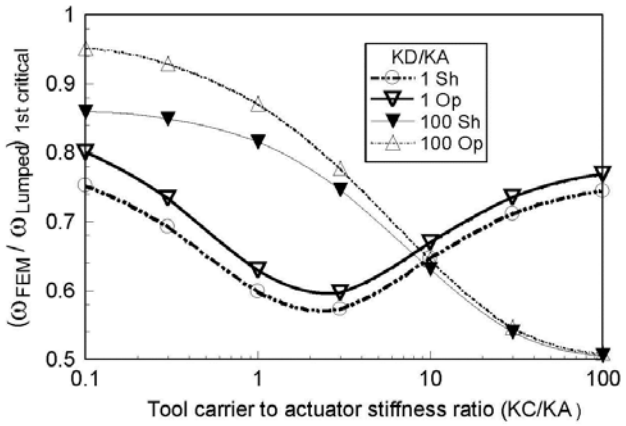

Fig. 5: First critical frequency ratio of FEM to lumped mass solutions versus (KC/KA) at different (KD/KA) for open (Op) and short (Sh) circuits

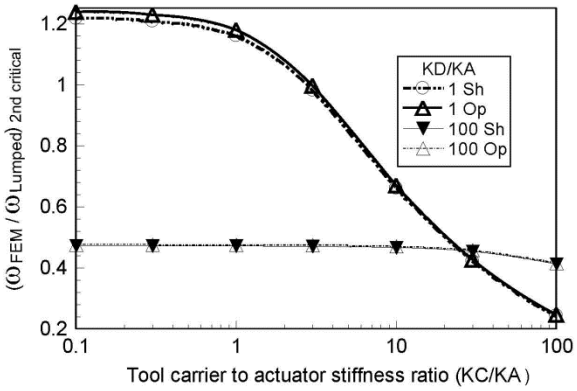

Fig. 6 Second critical frequency ratio of FEM to lumped mass solutions versus (KC/KA) at different (KD/KA) for open (Op) and short (Sh) circuits

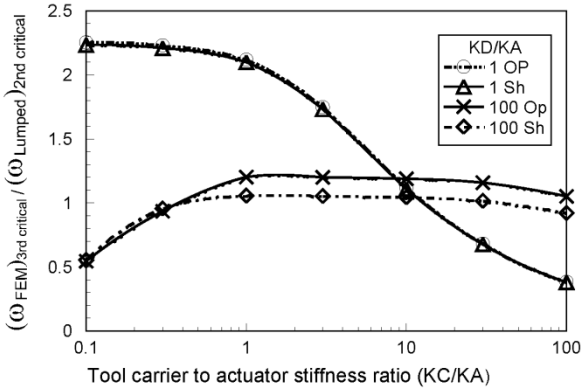

Fig. 7: Ratio of FEM third critical to second lumped mass critical frequency versus (KC/KA) at different (KD/KA) for open (Op) and short (Sh) circuits

Figure 5 indicates significant dependence of $(\omega_{FEM})_{1st}/(\omega_{Lumped})_{1st}$ for 1st critical with the variations in tool carrier to actuator stiffness (KC/KA) and diaphragm to actuator stiffness ratio (KD/KA). The availability of such results would help to work out a lumped mass model that has a more realistic response based on problem assumptions. The difference between first critical frequency ratios for short (sh) and open (Op) circuit conditions diminish at high (KC/KA) especially when (KD/KA) is relatively high.

The second critical frequency ratio $(\omega_{FEM})_{2nd}/(\omega_{Lumped})_{2nd}$ on the semi-log plot of Figure 6 shows independency of such ratio on tool carrier stiffness when selecting higher ratio of (KD/KA) which is not recommended for actuator design. At low (KD/KA) the dependency of frequency ratio on (KC/KA) is much more distinguished. In general the frequency ratio is tending to change remarkably when (KC/KA) goes beyond ten.

Ratio of the FEM third critical frequency $(\omega_{FEM})_{3rd}$ to the second critical frequency $(\omega_{Lumped})_{2nd}$ of lumped model shown in Figure 7 have a similar trend

as in Figure 6. The considerable difference between open and short circuit conditions occurs at high (KD/KA) only. Results indicate a possibility for $(\omega_{FEM})_{3rd}$ to be lower than $(\omega_{Lumped})_{2nd}$. Such disagreement between lumped mass models and FEM solution requires more awareness in vibration controller design using smart materials.

IV. Toolpost Force Generation Versus Displacement

Effective tool error attenuation depends on PZT actuator capabilities for resisting tool axial force within the required limited range of motion. To obtain such data a force versus displacement curve is developed for the investigated toolpost in Figure 1. Figure 8 shows the force-displacement characteristics for different values of tool carrier to actuator stiffness ratio (KC/KA). The plotted curves in Figure 8 are emphasizing the importance of increasing (KC/KA). Similar plots are generated to obtain the effects of increasing (KT/KA) and (KT/KA). Resulted figures indicate the worth of reducing the structural support stiffness (diaphragm) in the direction of PZT activation to improve actuation force for error attenuation. Guessing first actuator design can be conducted according to information offered by force-displacement calculations. A special treatment for dynamic effects during machining is discussed in the next sections. The smart material data and, the investigated toolpost dimensions that applied to both static and dynamic calculations are given in Table 1. A general theory for a piezoelectric actuator subjected to mechanical excitations and feedback voltages is discussed in (Tzou 1991).

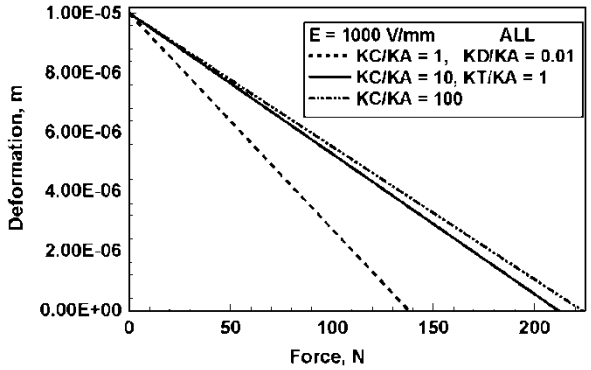

Figure 8: Smart toolpost displacement versus the applied force for different tool carrier to actuator stiffness ratio.

Table 1 : Toolpost dimension and material

Item	Value	Units
Cylindrical PZT-8 Stack		
PZT Thickness	0.09e-03	m
Electrode Thickness	0.03e-03	m
Structural support	0.03e-03	m
Adhesive Thickness	10.0e-06	m
Number of layers	500	
Effective Radius	5.0e-3	m
Steel Cylindrical Tool Carrier (holder)		
Radius	10.0e-3	m
Length	55.0e--3	m
Steel Tool Bit Effective Length		
Assumed Effective Length	20.0e-3	m
Steel Diaphragm		
Thickness	0.5e-3	m
Outside Radius	20.0e-3	m

V. Neurofuzzy Algorithm for Voltage Activation

Obtained results from Figures 5-7 prove significant deviation of lumped mass modeling from the finite element solution of the continuous elastic structure especially in the range of low (KD/KA) and high (KC/KA) where the PZT actuation is maximum as pointed out in Figure 8. Therefore the finite element method is the only reliable and available tool of solution in assessing switching methodology and system damping in the smart toolpost toward effective error reduction. Transient solution for tool displacement is achieved by solving Eq. (4) in the time domain for the system shown in Figure 1. The smart toolpost configuration and its associated data are given in Table 1.

a) PWM Modeling

The possibility of reducing tool tip position error is conducted by appropriate voltage activation to the smart material. Using Pulse Width Modulation (PWM) is an economical implement for smart material activation for such application. It is a common technique used with microcontroller units (MCU) to govern the time average of power input to the actuators. The associated time dependent motion accompanying tool vibration during error reduction is our next concern.

The voltage activation to the smart material is either triggered by a piezo stack with force sensing layer or by using a suitable type of displacement sensor. In both methods sensing the location should reflect cutting tool position error correctly. Switching circuits design is not discussed in this work; however the required voltage intensity level and the resulted motion are emphasized in this work.

Setting up the switching voltage by a series of PWM cycles should be judged by a sensed cutting force value from the peak force spectrum at the peak force

frequency (ω_f), then, the initial peak voltage is estimated from Figure 8. A complete period of the peak force cycle (T_f) is divided into number of duty cycles (N_{PWM} or NPWM). Then, for any of these divisions, the time duration of the PWM high DC-voltage is calculated based on the obtained voltage factor from the neurofuzzy algorithm that will be discussed next. A time delay in voltage activation can be incorporated as a function of the peak force frequency period. Two switching's are associated with each PWM cycle segment, therefore switching rate is $2N_{PWM}\omega_f$. Effects of switching voltage input, forcing frequency ω_f , and, damping level upon toolpost time response are parameters to be discussed in a smart toolpost transient solution.

b) Controller Configuration

It is difficult to acquire a controller that ensures continuous error tracking under stabilized condition for smart toolpost under continuous exposal to an erratic real time force inputs. The use of intelligent controller is generated by the random nature of system excitations which largely depends on unpredictable parameters such as structural properties, friction, and other variable dynamic forces. A neural network can model the response of such system by means of a nonlinear regression in the discrete time domain. The result is a network, with adjustable weights, that might approximate the system dynamics. Though it is a problem since the knowledge is stored in an opaque fashion and the learning results in a large set of parameter values which almost impossible to be interpreted in words. Conversely using a fuzzy rule based controller that consists of readable if-then statements which is almost a natural language, cannot learn new rules alone. The neurofuzzy controller might be preferred over the others for such application since it combines the two and it has a learning architecture (Lin, J. and Chao, W.S., 2009). To construct a neurofuzzy controller with ANFIS (Adaptive Neuro Fuzzy Inference System), we need a set of input-output data. In this work, two input signals are considered. The first input is normalized error defined by representing the negative error by the tool tip displacement away from the work piece axis. Then is the negative of the normalized tool tip error with respect to the maximum static displacement of the peak radial cutting force? The universe of discourse of the input variable is defined to be within the range [0, 1]. The second input is the normalized rate of change in error . Basically represent the time rate of change of error calculated every one tenth of the force period and given a universe of discourse [-0.2, 0.2]. The output signal is VF a multiplication factor for the estimated voltage from the static tool force-displacement chart in Figures 9 and 10 and given a universe of discourse [0, 1]..

Control strategies under different design parameters that might be difficult to implement in a real experimental setup can be tested by using the finite element dynamic simulation with ordinary Sugeno's Fuzzy controller. All problem components are integrated through visual basic as shown in Figures 9 and 10. Data sets are collected for training and adapting the Neurofuzzy controller in the next stage. The cost effectiveness of such simulation definitely adds to its flexibility in exploring different dynamic parameters that might be difficult to introduce in actually built system.

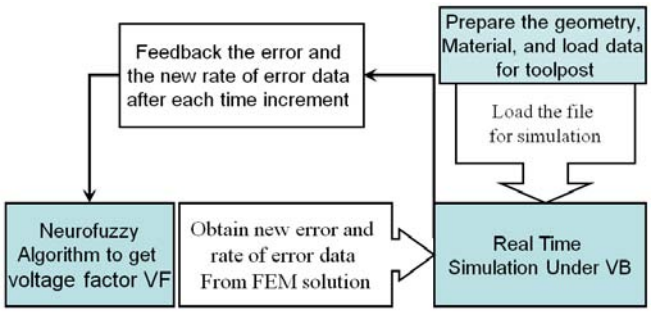

Fig. 9 Simulation flow chart

c) Takagi-Sugeno model

The general Takagi-Sugeno rule structure is:

If $g\,(e_1 \text{ is } A_1, e_2 \text{ is } A_2, \ldots, e_k \text{ is } A_k)$ then

$$y = f(e_1, e_2, \ldots, e_k) \qquad (10)$$

Here f is the logical function which connects the sentences that form the implemented conditions, y is the output, and, f is a function of the inputs $e_1, e_2, \ldots$,and e_k. The inputs in this work are the normalized error ε and the normalized rate of change in error $\dot{\varepsilon}$, while the output is the voltage factor VF.

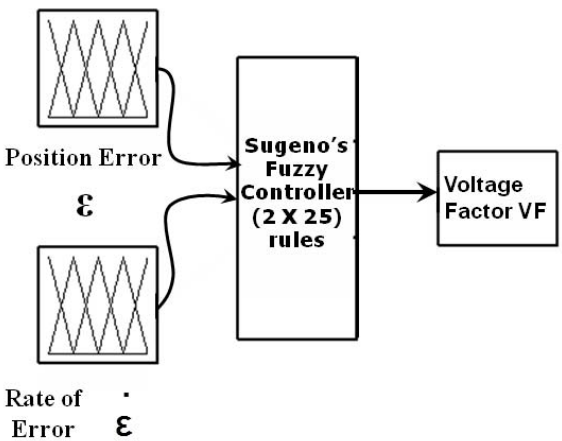

Fig. 10. Sugeno's Controller Layout

The rules can be structured according to the importance of the actual parameters involved in the targeted application based on the simulated dynamic model. The Takagi and Sugeno's fuzzy model can be formulated as the following:

$$L^i: \text{ IF } e_1 \text{ is } A_1^i \text{ and } .....\text{and } e_k \text{ is } A_k^i \text{ THEN}$$
$$y^i = f_i = a_0^i + a_1^i.e_1 + ... + a_k^i.e_k \quad (11)$$

where, $L^i (i = 1,2,....n)$ denotes the i-th rule, n is the number of fuzzy rules, y^i *or* f_i is the output from the i-th rule (implication), $a_p^i (p = 0,1,..., k)$ are consequent parameters, $e_1, e_2, \ldots, e_k$ are the input variables, and A_p^i are fuzzy sets whose membership functions are denoted by the same symbols as the fuzzy values. Given an inputs $(e_1, e_2, \ldots, e_k)$ the final output of the fuzzy model is inferred by taking the weighted average of the f_i is:

$$y = \frac{\sum_{i=1}^{n} w_i f_i}{\sum_{i=1}^{n} w_i} \quad (12)$$

where $w_i \rangle 0$ and f_i is calculated for the input by consequent equation of the i-th rule, and the weight w_i implies the overall truth value of premise of the i-th rule for input calculated as

$$w_i = \prod_{p=1}^{k} A_p^i.e_p \quad (13)$$

d) The Neuro-fuzzy control algorithm

To facilitate the learning (or adaptation) of the Takagi-Sugeno fuzzy model, it is convenient to implement the fuzzy model into a framework of adaptive network that can compute gradient vectors systematically. The resultant network architecture called ANFIS (Adaptive Neuro-Fuzzy Inference System). ANFIS is described by a similar Takagi-Sugeno model with a single difference that in this case the inputs, e_1 (ε -Error) and, e_2 ($\dot{\varepsilon}$ - Rate of Error) are range values. The fuzzy set for ε being $\mathbf{A_1}$ = { L="Low", M/L="Medium to low", M="Medium", M/H="Medium to High" and H="High"}, and fuzzy set for being $\mathbf{A_2}$ = { L="Low", M/L="Medium to low", M="Medium", M/H="Medium to High" and H="High"}. Fig. 11 illustrate graphically the neurofuzzy reasoning mechanism to derive an output y from a given inputs ε and $\dot{\varepsilon}$. Output f_i is one of the voltage factor VF for i-th rule where the size of the rule base is 25. The dynamic simulation is conducted with several types and sizes of membership functions for the fuzzy sets $\mathbf{A_1}$ and, $\mathbf{A_2}$. The triangular membership functions and a size of five for each of the two fuzzy sets were found the simplest and best suited for this case.

The square elements in Fig. 11 represent the adaptive nodes depending on the parameter set of the adaptive network. The circles represent fixed nodes, which are independent of the parameter set. The first layer is composed of adaptive nodes representing the triangular membership functions (Jang, J.-S. R.; Sun, C.-T. & Mizutani, E. 1996) associated with each linguistic value. The second layer implements the fuzzy rules. Each node in this layer calculates the firing strength of a rule by means of multiplication between the membership degrees of the two inputs. The third layer consists of adaptive nodes which include the output membership.

The other two layers consist of fixed nodes that implement the weighted average procedure to obtain the voltage factor VF as shown in Fig. 11. As the size of the rule base of the Sugeno fuzzy inference system (SFIS) is 25, we will have to identify 75 consequent parameters $\{a_0^1, ..., a_0^{25}, a_1^1, ..., a_1^{25}, a_2^1, ..., a_2^{25}\}$ as indicated in Jang, J.-S. R.; Sun, C.-T. & Mizutani, E. (1996). This can be obtained from the neural network (NN) using training set $\{\varepsilon, \dot{\varepsilon}, \text{VF}\}$ which are collected from the dynamic simulation results by using the Sugeno fuzzy inference system. A back-propagation learning algorithm is used to identify these parameters in two steps. In the forward pass, the input membership functions are fixed and consequent parameters associated with the output are calculated by applying the least square estimation method. Using these parameters, the NN generates an estimate of the output voltage factor VF. The difference between this estimate and the motor's value from the training set is then back-propagated in a second pass when the premise parameters associated with the input membership functions are calculated

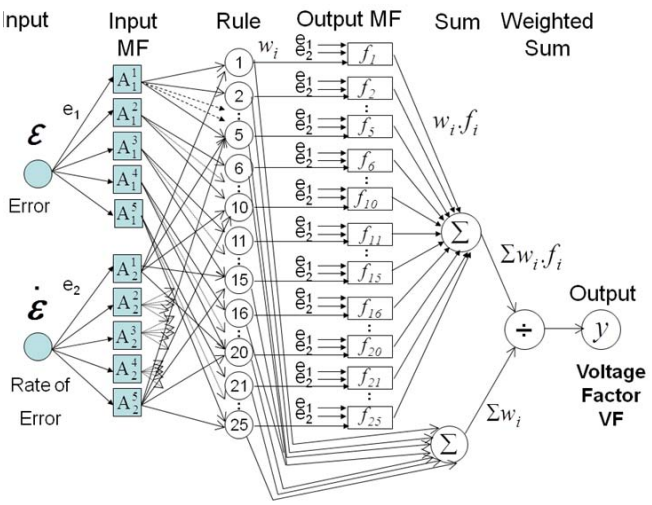

Fig.11 ANFIS architecture

e) Solution Method for Dynamic Equations

The system of equations for such a nonlinear problem is best solved by classical Newmark algorithms (Abboud, et al. 1998). Time step-by-step integration is used in solving Eq. (4). Basically the final results are obtained by attaining the solution at present time step from known solution at the previous time step. This approach takes into consideration the higher order time

approximations. Also it assumes a constant acceleration over a small time interval (time-step). By considering the Taylor series quadratic expansion for the function $\{u\}$ and its derivatives, (Abboud, et al. 1998) then,

$$\left.\begin{aligned}\{u_i\}_{n+1} &= \{u_i\}_n + \Delta t\{\dot{u}_i\}_n + \frac{1}{2}(1-\beta_2)\Delta t^2\{\ddot{u}_i\}_n + \\ &\frac{1}{2}\beta_2\Delta t^2\{\ddot{u}_i\}_{n+1} = \{\dot{u}_i\}_{n+1} + \frac{1}{2}\beta_2\Delta t^2\{\ddot{u}_i\}_{n+1} \\ \{\dot{u}_i\}_{n+1} &= \{\dot{u}_i\}_n + (1-\beta_1)\Delta t\{\ddot{u}_i\}_n + \beta_1\Delta t\{\ddot{u}_i\}_{n+1} \\ &= \{\ddot{u}_i\}_{n+1} + \beta_1\Delta t\{\ddot{u}_i\}_{n+1}\end{aligned}\right\} \quad (14)$$

From the dynamic equation Eq. (5) we have

$$[m_{uu}]\{\ddot{u}_i\}_{n+1} + [c_{uu}]\{\dot{u}_i\}_{n+1} + [k_{uu}]\{u_i\}_{n+1} + [k_{u\phi}]\{\phi_i\}_{n+1} = \{f_i\}_{n+1} \quad (15)$$

Equations (14) and (15) allows three unknowns $\{u_i\}_{n+1}, \{\dot{u}_i\}_{n+1}$ and, $\{\ddot{u}_i\}_{n+1}$ to be determined and for brevity the detail of solving these equations and the values of β_1 and, β_2 are given in (Abboud, et al. 1998). The step-by-step integration scheme assumes a known structural damping. The damping matrix is assumed to be a linear combination of stiffness and mass matrices (Rayleigh damping) (Bathe 1982):

$$[c_{uu}] = \alpha[m_{uu}] + \beta[k_{uu}] \quad (16)$$

Where α and β are constants to be determined from two assumed modal damping ratios (ξ_i) (1% and 5%) for first and second natural frequencies respectively which are related to modal damping by the available established relations.

VI. Results of Fuzzy Controlled Response for Integrated Toolpost

Requirements to reduce tool holder size and weight encourage developing new tactics of using smart actuators to attain high precision by compensating unfavorable motion errors. Estimation of cutting tool radial force might involve several variables. In general the static force relation (Frankpitt 1995) which expressed in terms of depth of cut (d , m m), cutting speed (V , mm/s), feed rate (f , m m/rev), and, coefficients describing the nonlinear relationships ($\kappa, \lambda, and, \gamma$) can be used as a first guess in error attenuation:

$$F_r = K_r d^{\lambda} V^{\gamma} f^{\kappa}(t) \quad (17)$$

K_r a general constant K_r , λ , γ and, κ are to be calibrated for each tool-workpiece, tool-work material combinations, process types, tool-wear condition, workpiece hardness, tool geometry, and speed. For the presented results, the applied voltage to the actuator is estimated first from both Eq. (17) and Figure 8. The subsequent applied voltage values are then obtained from the neurofuzzy output voltage factor of Figure 11 based on the resulted error and the rate of error values. Actuator data for the obtained final results are given in Table 1. Using few numbers of PWM cycles per force period can cause unfavorable switching dynamic excitation by the actuator to tool post. The results in Figure 12are the outcome of five PWM cycles, twenty PWM cycles per force period produce more favorable results but more than twenty have little effect. Cutting force fluctuations have a component that is proportional to the undeformed chip thickness and a component due to the rate of penetration called a plowing effect. For comparison, the results of increasing β in equation (16) by ten folds of the selected datum of 1% damping ratio for first mode and 5% for the second mode indicated a significant reduction in tool tip normalized error. In addition to the effectiveness of the Neurofuzzy algorithm both damping and NPWM (N_{PWM}) have contributed to the reduction in normalized error as shown in Figure 12. The results of Figure 12 points out that high damping alone do not ensure the minimum error attenuation. Sample results showing the effectiveness of the developed Neurofuzzy algorithm for error attenuation at different dampings are shown in Figure 12.

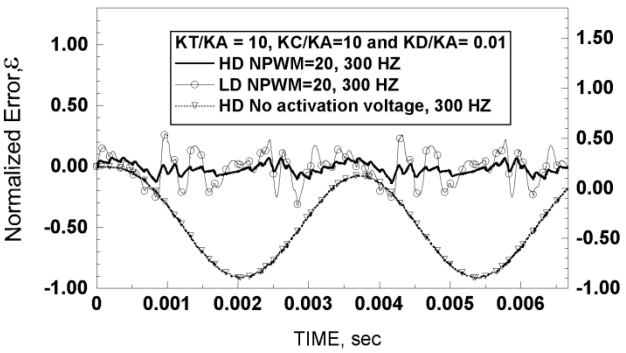

Figure 12: Normalized tool tip error versus time for neurofuzzy controller at high damping (HD), low damping (LD) and different NPWM's

The negative normalized error in Figures 12-13 indicates outward tool tip retraction away from workpiece axis. Tool bit to actuator stiffness ratio (KT/KA) has an importance in terms of force availability for tool tip error elimination and accurate displacement sensing as shown in Figure 8. Stiffness ratios greater than ten produce identical displacements between the tool tip and tool carrier main body. Taking into consideration the geometrical factors, significant deviation starts when stiffness ratio (KT/KA) drops below one. The importance of such parameter depends on the design configuration of the tool post and the acceptable range for the tool error.

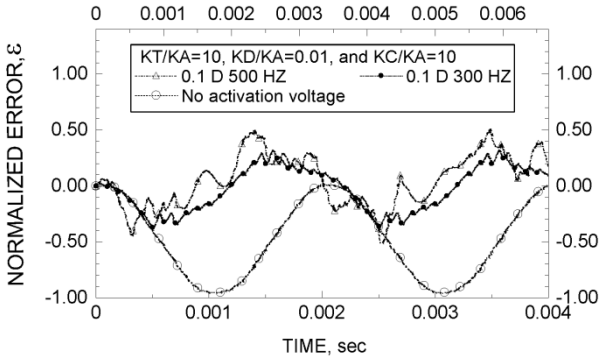

Fig. 13 Comparison between normalized tool tip errors at different frequencies for no delay (ND) and with 10% time delay (0.1 D)

of tool tip errors. Results are compared for two frequencies as shown in Figure 13.

VII. Conclusions

The application of neurofuzzy techniques to control a smart tool post has been presented. An adaptive learning algorithm for the neurofuzzy controller has been developed. The advantages of the proposed schemes are that an accurate model to describe the dynamics of the tool post is no longer needed, and the choice of learning parameters for the controller is not critical. With the proposed method, the controller can be easily designed and expanded. Designing against cutting tool error in turning machines using smart material reduce industrial waste, save money and, improve design flexibility for future tool generations. In this work critical frequencies of two modeling schemes are compared for a smart tool post under open and short circuit conditions. The results indicate significant differences between lumped mass modeling and FEM solution at low diaphragm to actuator stiffness ratio (KD/KA) and high tool carrier to actuator stiffness (KC/KA). This range of stiffness ratio has been investigated to ensure better error attenuation in smart material actuation for such applications. The work outcome can identify the stiffness range of lumped mass modeling that has more realistic representation of the dynamic response control. Also, suggest the use of high tool bit to tool carrier stiffness for better actuation capability and smaller tool tip error. Generated results suggest a reasonable number of at least twenty PWM segments should be used in representing the force cycle to reduce switching dynamic transient effects. The developed methodology in generating voltage activation factor to modify the static voltage-force-displacement value proved absolute effectiveness in error attenuation. The developed neurofuzzy algorithm to predict the voltage activation factor is based on both normalized error and rate of change in error and proved an ultimate success independent of forcing frequency. The neurofuzzy algorithm for voltage activation has contributed in reducing the too post error.

References Références Referencias

1. Abboud, N. N., Wojcik, G. L., Vaughan, D. K., Mould, J., Powell, D. J., and, Nikodym, L., 1998 "Finite Element Modeling for Ultrasonic Transonic Transducers," Proceedings SPIE Int. Symposium on Medical Imaging, San Diego, Feb 21-27, pp. 1-24.
2. Allik, H., and, Hughes, T. J. R.: Finite element method for piezoelectric vibration. International Journal for Numerical Methods in Engineering, 2, pp. 151–157 (1970).
3. Bathe, K. J., 1982 "Finite Element Procedures in Engineering Analysis" Prentice-Hall Inc, pp.511-537.
4. Frankpitt, B. A., 1995 "Model of the Dynamics of a Lathe Toolpost that Incorporates Active Vibration Suppression. Institute for System Research," University of Maryland at College Park.
5. Frankpitt, B. A., 1995 "Model of the Dynamics of a Lathe Toolpost that Incorporates Active Vibration Suppression," Institute for System Research, University of Maryland at College Park.
6. Gopalakrishnan, V., Fedewa, D., Mehrabi, M. G., Kota, S., and, Orlandea, N., 2002, "Design of Reconfigurable Machine Tools," ASME J. Manuf. Sci. Eng., Technical Briefs, 124, pp. 483-485.
7. Harms, A., Denkena, B., and, Lhermet, N., 2004, "Tool adaptor for Active Vibration Control in Turning Operations," Actuator, 9th International Conference on New Actuators, Bremen, Germany. Pages 694 – 697.
8. Jang, J. J., Chuen-Tsai Sun, C. T., Mizutani, E., 1996,"Neuro-Fuzzy and Soft Computing: A Computational Approach to Learning and Machine Intelligence," Prentice Hall.
9. Kalinski, K J., Galewski, M A. 2011, "Chatter vibration surveillance by the optimal-linear spindle speed control", Mechanical Systems and Signal Processing, 25, pp 383–399
10. Lerch, R., 1990 "Simulation of piezoelectric devices by two and three dimensional finite elements," IEEE Transactions on Ultrasonics, Ferroelectrics, and Frequency Control, 37(3), pp. 233–247.
11. Lin, J. and Chao, W.S., 2009 "Vibration Suppression Control of Beam-cart System with Piezoelectric Transducers by Decomposed Parallel Adaptive Neuro-fuzzy Control," Journal of Vibration and Control, December , vol. 15 no. 12 1885-1906
12. Moon, Y., and, Kota, S., 2002, "Design of Reconfigurable Machine Tools", ASME J. Manuf. Sci. Eng., Technical Briefs, 124, Nov., pp. 480-483.
13. Park, G.a , Bement, M.T.a , Hartman, D.A.b , Smith, R.E.c , Farrar, C.R., 2007, "The use of active materials for machining processes: A review", International Journal of Machine Tools and Manufacture, Volume 47, Issue 15, pp 2189-2206

14. Piefort, V., 2001 "Finite Element Modeling of Piezoelectric Active Structures" Ph.D. Thesis, ULB, Active Structures Laboratory - Department of Mechanical Engineering and Robotics.
15. Radecki, P.P., Farinholt, K.M., Park, G. , Bement, M.T., 2010, " Vibration suppression in cutting tools using a collocated piezoelectric sensor/actuator with an adaptive control algorithm", ASME Journal of Vibration and Acoustics, 132, 5, pp 0510021-0510028
16. Rashid, M.K., .2005, "Simulation Study on the Improvements of Machining Accuracy by Using Smart Materials" Robotics and Computer-Integrated Manufacturing, Elsevier Science, Volume 21, Issue 3, June, Pages 249-257
17. Rashid, M.K., and, Shihab, K.I., 2006 "Intelligent Design of Cutting Tools Using Smart Material" International Journal of Mechanics and Materials in Design, Volume 3, Number 1, March, Pages 17-27 .
18. Roark R. J. and Young W. C., 1975 "Formulas for Stress and Strain" 5th edn, New York: McGraw-Hill, p 337 (table 24-1j).
19. Tzou, H. S., 1991 "Design of a piezoelectric exciter/actuator for micro-displacement control: theory and experiment," Precision Engineering, Vol. 13, No. 2, pp.104-110.
20. Zienkiewicz, O. C., and, Taylor, R. L., 2000a "The Finite Element Method" Fifth edition Vol.1: The Basis. Butterworth-Heinemann.
21. Zienkiewicz, O. C., and, Taylor, R. L., 2000b "The Finite Element Method" Fifth edition Vol.2: Solid Mechanics. Butterworth-Heinemann, pp. 423-424.

Global Journal of researches in engineering
Mechanical and mechanics engineering
Volume 11 Issue 7 Version 1.0 December 2011
Type: Double Blind Peer Reviewed International Research Journal
Publisher: Global Journals Inc. (USA)
Online ISSN: 2249-4596 Print ISSN:0975-5861

The Characteristics of Brazed Plate Heat Exchangers with Different Chevron Angles

By S. Muthuraman
Professor, Higher College of Technology, Oman.

Introduction - Plate heat exchangers (PHEs) were introduced in the 1930s and were almost exclusively used as liquid/liquid heat exchangers in the food industries because of their ease of cleaning. Over the years, the development of the PHE has generally continued towards larger capacity, as well as higher working temperature and pressure. Recently, a gasket sealing was replaced by a brazed material, and each thermal plate was formed with a series of corrugations (herringbone or chevron). These greatly increased the pressure and the temperature capabilities.

Keywords : Compact heat exchanger, narrow channel, corrugation, CFD, Nusselt number, pressure drop, condensation, brazed plate heat exchanger, R410a, chevron angle, correlation.

GJRE-A Classification: FOR Code: 091305

Strictly as per the compliance and regulations of:

The Characteristics of Brazed Plate Heat Exchangers with Different Chevron Angles

S. Muthuraman

Keywords : *Compact heat exchanger, narrow channel, corrugation, CFD, Nusselt number, pressure drop, condensation, brazed plate heat exchanger, R410a, chevron angle, correlation.*

I. Introduction

Plate heat exchangers (PHEs) were introduced in the 1930s and were almost exclusively used as liquid/liquid heat exchangers in the food industries because of their ease of cleaning. Over the years, the development of the PHE has generally continued towards larger capacity, as well as higher working temperature and pressure. Recently, a gasket sealing was replaced by a brazed material, and each thermal plate was formed with a series of corrugations (herringbone or chevron). These greatly increased the pressure and the temperature capabilities.

The corrugated pattern on the thermal plate induces a highly turbulent fluid flow. The high turbulence in the PHE leads to an enhanced heat transfer, to a low fouling rate, and to a reduced heat transfer area. Therefore, PHEs can be used as alternatives to shell-and-tube heat exchangers. Due to ozone depletion, the refrigerant R22 is being replaced by R410A (a binary mixture of R32 and R125, mass fraction 50 %/50 %). R410A approximates an azeotropic behavior since it can be regarded as a pure substance because of the negligible temperature gliding. The heat transfer and the pressure drop characteristics in PHEs are related to the hydraulic diameter, the increased heat transfer area, the number of the flow channels, and the profile of the corrugation waviness, such as the inclination angle, the corrugation amplitude, and the corrugation wavelength. These geometric factors influence the separation, the boundary layer, and the vortex or swirl flow generation. However, earlier experimental and numerical works were restricted to a single-phase flow. Since the advent of a Brazed PHE (BPHE) in the 1990s, studies of the condensation and/or evaporation heat transfer have focused on their applications in refrigerating and air conditioning systems, but only a few studies have been done. Much work is needed to understand the features of the two-phase flow in the BPHEs with alternative refrigerants. Xiaoyang et al., [1] experimented with the two-phase flow distribution in stacked PHEs at both vertical upward and downward flow orientations. They indicated that non-uniform distributions were found and that the flow distribution was strongly affected by the total inlet flow rate, the vapor quality, the flow channel orientation, and the geometry of the inlet port Holger [2].Theoretically predicted the performance of chevron-type PHEs under single-phase conditions and recommended the correlations for the friction factors and heat transfer coefficients as functions of the corrugation chevron angles. Lee et al., [3] investigated the characteristics of the evaporation heat transfer and pressure drop in BPHEs with R404A and R407C. Kedzierski [4] reported the effect of inclination on the performance of a BPHE using R22 in both the condenser and the evaporator. Several single-phase correlations for heat transfer coefficients and friction factors have been proposed, but few correlations for the two-phase flow have been proposed. Yan et al., [5] suggested a correlation of condensation with a chevron angle of 30 for R134a. Yan et al., reported that the mass flux, the vapor quality, and the condensation pressure affected the heat transfer coefficients and the pressure drops. Hieh and Lin [6] developed the correlations for evaporation with a chevron angle of 30 for R410A.

The main objective of this work was to experimentally investigate the heat transfer coefficients and the pressure drops during condensation of R410A inside BPHEs. Three BPHEs with different chevron angles of 45, 35, and 20 were used. The results were then compared to those of R22. The geometric effects of the plate on the heat transfer and the pressure drop were investigated by varying the mass flux, the quality, and the condensation temperature. From the results, the geometric effects, especially the chevron angle, must be considered to develop the correlations for the Nusselt number and the friction factor. Correlations for the Nusselt number and the friction factor with the geometric parameters are suggested in this study.

Experiments to measure the condensation heat transfer coefficient and the pressure drop in brazed plate heat exchangers (BPHEs) were performed with the refrigerants R410A and R22. Brazed plate heat exchangers with different chevron angles of 45°, 35°, and 20° were used. Varying the mass flux, the condensation temperature, and the vapor quality of the refrigerant, we measured the condensation heat transfer coefficient and the pressure drops. Both the heat transfer coefficient and the pressure drop increased proportionally with the mass flux and the vapor quality

Author : *Professor, Higher College of Technology, Oman.*

and inversely with the condensation temperature and the chevron angle.

Correlations of the Nusselt number and the friction factor with the geometric parameters are suggested for the tested BPHEs. In an effort to study and optimize the design of a plate heat exchanger comprising of corrugated walls with herringbone design, a CFD code is employed. Due to the difficulties induced by the geometry and flow complexity, an approach through a simplified model was followed as a first step. This simple model, comprised of only one corrugated plate and a flat plate, was constructed and simulated. The Reynolds numbers examined are 400, 900, 1000, 1150, 1250 and 1400. The SST turbulence model was preferred over other flow models for the simulation.

The case where hot water (60oC) is in contact with a constant-temperature wall (20oC) was also simulated and the heat transfer rate was calculated. The results for the simplified model, presented in terms of velocity, shear stress and heat transfer coefficients, strongly encourage the simulation of one channel of the typical plate heat exchanger, i.e. the one that comprises of two corrugated plates with herringbone design having their crests nearly in contact. Preliminary results of this latter work, currently in progress, comply with visual observations.

In recent years, compact heat exchangers with corrugated plates are being rapidly adopted by food and chemical process industries, replacing conventional shell-and-tube exchangers. Compact heat exchangers consist of plates embossed with some form of corrugated surface pattern, usually the chevron (herringbone) geometry[1].The plates are assembled being abutting, with their corrugations forming narrow passages. This type of equipment offers high thermal effectiveness and close temperature approach, while allowing ease of inspection and cleaning [1],[2]. In order to be able to evaluate its performance, methods to predict the heat transfer coefficient and pressure drop must be developed. In this direction, CFD is considered an efficient tool for momentum and heat transfer rate estimation in this type of heat exchangers.

The type of flow in such narrow passages, which is associated with the choice of the most appropriate flow model for CFD simulation, is still an open issue in the literature. Due to the relatively high pressure drop, compared to shell-and-tube heat exchangers for equivalent flow rates, the Reynolds numbers used in this type of equipment must be lower so as the resulting pressure drops would be generally acceptable[1]. Moreover, when this equipment is used as a reflux condenser, the limit imposed by the onset of flooding reduces the maximum Reynolds number to a value less than 2000[3]. Ciofalo et al.[4], in a comprehensive review article concerning modeling heat transfer in narrow flow passages, state that, for the Reynolds number range of 1,500-3,000, transitional flow is expected, a kind of flow among the most difficult to simulate by conventional turbulence models.

On the other hand, Shah & Wanniarachchi[1] declare that, for the Reynolds number range 100-1500, there is evidence that the flow is already turbulent, a statement that is also supported by Vlasogiannis et al.[5], whose experiments in a plate heat exchanger verify that the flow is turbulent for Re>650. Lioumbas et al.[6], who studied experimentally the flow in narrow passages during counter-current gas-liquid flow, suggest that the flow exhibits the basic features of turbulent flow even for the relatively low gas Reynolds numbers tested (500<Re<1200).Focke & Knibbe[7] performed flow visualization experiments in narrow passages with corrugated walls. They concluded that the flow patterns in such geometries are complex, due to the existence of secondary swirling motions along the furrows of their test section and suggest that the local flow structure controls the heat transfer process in such narrow passages.

The most common two-equation turbulence model, based on the equations for the turbulence energy k and its dissipation ε, is the k-ε model[8]. To calculate the boundary layer, either "wall functions" are used, overriding the calculation of k and ε in the wall adjacent nodes[8], or integration is performed to the surface, using a "low turbulent Reynolds (*low-Re*) k-ε" model[9]. Menter & Esch[9] state that, in standard k-ε the wall shear stress and heat flux are over predicted (especially for the lower range of the Reynolds number encountered in this kind of equipment) due to the over prediction of the turbulent length scale in the flow reattachment region, which is a characteristic phenomenon occurring on the corrugated surfaces in these geometries. Moreover, the standard k-ε, model requires a course grid near the wall, based on the value of y+=11 [9],[10], which is difficult to accomplish in confined geometries. The low-Re k-ε model, which uses "dumping functions" near the wall[8],[9], is not considered capable of predicting the flow parameters in the complex geometry of a corrugated narrow channel[4], requires finer mesh near the wall, is computationally expensive compared to the standard k-ε model and it is unstable in convergence.

An alternative to k-ε model, is the k-ω model, developed by Wilcox[11]. This model, which uses the turbulence frequency ω instead of the turbulence diffusivity ε, appears to be more robust, even for complex applications, and does not require very fine grid near the wall[8]. However, it seems to be sensitive to the free stream values of turbulence frequency ω outside the boundary layer. A combination of the two models, k-ε and k-ω, is the SST (Shear-Stress Transport) model, which, by employing specific "blending functions", activates the Wilcox model near the wall and the k-ε model for the rest of the flow[9] and thus it benefits from the advantages of both models. Some efforts have been made wards the effective simulation of a plate heat exchanger. Due to the modular nature of a

compact heat exchanger, a common practice is to think of it as composed of a large number of unit cells (Representative Element Units, RES) and obtain results by using a single cell as the computational domain and imposing periodicity conditions across its boundaries[4],[12]. However, the validity of this assumption is considered another open issue in the literature [4].

II. Experimental Facility

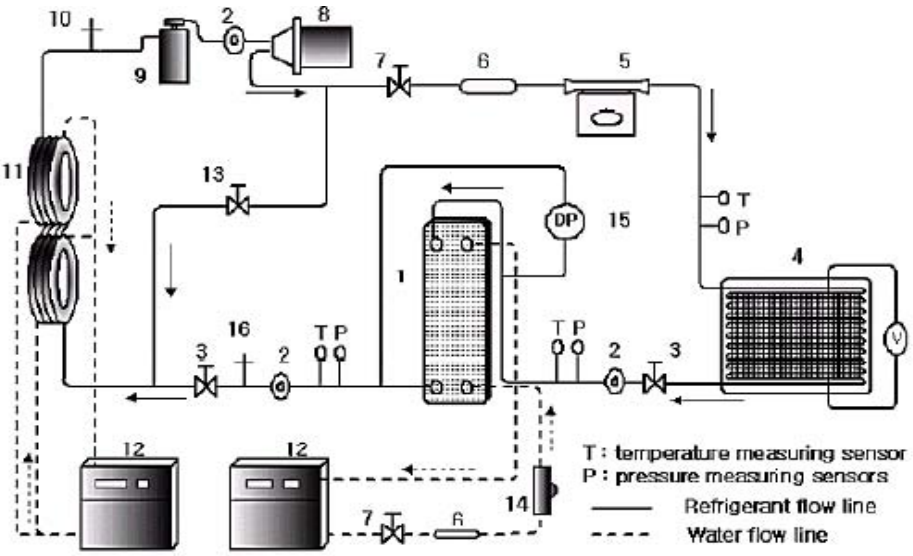

1. Plate heat exchanger	9. Liquid receiver
2. Sight glass	10. Charging port
3. On-off valve	11. Double-pipe heat exchanger
4. Pre-heater	12. Chiller
5. Mass flow meter	13. By-pass valve
6. Filter & dryer	14. Volumetric flow meter
7. Check valve	15. Differential pressure transducer
8. Magnetic gear pump	16. Discharge port

Fig. 1. Schematic diagram of the experimental system.

The experimental facility is capable of determining in plate heat transfer coefficients and measuring the pressure drops for the refrigerants. It consists of four main parts: a test section, a refrigerant loop, two water loops, and a data-acquisition system. A schematic of the test facility used in this study is shown in Figure-1, and detailed descriptions of the four main parts are mentioned below.

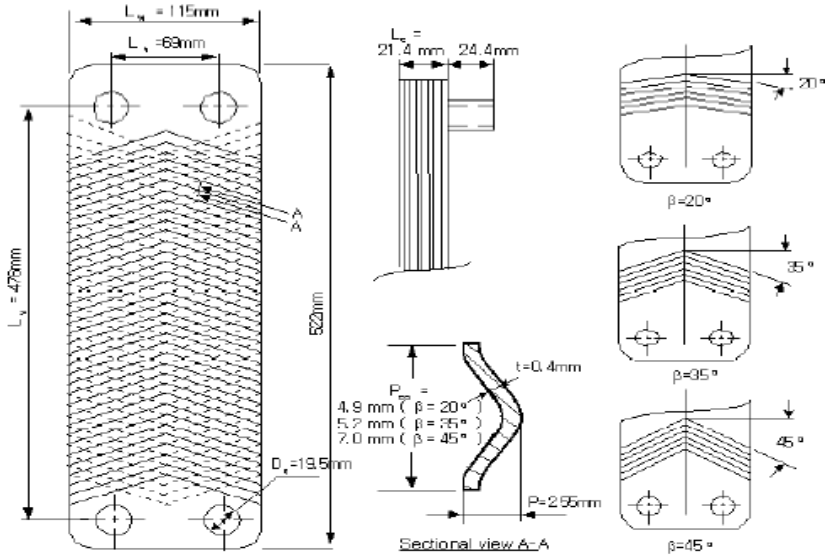

Fig. 2. Dimensions of the brazed plate heat exchangers.

a) Brazed plate heat exchangers

Three BPHEs with chevron angles of 45°, 35°, and 20° were used as the test sections. The angles of corrugation were measured from the horizontal axis. Each BPHE was composed of 4 thermal plates and 2 end plates, forming 5 flow channels. The dimensions of the BPHEs are shown in Figure-2. The refrigerant and cooling water were directed into the alternate passages between the plates through corner ports, creating counter flow conditions. The cooling water owed from the bottom to the top of every other channel on the basis of a central channel. On the other hand, the refrigerant owed from the top to the bottom in the rest of them.

b) Refrigerant loop

Refrigerant was supplied to the test section at specific conditions (i.e., temperature, flow rate, and quality) through the refrigerant loop. This loop contained a pre-heater, a double-pipe heat exchanger, a receiver, a magnetic gear pump, a differential pressure transducer, and a mass flow meter. Also included were thermocouples probes and pressure taps at the inlet/outlet of the test section. The refrigerant pump was driven by a DC motor which was controlled by a variable DC output motor controller.

The refrigerant flow rate was measured by using a mass flow meter installed between the magnetic gear pump and the pre-heater with an accuracy of _0.5 %. The pre-heater located before the test section was used to evaporate the refrigerant to a specified vapor quality at the inlet of the test section. The pressure drop of the refrigerant owing through the test section was measured with the differential pressure transducer, to an accuracy of _0.25 kPa. The refrigerant through the test section was subcooled at a double-pipe heat exchanger by the water cooled by the chiller and went into a liquid receiver. The subcooled refrigerant returned to the magnetic gear pump and circulated through the refrigerant loop repeatedly. Calibrated T-type thermocouples were used to measure the temperatures of the refrigerant at the inlet/outlet of the test section. The entire loop was insulated with fiberglass to prevent heat transfer to the environment.

c) Water loop

There are two closed water loops in this facility. One is for determining the condensation heat flux at the test section. The other is for making the subcooled refrigerant state at two double-pipe heat exchangers before it enters the magnetic gear pump. The water flow rates of the test section were measured by using a turbine flow meter, and T-type thermocouples were installed to evaluate the gain of the heat flux of the water of the test section.

d) Data acquisition

The data were recorded by a computer-controlled data-acquisition system with 40 channels scanned at the speed of 30 data per minute. The temperature and the pressure of both fluids were continuously recorded, and the thermodynamic properties of the refrigerant were obtained from a computer program. After steady-state conditions had been reached in the system, all measurements were taken for 10 minutes.

III. Data Reduction and Uncertainty Analysis

The hydraulic diameter of the channel, D_h, is defined as

$$D_h = \frac{4 \times \text{channel flow area}}{\text{wetted perimeter}} = \frac{4bL_w}{2L_w\phi} = \frac{2b}{\phi}, \qquad (1)$$

Where is φ=1.17. This value is given by the manufacturer.

The mean channel spacing, b, is defined as

b = p - t; t= Plate Thickness (2)

and the plate pitch p can be determined as, N_t=Total Number of plates

$$p = \frac{L_c}{N_t - 1}. \qquad (3)$$

The procedures to calculate the condensation heat transfer coefficient of the refrigerant side are described below. At first, the refrigerant quality at the inlet of the test section (x_{in}) should be selected to evaluate the condensation heat at a given quality. Its value is calculated from the amount of heat given by a pre-heater, which is the summation of the sensible heat and the latent heat:

$$\begin{aligned} Q_{pre} &= Q_{sens} + Q_{lat} \\ &= \dot{m}_r C_{p,r}(T_{r,sat} - T_{r,pre,in}) + \dot{m}_r i_{fg} x_{in}. \end{aligned} \qquad (4)$$

The refrigerant quality at the inlet of the test section can be written as

$$x_{in} = \frac{1}{i_{fg}}\left[\frac{Q_{pre}}{\dot{m}_r} - C_{p,r}(T_{r,sat} - T_{r,pre,in})\right]. \qquad (5)$$

The power gained by the pre-heater is calculated by measuring the voltage and the current with a power meter. The change in the refrigerant quality inside the test section was evaluated from the heat transferred in the test section and the refrigerant mass flow rate (6)

$$\Delta x = x_{in} - x_{out} = \frac{Q_w}{\dot{m}_r \times i_{fg}}. \qquad (6)$$

The condensing heat in the test section was calculated from an energy balance with water:

$$Q_w = \dot{m}_w C_{p,w}(T_{w,out} - T_{w,in}). \qquad (7)$$

The heat transfer coefficient of the refrigerant side (hr) was evaluated from the following equation:

$$\frac{1}{h_r} = \frac{1}{U} - \frac{1}{h_w} - R_{wall}. \quad (8)$$

The overall heat transfer coefficient was determined using the log mean temperature difference

$$U = \frac{Q_w}{A \times LMTD},$$

$$LMTD = \frac{(T_{r,out} - T_{w,in}) - (T_{r,in} - T_{w,out})}{\ln\{(T_{r,out} - T_{w,in})/(T_{r,in} - T_{w,out})\}}. \quad (9)$$

The heat transfer coefficient of the water side (h W) was obtained by using Eq. (10). Equation (10) was developed from the single-phase water to water pre tests by K_{im} [7]. If the least-squares method and the multiple regression method are used, the heat transfer coefficient of the water side is correlated in terms of the Reynolds number, the Prandtl number, and the chevron angle:

$$h_w = 0.295 \left(\frac{k_w}{D_{Eq}}\right) Re^{0.64} Pr^{0.32} \left(\frac{\pi}{2} - \beta\right)^{0.09}. \quad (10)$$

The thermal resistance of the wall is negligible compared to the effect of convection.

For the vertical downward flow, the total pressure drop in the test section is defined as

$$\Delta P_{total} = \Delta P_{fr} + \Delta P_a + \Delta P_s + \Delta P_p, \quad (11)$$

And ΔP_{total} is measured by using a differential pressure transducer. The two-phase friction factor, f, is defined as

$$\Delta P_{fr} = f \frac{L_v N_{cp}}{D_h} \frac{G_{Eq}^2}{\rho_f}. \quad (12)$$

The port pressure loss in this experiment was less than 1 % of the total pressure loss. The static head loss can be written as and it has a negative value for vertical downward flow. The acceleration pressure drop for condensation is expressed as

$$\Delta P_p = 1.4 G_p^2/(2\rho_m), \quad (13)$$

An uncertainty analysis was done for all the measured data and the calculated quantities based on the methods described by Moffat [9]. The detailed results of the uncertainty analysis are shown in Table-1.

Table 1 : Estimated Uncertainty

Parameters	Uncertainty
Temperature	±0.2 ° C
Pressure	±4.7KPa
Pressure drop	±250Pa
Water flow rate	±2%
Refrigerant mass flux	±0.5%
Heat flux of Test Section	±5.7%
Vapour quality	±0.03
Heat transfer Coefficients of Water side	±10.1%
Heat transfer Coefficients of Refrigerant	±9.1%

where

$$G_p = 4\dot{m}_{Eq}/\pi D_p^2 \quad (14)$$

and

$$(1/\rho_m) = (x/\rho_g) + [(1-x)/\rho_f]. \quad (15)$$

The equivalent mass flow rate, $\dot{m}_{Eq}$, is defined as

$$\dot{m}_{Eq} = \dot{m}\left[1 - x + x\left(\frac{\rho_f}{\rho_g}\right)^{0.5}\right]. \quad (16)$$

The port pressure loss in this experiment was less than 1 % of the total pressure loss. The static head loss can be written as

$$\Delta P_s = -\rho_m g L_v \quad (17)$$

and it has a negative value for vertical downward flow. The acceleration pressure drop for condensation is expressed as

$$\Delta P_a = -\left[(G_{Eq}^2 x/\rho_{fg})_{in} - (G_{Eq}^2 x/\rho_{fg})_{out}\right]. \quad (18)$$

IV. Results and Discussions

The condensation heat transfer coefficients and the pressure drops of R410A and R22 were measured in three BPHEs with chevron angles of 20°, 35°, and 45° by varying the mass flux (13 - 34 kg/m2s), the vapor quality (0.9 - 0.15), and the condensing temperature (20°C and 30°C) under a given heat flux condition (4.7 -5.3 kW/m2). R22 was tested under identical experimental conditions for comparison with R410A.

a) Flow regime

Before the behaviors of heat transfer are considered, it is necessary to predict what flow regime exists at a given set of operating conditions. The detailed flow regime map for the PHE has not been proposed yet because of the difficulty of flow visualization. Vlasogiannis et al., [10] suggested the criterion of a two-phase flow regime for a PHE in terms of superficial liquid (jf) and vapor velocities (jg) by using water and air under adiabatic conditions. They only simulated a mixture of water and air as a two-phase fluid. According to their work, the flow patterns in a PHE are significantly different from those inside the vertical round tubes. They detected 3 types of flow patterns. The

first was a gas continuous pattern with a liquid pocket at flow water flow rates (jf < 0.025 m/s) over wide range of air flow rates.

The second was the slug flow pattern, which was detected at sufficiently high air (jg > 2 m/s) and water flow rates (jf > 0.025 m/s). Thirdly, the liquid continuous pattern with a gas pocket or a gas bubble at the high water flow rates (jf >0.1 m/s) and low air flow rates (jg < 1 m/s).According to the flow regime map proposed by Vlasogiannis et al., the expected flow pattern in this experimental study is the gas continuous flow pattern with liquid pockets. However, their flow regime map has a significant limitation for use since many important features, such as the phase-change, the heating or cooling conditions, the densities or specific volumes of the working fluids, the geometries of the PHEs, etc., were not considered in detail. According to the flow regime map proposed by Crawford et al. [11], which was developed for vertical downward flow in a round tube, all experimental flow patterns are located in the intermittent flow regime, but this flow regime cannot represent the correct flow regime in a BPHE due to the different geometries.

b) Condensation heat transfer

Figure-3 shows the effects of the refrigerant mass flux, the chevron angle, and the condensation temperature on the averaged heat transfer coefficient for R410A. The term "averaged heat transfer coefficient" means the average of the heat transfer coefficients calculated by varying the quality of the refrigerant from 0.15 to 0.9, and the coefficients were obtained from Eq. (19):

$$h_{averged} = \frac{\Sigma h_{local} x_{local}}{\Sigma x_{local}}, \qquad (19)$$

Where $\sum h_{local} x_{local}$ is the local heat transfer coefficient at the local vapor quality. The experimental results indicate that the averaged heat transfer coefficients vary proportionally with the mass flux and inversely with the chevron angles and the condensation temperature. The small chevron angle forms narrow pitches to the flow direction, creating more abrupt changes in the velocity and the flow direction, thus increasing the effective contact length and time in a BHPE. The zigzag flow increases the heat transfer, and the turbulence created by the shape of the plate pattern is also important in addition to the turbulence created by the high flow rates. Increasing the mass flux at a given condensation temperature showed that the differences in the averaged heat transfer coefficients were significantly enlarged with decreasing chevron angle. This indicates that a PHE with the small chevron angle is more effective at a large mass flux ($Gc > 25\ kg/m^2s$) than at a small mass flux.

The averaged heat transfer coefficient of R410A decreases with increasing condensation temperature. The vapor velocity is a more influential factor than the liquid film thickness for the heat transfer. Vapor bubbles in the flow enhance the disturbance in the bubble wake as a turbulence promoter, and the turbulence induced by the vapor bubbles increases with the vapor velocity. Also, since the specific volume of the vapor increases with decreasing condensation temperature, the vapor velocity increases for a fixed mass flux and quality. The vapor velocity at 20°C is faster than that at 30°C. The rates of the averaged heat transfer coefficients between condensation temperatures of 20°C and 30°C increased 5 % for a chevron angle of 45°, 9 % for 35°, and 16 % for 20°. These results show that different chevron angles lead partly to different flow pattern. Thus, we may conclude that the flow regime map should be modified by geometric considerations. The heat transfer coefficients in the high-quality region (fast velocity region) are larger than those in the low-quality region (slow velocity region). As mentioned above, this happens because the vapor velocity is the dominant effect on the heat transfer mechanism.

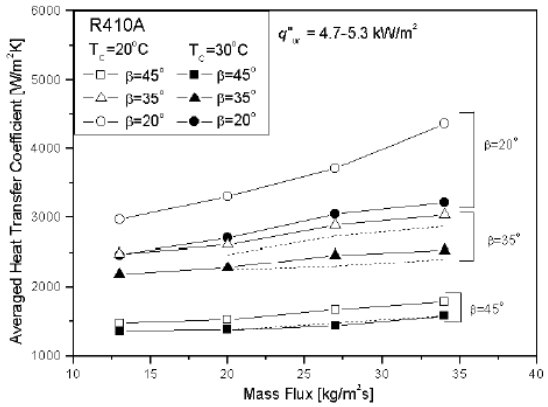

Fig. 3. Effect of mass flux on the averaged condensation heat transfer coefficient.

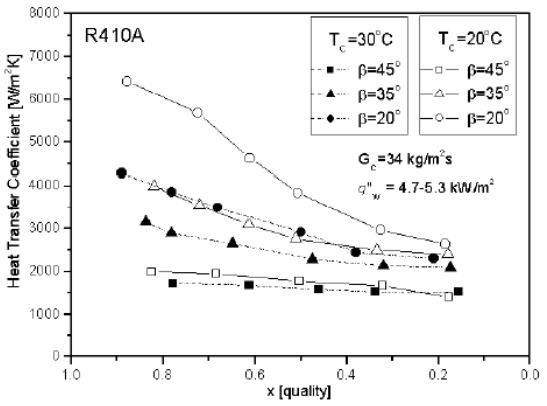

Fig. 4. Effect of quality on the condensation heat transfer coefficient.

Increasing the vapor quality at the same mass flux induces a faster bubble velocity, which increases the turbulence level and the convection heat transfer coefficient. The difference of heat transfer coefficients between the low-quality region and the high-quality region becomes larger with decreasing chevron angle. The PHE with a low chevron angle shows a better heat transfer performance in the high-quality region (i.e., the high vapor velocity region). Figure-4 also shows the variation of the heat transfer coefficients with the condensation temperatures. Like Figure-3, the heat transfer coefficients decreased with increasing condensation temperature. Also, the variations of the heat transfer coefficients with the condensation temperature are larger in the high-quality region. From the experimental results in Figures, 3 and 4, lowering the chevron angle and the condensation temperature gives the desired heat transfer effect.

c) Frictional pressure loss

The frictional pressure loss in a BPHE is obtained by subtracting the acceleration pressure loss, the static head loss, and the port pressure loss from the total pressure loss. Figure-5 shows the trend of the pressure drop along the mass flux, and Figure-6 shows the trend of the pressure drop along the quality at a mass flux of 34 kg/m^2s and a heat flux of 4.7-5.3 kW/m^2. The frictional pressure drops in the BPHEs increase with increasing mass flux and quality and decreasing condensation temperature and chevron angle. This trend is similar to that of the condensation heat transfer. As mentioned above, since the vapor velocity is much faster than the liquid velocity during the two-phase flow in the tube, the vapor velocity is the dominant influence on the pressure drop, as well as the heat transfer. A high vapor velocity also tends to increase the turbulence of the flow. From Figures 3, 4, 5 and 6, we may concluded that since the trends of the the condensation heat transfer and the pressure loss in BPHEs are similar, those effects must be carefully considered in the design of a BPHE.

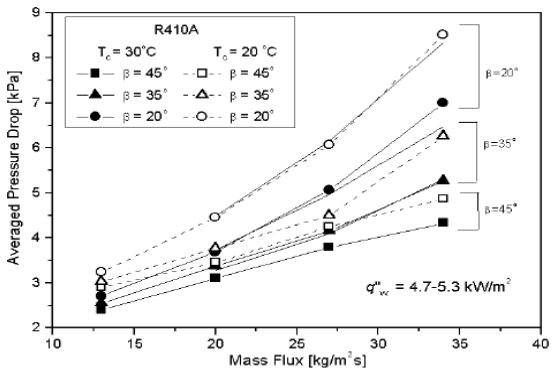

Fig. 5. Variation of the averaged condensation pressure drop with mass flux.

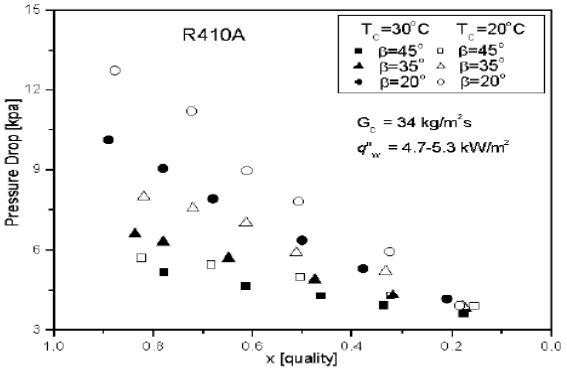

Fig. 6. Variation of the condensation pressure drop with quality.

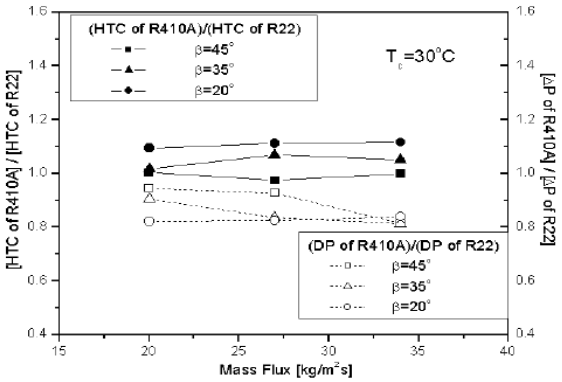

Fig. 7. Condensation heat transfer coefficient ratio and pressure drop ratio between R410A and R22.

d) Comparison of R410A with R22

The ratios of R410A to R22 for the condensation heat transfer coefficients and pressure drops at a condensation temperature of 30°C are shown in the Figure-7. The ratios for the heat transfer coefficients are relatively constant in the range of 1 -1.1, regardless of the mass flux, while the ratios for the pressure drops decrease with increasing mass flux, except for the data at a chevron angle of 20° in the present experimental range. For a chevron angle of 20°, the heat transfer ratios of R410A to R22 are about 1.1, and the pressure drop ratios about 0.8, which is a 10 % higher heat transfer and a 20 % lower pressure drop.The smaller specific volume of the vapor of R410A relative to that of R22 makes the vapor velocity slower and yields a small pressure drop under the same conditions of the mass flux. While the two fluids have almost equal values of their latent heats, the liquid-phase thermal conductivity of R410A is larger than that of R22. The higher thermal conductivity for R410A helps to produce better heat transfer even if a reduction in the specific volume occurs. Also, a BPHE with a small chevron angle is known to have more effective performance from the ratios when replacing R22 with R410A.

e) Correlations of Nusselt number and friction factor for tested BPHEs

Based on the experimental data, the following correlations for Nu and f during condensation for the tested BPHEs are established: Where G_{e1}, G_{e2}, G_{e3}, and G_{e4} are non-dimensional geometric parameters that involve the corrugation pitch, the equivalent diameter, and the chevron angle. Re_{Eq} is the equivalent Reynolds number, and G_{Eq} the equivalent mass flux: where G_c is the channel mass flux. The suggested correlations for the Nusselt number and the friction factor can be applied in the range of Re_{Eq} from 300 to 4000. Figure-8(a) shows a comparison of the Nusselt number among the experimental data, the correlation proposed in this paper, and the correlation of Yan et al., [5]. The correlation of Yan et al., is

$$Nu = Ge_1 Re_{Eq}^{Ge_1} Pr^{1/3}, \tag{20}$$

$$Ge_1 = 11.22\left(\frac{p_{co}}{D_h}\right)^{-2.83}\left(\frac{\pi}{2}-\beta\right)^{-4.5}, \tag{21}$$

$$Ge_2 = 0.35\left(\frac{p_{co}}{D_h}\right)^{0.23}\left(\frac{\pi}{2}-\beta\right)^{1.48}, \tag{22}$$

$$f = Ge_3 Re_{Eq}^{Ge_4}, \tag{23}$$

$$Ge_3 = 3521.1\left(\frac{p_{co}}{D_h}\right)^{4.17}\left(\frac{\pi}{2}-\beta\right)^{-7.75}, \tag{24}$$

$$Ge_4 = -1.024\left(\frac{p_{co}}{D_h}\right)^{0.0925}\left(\frac{\pi}{2}-\beta\right)^{-1.3}, \tag{25}$$

$$Re_{Eq} = \frac{G_{Eq} D_h}{\mu_f}, \tag{26}$$

$$G_{Eq} = G_c[1 - x + x(\rho_f/\rho_g)^{1/2}], \tag{27}$$

$$G_c = \frac{\dot{m}}{N_{cp} b L_w}, \tag{28}$$

and is obtained from one PHE with a chevron angle of 30° for R134a. Regardless of the BPHE types and refrigerants, most of the experimental data are within 20 % for the correlation proposed in this paper.

The correlation of Y an et al.(5), matched the data relatively well for β : 20 and 35 within30 %, but over-predicted the data quite a bit for 45. This discrepancy results from the correlation of Yan et al., being developed for only a+30 PHE. Also,the correlation of Yan et al.

$$Nu = 4.118 Re_{Eq}^{0.4} Pr^{1/3}, \tag{29}$$

for the Nusselt number only adopted the equivalent Reynolds number and Prandtl number without any geometric parameters. Because a BPHE has a strong geometric effect, the correlation with geometric parameters must be developed for general applications. The root-mean-square (r.m.s.) of the deviations is defined as

$$r.m.s. = \sqrt{\frac{1}{N_{data}}\sum\left(\frac{Nu_{pred} - Nu_{\exp}}{Nu_{\exp}}\right)^2} \times 100(\%). \tag{30}$$

The r.m.s. deviation for the correlation of Yan et al., [Eq. (29)] is 50.2 % and for Eq. (20), it is only 10.9 %. Figure-8(b) shows a comparison of the friction factor between the experimental data and the proposed correlation. Similar to the correlation of the Nusselt number, the correlation of the friction factor includes the equivalent Reynolds number and the geometric parameters. Regardless of the BPHE types and refrigerants, most of the experimental data are within 15 % of the correlation proposed in this paper; the r.m.s. deviation for Eq. (23) is 10 %.

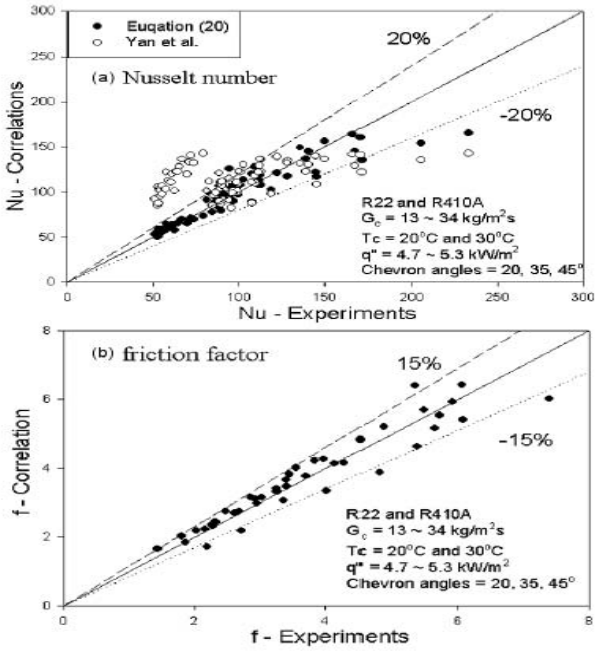

Fig. 8. Comparison of the correlations with the experimental data.

V. Study of A Simplified Geometry

In an effort to simulate the flow configuration, a simple channel was designed and constructed in order to conduct experiments and obtain formation on the flow pattern prevailing inside the furrows of the conduit. The flow configuration, apart from affecting the local momentum and heat transfer rates of a plate heat exchanger, suggests the appropriate flow model for the CFD simulation. A module of a plate heat exchanger is a single pass of the exchanger, consisting of only two plates. The simple channel examined is a single pass made of Plexiglas (Figure 9). It is formed by only one corrugated plate comprised of fourteen equal sized and uniformly spaced corrugations as well as a flat plate and it is used for pressure drop measurements and flow visualization. Details of the plate geometry are presented in Table 2. This model was chosen in an attempt to simplify the complexity of the original plate

heat exchanger and to reduce the computational demands. The geometry studied in the CFD simulations (similar to the test section) is shown in Figure 10. The Reynolds numbers examined are 400, 900, 1000, 1150, 1250 and 1400, which are based on the distance between the plates at the entrance (d=10mm), the mean flow velocity and the properties of water at 60oC. In addition to isothermal flow, heat transfer simulations are carried out for the same Reynolds numbers, where hot water (60oC) is cooled in contact with a constant-temperature wall (20oC). The latter case is realized in condensers and evaporators. Additionally, it is assumed that heat is transferred only through the corrugated plate, while the rest of the walls are considered adiabatic.

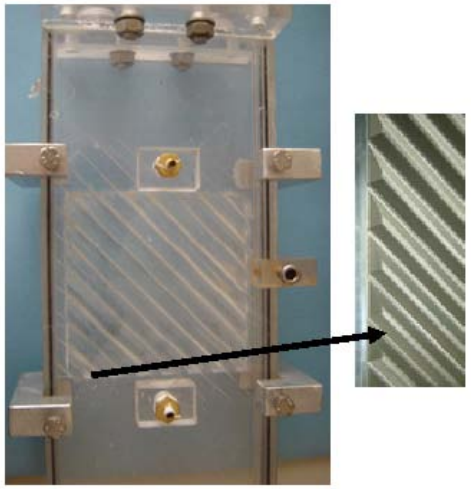

Figure 9 Simplified model and detail of the corrugated plate

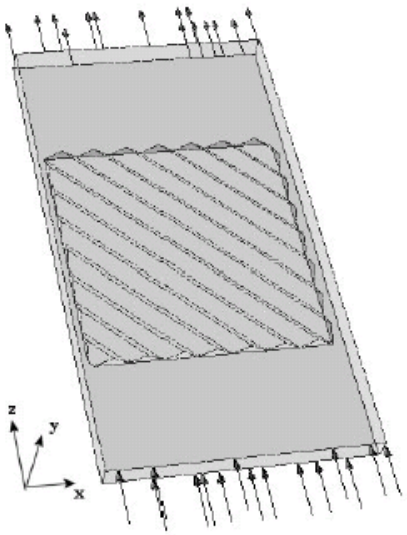

Figure 10 CFD model

A commercial CFD code, namely the CFX ® 5.6 code developed by AEA Technology, was employed to explore its potential for computing detailed characteristics of this kind of flow. In general, the models used in CFD codes give reasonably good results for single-phase flow systems. The first step in obtaining a solution is the division of the physical domain into a solution mesh, in which the set of equations is discretised.

The grid size used is selected by performing a grid dependence study, since the accuracy of the solution greatly depends on the number and the size of the cells. The resulting mesh was also inspected for inappropriate generated cells (e.g. tetrahedral cells with sharp angles) and fixed, leading to a total number of 870,000 elements. The SST model was employed in the calculations for the reasons explained in the previous chapter. The mean velocity of the liquid phase was applied as boundary condition at the channel entrance (i.e. Dirichlet BC on the inlet velocity) and no slip conditions on the channel walls. A constant temperature boundary condition was applied only on the corrugated wall, whereas the rest of the walls are considered adiabatic. Calculations were performed on a SGI O2 R10000 workstation with a 195MHz processor and 448Mb RAM. The CFX ®5.6 code uses a finite volume method on a non-orthogonal body-fitted multi-block grid. In the present calculations, the SIMPLEC algorithm is used for pressure-velocity coupling and the QUICK scheme for discretisation of the momentum equations [31],[32].

Plate length	0.200 m
Plate width	0.110 m
Maximum spacing between plates	0.010 m
Number of corrugations	14
Corrugation angle	45°
Corrugation pitch	0.005 m
Corrugation width	0.014 m
Plate length before and after corrugations	0.050 m
Heat transfer area	2.7×10^{-2} m^2

Table 2 Simple channel's plate geometric characteristics.

The results of the present study suggest that fluid flow is mainly directed inside the furrows and follows them (Figure 11a). This type of flow behavior is also described by Focke & Knibbe[7], who made visual observations of the flow between two superposed corrugated plates (Figure 11b). They confirm that the fluid, after entering a furrow, mostly follows it until it reaches the side wall, where it is reflected and enters the anti-symmetrical furrow of the plate above, a behavior similar to the one predicted by the CFD simulation. It seems that, in both cases, most of the flow passes through the furrows, where enhanced heat transfer characteristics are expected.

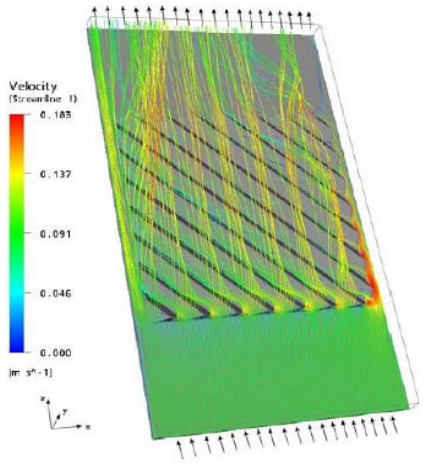

Figure 11.a Typical flow pattern for the: a) simple channel, CFD results, Re=900

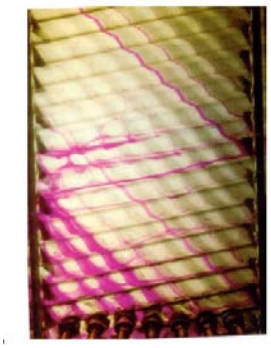

Figure 11.b) Flow visualization by Focke & Knibbe[7], Re=125

Figure 12 shows details of the flow inside a furrow for the simple model, where swirling flow is identified. This secondary flow is capable of bringing new fluid from the main stream close to the walls, augmenting heat transfer rates. Focke & Knibbe[18], who performed visualization experiments in similar geometries, also describe this kind of swirling flow. The values of the z-component of shear stress (Figure13a) increase with the Reynolds number –as expected–and the maximum value occurs at the crests of the corrugations. It may be argued that, during gas-liquid counter-current flow in such geometries, the shear stress distribution tends to prevent the liquid layer from falling over the crest of the corrugations and to keep it inside the furrows. The visual observations of Paras et al.[14] seem to confirm the above behavior. The heat flux through the wall of the corrugated plate was calculated by the CFD code. In addition, the local Nusselt number was calculated (by a user-Fortran subroutine) using the expression:

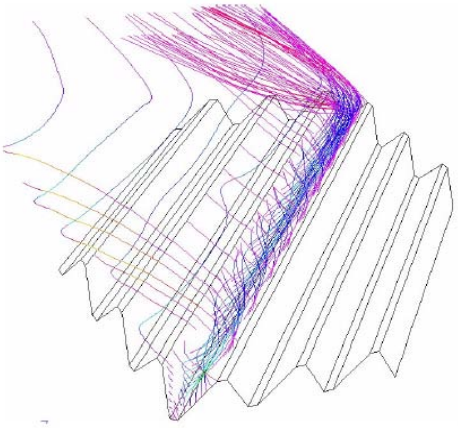

Figure 12 Swirling flow inside a furrow; Re=900

$$Nu_x = \frac{\dot{q}d}{(T_b - T_w)k} \qquad (31)$$

Where q' is the local wall heat flux, d the distance between the plates at the entrance, T_w the wall temperature, T_b the local fluid temperature and k the thermal conductivity of the fluid. In addition to the local Nusselt number, mean Nusselt numbers were calculated as follows:

- A mean Nu calculated by numerical integration of the local Nu over the corrugated area only, and
- An overall average Nu calculated using the total wall heat flux through the whole plate and the fluid temperatures at the channel entrance/exit.

The comparison of the values of the above Nusselt numbers shows that they do not differ more that 1%; therefore, the smooth part of the corrugated plate does not seem to influence the overall heat transfer. Figure 13b shows a typical local Nusselt number distribution over the corrugated wall for Re=900. All the Reynolds numbers studied exhibit similar distributions.

It is noticeable that local Nusselt numbers attain their maximum value at the top of the corrugations. This confirms the strong effect of the corrugations, not only on the flow distribution, but also on the heat transfer rate. To the best of author's knowledge, experimental values of heat transfer and pressure drop are very limited in the open literature for the corrugated plate geometry, since these data are proprietary. Therefore, the data of Vlasogiannis et al.[16] were used to validate the simulation results. These data concern heat transfer coefficients measurements of both single (Re<1200) and two-phase flow in a plate heat exchanger with corrugated walls and a corrugation inclination angle of 60o. Heavner et al.[14] proposed a theoretical approach, supported by experimental data, to predict heat transfer coefficients of chevron-type plate heat exchangers. Figure14 presents the experimental friction factors, obtained from the Plexiglas test section of Figure 9, as well as the CFD predictions for the simple geometry studied, as a function of the Reynolds number. It appears that the experimental values follow a power law of the form:

$$f = m\,\mathrm{Re}^{-n} \qquad (32)$$

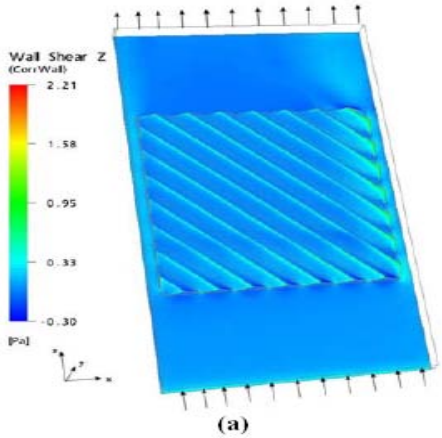

Figure 13. : Typical results of the CFD simulation for Re=900; distributions of: (a) z-shear stress component

Where m and n constants with values 0.27 and 0.14 respectively. Heavner et al.[14] proposed a similar empirical correlation based on their experimental results on a single pass of a plate heat exchanger with 45o corrugation angle, but with two corrugated plates. In spite of the differences in geometry, it appears that the present results are in good agreement with the experimental data of Heavner et al.[14] (0.687 and 0.141 for the variables m and n, respectively).

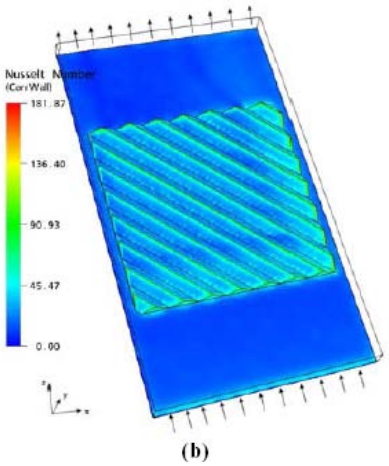

Figure 13. : Typical results of the CFD simulation for Re=900; distributions of: (b) local Nusselt number

It must be noted that Focke et al.[15] , who also measured heat transfer coefficients in a corrugated plate heat exchanger having a partition of celluloid sheet between the two plates, reported that the overall heat transfer rate is the 65% of the corresponding value without the partition. Figure 15 shows that the mean j-Colburn factor values calculated using the overall Nusselt number are practically equal to the 65% of the values measured by Vlasogiannis et al. This holds true for all Reynolds numbers except the smallest one

(Re=400). In the latter case the Nusselt number is greatly overpredicted by the CFD code. This is not unexpected, since the two-equation turbulence model is not capable to predict correctly the heat transfer characteristics for such low Reynolds number.The CFD results reveal that the corrugations enhance the heat transfer coefficient, whereas the pressure losses due to the augmentation of friction factor f are increased (Table 3), compared to a smooth-wall plate heat exchanger. Additionally, comparison of the normalized values of Nusselt number and the friction factor, with respect to the corresponding values for the smooth plate (*fsm, Nusm*), indicates that as the Reynolds number increases, heat transfer enhancement is slightly reduced, while the friction factor ratio, f/f , is increased. This is typical for plate heat exchangers with corrugations [16].

Re	Nu_{vlasog}	$65\%\ Nu_{vlasog}$	Nu_{all}	Nu_{sm}	$\frac{Nu_{ave}}{Nu_{sm}}$	$\frac{f}{f_{sm}}$
400	13.2	8.6	20.5	-	-	-
900	38.0	24.7	27.3	9.4	2.9	12.4
1000	41.2	26.8	28.6	10.2	2.8	12.8
1150	44.2	28.7	28.8	11.0	2.7	13.5
1250	46.8	30.4	30.9	11.7	2.7	13.9
1400	49.5	32.2	32.0	12.5	2.6	14.5

Table 3 Experimental values, calculated Nusselt numbers and normalized values of *Nu* and *f*

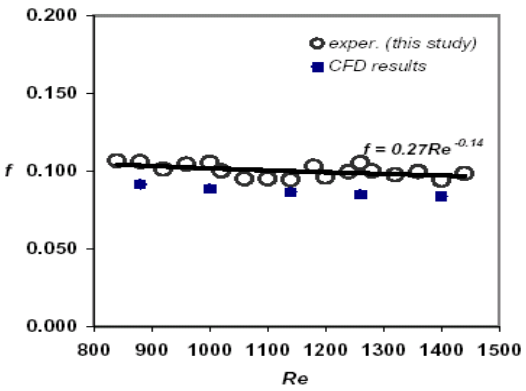

Figure 14. : Comparison of friction factor predictions (CFD) with experimental data

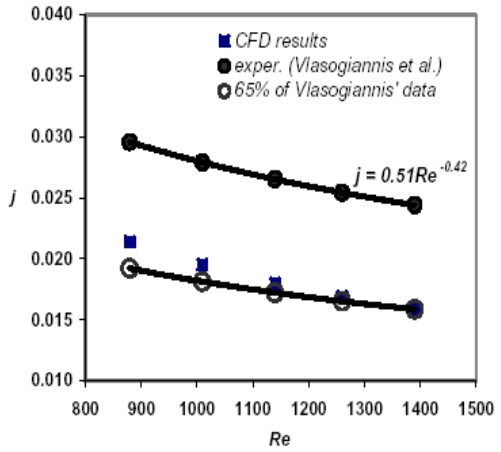

Figure 15 : Comparison of j-Colburn factor predictions (CFD) with experimental data

VI. Study of A Heat Exchanger Channel

The results for the simplified geometry confirm the validity of the CFD code and strongly encourage the simulation of a module (pass) consisting of two corrugated plates of a compact heat exchanger (Figure16a). In order to quantitatively evaluate the results of this simulation, the experimental setup of Vlasogiannis et al.[16] was used as the design model (Figure 16b). Due to the increased computational demands, an AMD AthlonXP 1.7GHz workstation with 1GB RAM was used. The geometric characteristics of the new model are presented in Table 4.

Plate length	0.430 m
Plate width	0.100 m
Mean spacing between plates	0.024 m
Corrugation angle	60°
Corrugation area length	0.352 m

Table 4 Geometric characteristics of the model with two-corrugated plates

Preliminary results of the present study, which is still in progress, are shown in Figure 17. It is obvious that the herringbone design promotes a symmetric flow pattern (Figure 16b). Focusing on the left half of the channel (Figure 17a), a close-up of the flow streamlines (Figure17b) reveals a "*peacock-tail*" pattern as the liquid flows inside the furrows and over the corrugations. The same flow pattern, which is characteristic for this type of geometry, has also been observed by Paras et al.[14] in similar cross-corrugated geometries (Figure17c), where "dry areas" of ellipsoidal shape are formed around the points where the corrugations come into contact. The

effect of fluid properties (e.g. surface tension, viscosity) on the shape and the extent of these areas, which are considered undesirable, will be examined in the course of this study.

(a)

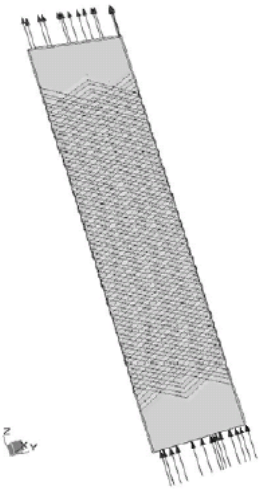

(b)

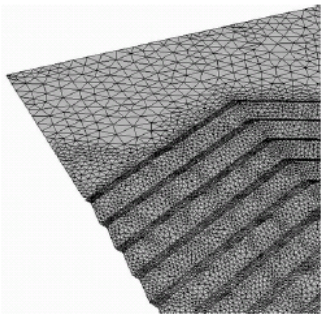

(c)

Figure 17. (a) : Module of a corrugated plate exchanger; (b) The CFD model and (c) Detail of the grid distribution over the corrugated wall.

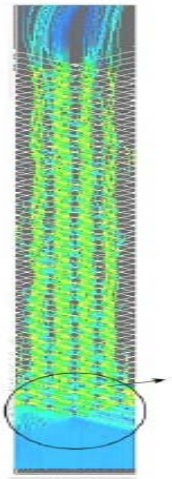

(a)

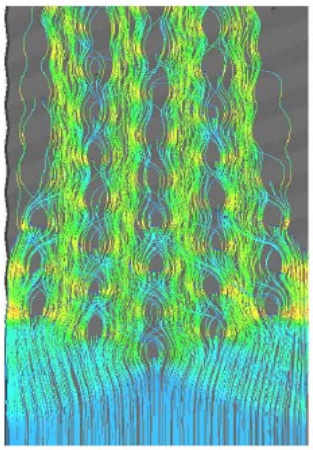

(b)

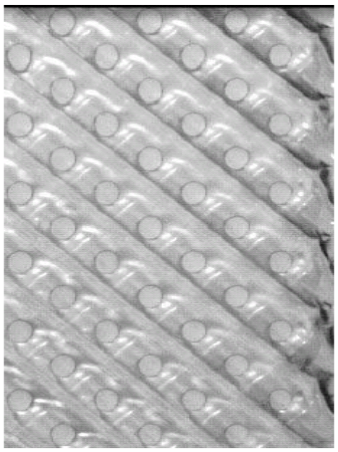

(c)

Figure 18. (a) : Streamlines in the left half of the channel; (b) Close up of the flow pattern; (c) Photo of the flow in the cross-corrugated geometry [14]

VII. Conclusion

An experimental investigation has been conducted to measure the condensation heat transfer coefficient and the pressure drop of R410A and R22 in

BPHEs with chevron angles of 20, 35, and 45 degrees. The experimental data were taken at two different condensation temperatures of 20°C and 30°C in the range of mass flux of 14-34 kg/m^2s with a heat flux of 4.7 -5.3 kW/m^2.

- Both the heat transfer coefficient and the pressure drop increased proportionally with the mass flux and the vapor quality and inversely with the condensation temperature and the chevron angle. Those effects must be carefully considered in the design of a BPHE due their opposing effects.
- A comparison of the data for R410A and R22 showed that the heat transfer coefficient for R410A was about 0 - 10 % larger and the pressure drop about 2- 21 % lower than those for R22. Therefore, R410A is a suitable alternative refrigerant for R22.
- Correlations for the Nusselt number and the friction factor with the geometric parameters were suggested for the tested BPHEs within 20 % (r.m.s. deviation: 10.9 %) for Nu and 15 % (r.m.s. deviation: 10 %) for f.

Although compact heat exchangers with corrugated plates offer many advantages compared to conventional heat exchangers, their main drawback is the absence of a general design method. The variation of their basic geometric details (i.e. aspect ratio, shape and angle of the corrugations) produces various design configurations, but this variety, although it increases the ability of compact heat exchangers to adapt to different applications, renders it very difficult to generate an adequate 'database' covering all possible configurations. Thus, CFD simulation is promising in this respect, as it allows computation for various geometries, and study of the effect of various design configurations on heat transfer and flow characteristics.

In an effort to investigate the complex flow and heat transfer inside this equipment, this work starts by simulating and studying a simplified channel and, after gaining adequate experience, it continues by the CFD simulation of a module of a compact heat exchanger consisting of two corrugated plates. The data acquired from former simulation is consistent with the single corrugated plate results and verifies the importance of corrugations on both flow distribution and heat transfer rate. To compensate for the limited experimental data concerning the flow and heat transfer characteristics, the results are validated by comparing the overall Nusselt numbers calculated for this simple channel to those of a commercial heat exchanger and are found to be in reasonably good agreement. In addition, the results of the simulation of a complete heat exchanger agree with the visual observations in similar geometries.

Since the simulation is computationally intensive, it is necessary to employ a cluster of parallel workstations, in order to use finer grid and more appropriate CFD flow models. The results of this study, apart from enhancing our physical understanding of the flow inside compact heat exchangers, can also contribute to the formulation of design equations that could be appended to commercial process simulators. Additional experimental work is needed to validate and support CFD results, and towards this direction there is work in progress on visualization and measurements of pressure drop, local velocity profiles and heat transfer coefficients in this type of equipment.

References Références Referencias

1. R. Xiaoyang, K. Masahiro and J. G. Burgers. 1995. ASME. 225: 115 (1995).
2. M. Holger. 1996. Chem. Eng. Proc. 35: 301.1996
3. G. J. Lee, J. Lee C. D. Jeon and O. K. Kwon. 1999. In: Proceedings of the 1999 Summer Meeting of the SAREK, edited by C. S. Yim (SAREK, Nov.). p. 144.
4. M. A. Kedzierski. 1997. Heat Trans. Eng. 18: 25.
5. Y. Y. Yan, H. C. Lio and T. F. Lin. 1999. Int. J. Heat and Mass Transfer. 42: 993.
6. Y. Y. Hsieh and T. F. Lin. 2002. Int. J. Heat and Mass Transfer. 45: 1033.
7. Y. S. Kim. 1999. M.S. Thesis. Yonsei University.
8. S. Kakac and H. Liu. 1998. Heat Exchangers Selection, Rating and Thermal Design. CRC Press, Boca Raton. p. 323.
9. R. J. Mo. 1982. ASME J. Fluids Eng. 107: 173.
10. P. Vlasogiannis, G. Karajiannis and P. Argyoropoulos. 2002. Int. J. Multiphase Flow. 28: 757.
11. T. J. Crawford, C. B. Weinberger and J. Weisman. 1985. Int. J. Multiphase Flow. 11: 297.
12. Shah, R.K., Wanniarachchi, A.S. (1991), Plate heat exchanger design theory, In: Buchlin, J.-M. (Ed.),Industrial Heat Exchangers, von Karman Institute Lecture Series 1991-04.
13. Kays, W.M. & London, A.L. (1998), Compact heat exchangers, 3rd Ed. Krieger Publ. Co., Florida.
14. Paras, S.V., Drosos, E.I.P., Karabelas, A.J, Chopard, F. (2001), "Counter-Current Gas/Liquid Flow Through Channels with Corrugated Walls–Visual Observations of Liquid Distribution and Flooding", World Conference on Experimental Heat Transfer, Fluid Mechanics & Thermodynamics, Thessaloniki, September 24-28.
15. Ciofalo, M. Collins, M.W., Stasiek, J.A. (1998), Flow and heat transfer predictions in flow passages of air preheaters: assessment of alternative modeling approaches, In: Computer simulations in compact heat exchangers, Eds. B. Sunden, M.Faghri, Computational Mechanics Publ. U.K.
16. Vlasogiannis, P., Karagiannis, G., Argyropoulos, P., Bontozoglou, V. (2002), "Air–water two-phase flow and heat transfer in a plate heat exchanger", Int. J. Multiphase Flow, 28, 5, pp. 757-772.
17. Lioumbas, I.S., Mouza, A.A., Paras, S.V. (2002), "Local velocities inside the gas phase in counter current two-phase flow in a narrow vertical channel", Chemical Engineering Research & Design, 80, 6, pp. 667-673.

18. Focke, W.W., Knibbe, P.G. (1986), "Flow visualization in parallel-plate ducts with corrugated walls", J.fluid Mech., 165, 73-77.
19. Davidson, L. (2001), An Introduction to Turbulence Models, Department of Thermo and Fluid Dynamics, Chalmers University of Technology, Götemberg, Sweden.
20. Menter, F., Esch, T. (2001), "Elements of Industrial Heat Transfer Predictions", 16th Brazilian Congress of Mechanical Engineering (COBEM), 26-30 Nov. 2001, Uberlandia, Brazil.
21. AEA Technology (2003), CFX Release 5.6 User Guide, CFX International, Harwell, Didcot, UK.
22. Wilcox,D(1988), "Reassessment of the scale-determining equation", AIAA Journal, 26,11.
23. Mehrabian, M.A., Poulter, R. (2000), "Hydrodynamics and thermal characteristics of corrugated channels: computational approach", Applied Mathematical Modeling, 24, pp. 343-364.

Appendix

Nomenclature

A	heat transfer area of plate [m^2]
b	mean channel spacing [m]
C_p	constant pressure specific heat [J/kg K]
D	diameter [m]
f	friction factor
G	mass flux [kg/m^2s]
Ge	non-dimensional geometric parameter
g	gravitational acceleration [m/s^2]
h	heat transfer coefficient [W/m^2K]
i	enthalpy [J/kg]
j	superficial velocity [m/s]
L_c	distance between the end plates [m]
L_h	distance between the ports [m]
L_v	vertical length of the fluid path [m]
L_w	horizontal length of the plates [m]
LMTD	log mean temperature difference [°C]
m	mass flow rate [kg/s]
N_{cp}	number of channels for the refrigerant
N_{data}	total number of data
N_t	total number of plates
Nu	Nusselt number
Nu_{exp}	Nusselt number obtained from experiment
Nu_{pred}	Nusselt number obtained from correlation
p	plate pitch [m]
p_{co}	corrugation pitch [m]
Pr	Prandtl number [v]
Q	heat transfer rate [W]
q	heat flux [W/m^2]
Re	Reynolds number
T	temperature [°C]
t	plate thickness [m]
U	overall heat transfer coefficient [W/m^2 K]
x	Vapour quality

Subscripts

a	acceleration
c	channel
Eq	equivalent
f	liquid
fg	difference the liquid phase and the vapor phase
fr	friction
g	vapour
in	inlet
lat	latent
m	mean
out	outlet
p	port
pre	pre-heater
r	refrigerant
s	static
sat	saturated
sens	sensible
w	water

This page is intentionally left blank

Global Journal of researches in engineering
Mechanical and mechanics engineering
Volume 11 Issue 7 Version 1.0 December 2011
Type: Double Blind Peer Reviewed International Research Journal
Publisher: Global Journals Inc. (USA)
Online ISSN: 2249-4596 Print ISSN:0975-5861

Vibration Study of a Cutting Tool By The Finite Element Method

By M. Rahou, A. Cheikh, F. Sebaa, A. Youcef
Department of genie mechanical Abou bekr Belkaid University, Tlemcen , Algeria.

Abstract - The problem of vibration cutting tools for machining has an important influence on the state of surface and manufacturing tolerances. In this paper, we presented a model of the dynamic behavior of a cutting tool; the goal is to be determined by the finite element method hierarchical trigonometric frequencies own a tool from the kinetic energy and energy deformation. A programme has been developed in FOLTRAN 77 can generate automatically calculate the frequencies.

Keywords : *Vibration, Cutting tool , FEM*

GJRE-A Classification: *FOR Code: 091304*

Strictly as per the compliance and regulations of:

Vibration Study of a Cutting Tool By The Finite Element Method

M. Rahou[α], A. Cheikh[Ω], F. Sebaa[β], A. Youcef[Ψ]

Abstract - The problem of vibration cutting tools for machining has an important influence on the state of surface and manufacturing tolerances. In this paper, we presented a model of the dynamic behavior of a cutting tool; the goal is to be determined by the finite element method hierarchical trigonometric frequencies own a tool from the kinetic energy and energy deformation. A programme has been developed in FOLTRAN 77 can generate automatically calculate the frequencies.

Keywords : Vibration, Cutting tool , FEM

I. Introduction

The phenomenon of the vibration of the cutting tools is a main issue which appears during the process of cut of metals. This problem with an influence very import on the qualitative level such as tolerances of manufacture, surface quality….Several studies were presented. Bourdim et al [1] illustrates an approach of the study of the dynamic stability of the system part-tool in the course of machining .In work of (Arfaoui et al) (Bourdim et al) (Wu D.W., Liu C.R) [2,3,4], the authors present a vibratory modeling of the cutting tool in turning, they showed that the vibratory be havior of the tool depends primarily on the angle of attack, angle strip, advance, depth of cut and the cutting speed . the work of Younes R. [5] a study was carried out on the influence cutting speed on the vibrations of chattering of the tool with an aim of proposing an analytical study by analogy with the model of Vander pole. The work of N. Ouelaa et al [6] presents an experimental semi study of the vibratory behavior of the cutting tool golds of the operation of slide-lathing, fact object of showing that it is possible to consider the roughness average of the part machined starting from displacement resulting from the nozzle of the tool and for the work of Vincent et al [7] a study was presented on the influence of the position of the tool on dynamic behavior in milling of thin walls.

In the last 20 years, the p-version finite element method has generated a lot of interest [8, 9]. The main reason for this interest is the remarkable convergence properties that the method has [10].The p version gets these convergence properties from the fact that it converges to the solution by increasing the order of element shape functions instead of increasing the number of elements as the h - version finite element approach does.

In our work a theoretical study on the vibrations of the cutting tools by the finite element method which makes it possible to choose a good system design starting from the Eigen frequencies.

II. Vibratory Behavior of The Cutting Tool Modeling

In general, we can consider that a structure or an element of structure will be of beam type if one of its dimensions (length) is large in front of the two others. The experiments [11] watch which we can make a known simplifying assumption under the name of assumption of Bernoulli-Euler who expresses himself as follows:

"Any normal plane section with average fiber before deformation remains plane and normal with this average fiber after deformation (effect of null shearing)" [11,13].In our case, we can modelize the cutting tool by a beam Clamped-Free (Figure1).

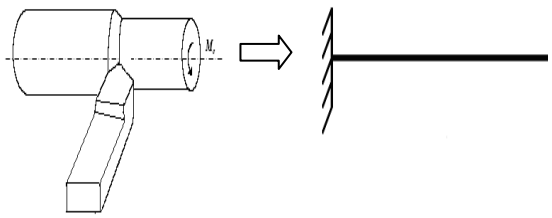

Figure 1 Modeling of the cutting tool

a) Beam element displacement field

The displacement of the point P of the cross-section (Figure2) is given by the system (1):

$$\begin{cases} U(x,y,z) = U_0(x) - y\theta \\ V(x,y,z) = V_0(x) \\ W(x,y,z) = 0 \end{cases} \quad (1)$$

With:

$U_0(x) = U(x,0,0)$: Longitudinal displacement

$V_0(x) = V(x,0,0)$: Transverse displacement

$-y\theta$: Displacement of with the rotation of the cross-section.

There: Position of a point M of the cross-section.

b) Deformation tensor

The components εij of the tensor of deformation are given by the relation (2):

Author [αΩβψ] : Faculty of technology, Department of genie mechanical Abou bekr Belkaid University, Tlemcen , Algeria.
Email[α] : am_rahou@yahoo.fr

$$\varepsilon_{ij} = \frac{1}{2}\left(\frac{\partial U_i}{\partial x_j} + \frac{\partial U_j}{\partial x_i}\right) \qquad i, j = 1,2,3 \qquad (2)$$

For $\varepsilon_{xx}, \varepsilon_{xy}, \varepsilon_{yy}$ we have the matrix (3) following:

$$\varepsilon = \begin{bmatrix} \frac{\partial U_0}{\partial x} - y\frac{\partial \theta}{\partial x} & \frac{1}{2}\left(\frac{\partial V_0}{\partial x} - \theta\right) \\ \frac{1}{2}\left(\frac{\partial V_0}{\partial x} - \theta\right) & 0 \end{bmatrix} \qquad (3)$$

In the form of the tensor, while noting:

- ε_0: it is the generalized relative deformation of the average line.

$$\varepsilon_0 = \frac{\partial U_0}{\partial x} \qquad (4)$$

- γ : it is the shearing strain.

$$\gamma = \frac{\partial V_0}{\partial x} - \theta \qquad (5)$$

- χ : it is the curve of the average line, with ρ $\varepsilon\eta\tau$ radius of the curvature.

$$\chi = \frac{\partial \theta}{\partial x} = \frac{1}{\rho} \qquad (6)$$

c) Shearing assumption

In the majority of the cases, the deflections longitudinal, corresponding has ε_{xx} due to the traction and compression and/or with the bending, are definitely more important than the deformations due to shearing. Noun let us can thus very often neglect the deformations due to shearing γ in the case of the long beams (L/h>20).

Therefore, by supposing γ=0 systematically, the following relation is obtained:

$$\frac{\partial V_0}{\partial x} - \theta = 0 \Longrightarrow \frac{\partial V_0}{\partial x} = \theta \qquad (7)$$

Lead:

$$\varepsilon = \begin{bmatrix} \frac{\partial U_0}{\partial x} - y\frac{\partial^2 V_0}{\partial x^2} & 0 \\ 0 & 0 \end{bmatrix} \qquad (8)$$

d) Stress Deformations Relations

The relation (9) is obtained starting from the generalization of the law of Hooke:

$$\sigma = D.\varepsilon \qquad (9)$$

e) Deformation energy

The deformation energy of the system, equation (10), it is the sum of deformation energies of each element.

$$U_\Sigma = \sum_{e=1}^{n} U_e \qquad (10)$$

The general form of the deformation energy will be given by the relation (11):

$$U_e = \frac{1}{2}\int_V \sigma_{ij} \,.\, \varepsilon_{ij}\, dv \qquad (11)$$

f) Kinetic energy

The kinetic energy of the system, equation (12), it is the kinetic sum of energy of each element:

$$E_\Sigma = \sum_{e=1}^{n} Ec_e \qquad (12)$$

The kinetic energy of an element moving, formula (13), it is the sum of the energy of the beam and the energy of the mass of the Mj engine:

$$Ec_e = Ec_p + Ec_{MJ} \qquad (13)$$

With

EcP : Kinetic energy of the beam, equation (14).

EcMj : Kinetic energy of the concentrated mass equation (15).

$$\begin{aligned} Ec_P = {} & \frac{1}{2}\rho\int_v \dot{h}^T.\dot{h}.dv + \frac{1}{2}\rho\int_v 2.\dot{h}^T\,\Omega.h.dv \\ & + \frac{1}{2}\rho\int_v h^T.\Omega^2.h.dv + \frac{1}{2}\rho\int_v 2\dot{h}^T(A^T\dot{r}_i + \Omega x)\,dv \\ & + \frac{1}{2}\rho\int_v 2h^T\,\Omega^T(A^T\dot{r}_i + \Omega x)\,dv \\ & + \frac{1}{2}\rho\int_v (\dot{r}_i^T\dot{r}_i + 2\dot{r}_i^T A\Omega x + x^T\Omega^T\Omega x)\,dv \end{aligned} \qquad (14)$$

$$\begin{aligned} Ec_{MJ} = {} & \frac{1}{2}\mathrm{M_j}\,[\dot{h}^T\dot{h} + 2.\dot{h}^T\,\Omega.h \\ & + h^T.\Omega^2.h + 2h^T\,\Omega^T(A^T\dot{r}_i + \Omega x) \\ & + 2\dot{h}^T(A^T\dot{r}_i + \Omega x) + (\dot{r}_i^T\dot{r}_i \\ & + 2\dot{r}_i^T A\Omega x + x^T\Omega^T\Omega x)]\,\Big|_{x=l} \end{aligned} \qquad (15)$$

g) Motion equations

The equations of Lagrange make it possible to obtain the equations of the movement of an element of the structure (element beam with mass concentrated at the end) starting from the expression of the kinetic and potential energy elementary, equation (16).

$$L(q_i, \dot{q}_i, t) = Ec - U \qquad (16)$$

III. Formulation by The Finite Element Method Hierarchical

The particular characteristic of the finite element method is that the field, in which an approximate solution is required is divided into under field called finite elements. The unknown quantity, such as displacement is represented in each element by polynomial functions simple. Its functions are called elementary functions of forms.

For a given formulation the choice of the subdivision (mesh) and functions of forms determines the precision of the approximation. The cutting tool is modelized by only one element, called hierarchical finite element, the field of displacement describe the element is given by (17):

$$\begin{Bmatrix} U \\ V \end{Bmatrix} = [N]^e \{q\}^e \qquad (17)$$

With:

$$\{q\}^T = \{X_1 \ldots X_p, Y_1 \ldots Y_p\}^T. \qquad n=1,\ldots,P$$

P: Many functions of form.

$$[N]^e = \begin{bmatrix} [N_u] & 0 \\ 0 & [N_v] \end{bmatrix}$$

Such as:

$$[N_u] = [f_1(\xi), f_2(\xi) \ldots f_P(\xi)]$$
$$[N_v] = [g_1(\xi), g_2(\xi) \ldots g_P(\xi)]$$

The components of the vector {E} necessary to the determination of rigidity are given in the system of coordinates Cartesian, relation (18).

$$\{e\} = [A]^e \begin{Bmatrix} U \\ V \end{Bmatrix} \qquad (18)$$

With:

$$[A]^e = \begin{bmatrix} \frac{1}{L}\frac{\partial}{\partial \xi} & \frac{-y}{L^2}\frac{\partial}{\partial \xi^2} \end{bmatrix}$$

The vector of deformation {E} is given according to {Q} in the matrix form (19) following:

$$\{e\} = [A]^e [N]^e \{q\}$$
$$\{e\} = [B]^e \{q\} \qquad (19)$$

With:

$$[B]^e = [A]^e [N]^e$$

a) Energy in the matrix form

The kinetic energy and of elementary deformation in the matrix form is given by the relation (20):

$$Ec_p = \frac{1}{2}\rho S L \int_0^1 \left\{\dot{q}\right\}^T [N]^T [N] \left\{\dot{q}\right\} d\xi + \frac{1}{2}\rho S L 2 \int_0^1 \left\{\dot{q}\right\}^T [N]^T \Omega [N] \{q\} d\xi + \frac{1}{2}\rho S L \Omega^2 \int_0^1 \{q\}^T [N]^T [N] \{q\} d\xi + \frac{1}{2}\rho S L 2 \int_0^1 \{q\}^T [N]^T \Omega^T (A^T \dot{r}_i + \Omega x) d\xi + \frac{1}{2}\rho S L 2 \int_0^1 \left\{\dot{q}\right\}^T [N]^T (A^T \dot{r}_i + \Omega x) d\xi + \frac{1}{2}\rho S L \int_0^1 (\dot{r}_i^T \dot{r}_i + 2\dot{r}_i^T A \Omega x + x^T \Omega^T \Omega x) d\xi \qquad (20)$$

The kinetic energy of the mass is given in the matrix form by the relation (21):

$$\begin{aligned} Ec_{MJ} = {} & \tfrac{1}{2} M_j \Big(\left\{\dot{q}\right\}^T [N]^T [N] \left\{\dot{q}\right\} \\ & + 2 \left\{\dot{q}\right\}^T [N]^T \Omega [N] \{q\} \\ & + \{q\}^T [N]^T \Omega^T \Omega [N] \{q\} \\ & + 2 \left\{\dot{q}\right\}^T [N]^T \Omega l + 2 \left\{\dot{q}\right\}^T [N]^T A^T \dot{r}_i \\ & + 2 \{q\}^T [N]^T \Omega^T \Omega l \\ & + \dot{r}^T \dot{r} + 2 \{q\}^T [N]^T \Omega^T A^T \dot{r}_i \Big) \end{aligned} \qquad (21)$$

The relation (22) presents the deformation energy in the matrix form.

$$U_e = \frac{1}{2}\frac{ES}{L}\int_0^1 \{q\}^T \left[N_{u,\xi}\right]^T \left[N_{u,\xi}\right] \{q\} \, d\xi + \frac{1}{2}\frac{EI}{L^3}\int_0^1 \{q\}^T \left[N_{v,\xi\xi}\right]^T \left[N_{v,\xi\xi}\right] \{q\} \, d\xi \qquad (22)$$

The equations of Lagrange are written in the matrix form, equation (23).

$$[M]^e \left\{\ddot{q}\right\} + [G]^e \left\{\dot{q}\right\} + \left([K]^e + [R]^e + [P]^e\right)\{q\} = \{r\} + \{F_{ext}\} \qquad (23)$$

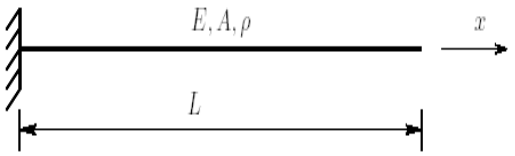

Figure 2: Cleanliness of the Clamped-Free beam

The matrix of rigidity is given by (24):

$$[K]^e = E\int_V [Be]^T [Be] dV \qquad (24)$$

The centrifugal matrix of rigidification is given par.

$$[R]_P = \rho \omega_3^2 \, S L \int_0^1 [N]^T [N] d\xi \qquad (25)$$

$$[R]_{MJ} = M_j \, \omega_3^2 \, [N(1)]^T [N(1)] \qquad (26)$$

The matrix of rigidification of angular acceleration [P] is given by:

$$[P]^e = [P]_P + [P]_{MJ} \quad (27)$$

$$[P]_P = \rho S L \int_0^1 [N]^T \dot{\Omega} [N] d\xi \quad (28)$$

$$[P]_{MJ} = M_j [N(1)]^T \dot{\Omega} [N(1)]^T \quad (29)$$

According to the kinetic energy the matrix mass is given by

$$[M] = [M]_P + [M]_{MJ} \quad (30)$$

By identification.

$$[M]_P = \rho S L \int_0^1 [N]^T [N] d\xi \quad (31)$$

$$[M]_{MJ} = M_j [N(1)]^T [N(1)] \quad (32)$$

According to the kinetic energy, the gyroscopic matrix is given by:

$$[G] = [G]_p + [G]_{MJ} \quad (33)$$

$$[G]_p = 2 \rho S L \int_0^1 [N]^T \Omega [N] d\xi \quad (34)$$

$$[G]_{MJ} = 2 M_j [N(1)]^T \Omega [N(1)] \quad (35)$$

b) Numerical example

The FORTRAN program in 77 allowing determining the dynamic characteristics of the structure beam (cutting tool) The first four pulsations are given in the following tables for various cases of boundary conditions. The resulting ones calculated are compared with the reference (M Geradin ,D Rixen), which is illustrated in table 1 in the case of a beam in rest or. The parameter of frequency and other parameters used for the validation of the model are given by

$$\omega^* = \sqrt{\frac{\rho A L^4}{E I_z}}\,\omega \quad , \quad \alpha = \sqrt{\frac{A L^2}{I_z}}$$

$$\Omega = \sqrt{\frac{\rho A L^4}{E I_z}}\,\omega_3$$

or ω^* , α and Ω are respectively the parameter of frequency, parameter speed and the parameter defining the type of beam used (Bernoulli or Timoshenko type).

- *Clamped-Free Beam:*

Table 1 illustrates the pulsation values for the solution of the hierarchical finite element method as well as the values of the exact solution, for a Clamped-Free beam

Table 1: Comparison of the values of pulsations for a beam (C-F):

Modes	Solution HFEM	Exact solution	% error
1	3.5160	3.1560	0,114
2	22.0348	22.0344	0,181E-04
3	61.7036	61.6972	0,103 E-03
4	120.9762	120.9019	0,614E-03

With:

$$\% = \frac{HFEM - EXACT.S}{EXACT.S}$$

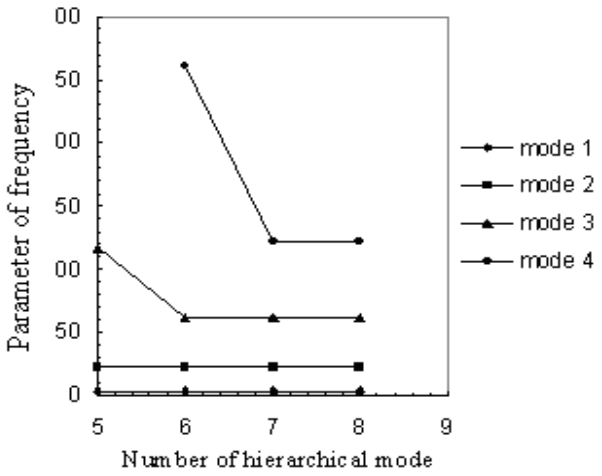

Figure 3 : Chart of the convergence of the pulsation values w * according to NHM in the case of beam (C-F).

In the graph, represented by Figure 3, in the case of give the variation of the first three parameters of frequency according to the number of hierarchical modes NMH a clamped-free beam (C-F), we notice that convergence is ensured starting from a number of modes equal to 8.

C. Influence speed Ω on the values of the pulsations $*\omega$:

The variation of the parameters of pulsation $*\omega$ of the first four modes for variations rotational speeds Ω are given by table 2.

Table 2 : Variation of the values of pulsations w* according to rotational speed Ω .

Ω	ω_1^*	ω_2^*	ω_3^*	ω_4^*
0	3,51601	22,0348	61,7036	109,958
0,1	3,51743	22,0350	61,7037	109,958
0,2	3,52167	22,0357	61,7039	109,959
0,3	3,52874	22,0368	61,7043	109,960
0,4	3,53860	22,0383	61,7048	109,962
1	3,65489	22,0568	61,7112	109,981
1,1	3,68338	22,0615	61,7128	109,986
1,2	3,71433	22,0665	61,7145	109,991
1,3	3,74767	22,0721	61,7164	109,996
1,4	3,78335	22,0780	61,7185	110,003
2	4,04256	22,1229	61,7339	110,049
2,1	4,09263	22,1319	61,7370	110,058
2,2	4,14445	22,1414	61,7402	110,068
2,3	4,19806	22,1512	61,7436	110,078
3	4,61556	22,2325	61,7717	110,162
3,1	4,68056	22,2458	61,7763	110,176
3,2	4,74673	22,2596	61,7811	110,190
3,3	4,81402	22,2738	61,7860	110,205
4	5,31259	22,3850	61,8246	110,320
5	6,08914	22,5793	61,8925	110,523
10	10,44095	24,1317	62,4549	112,208

Figure 4 presents the variation of the parameter of frequency according to the rotational speed for a variation from 0 to 110, we notice that the second, third and the fourth mode vary linearly for the values of Ω superior to 20, whereas the first mode varies almost exponentially.

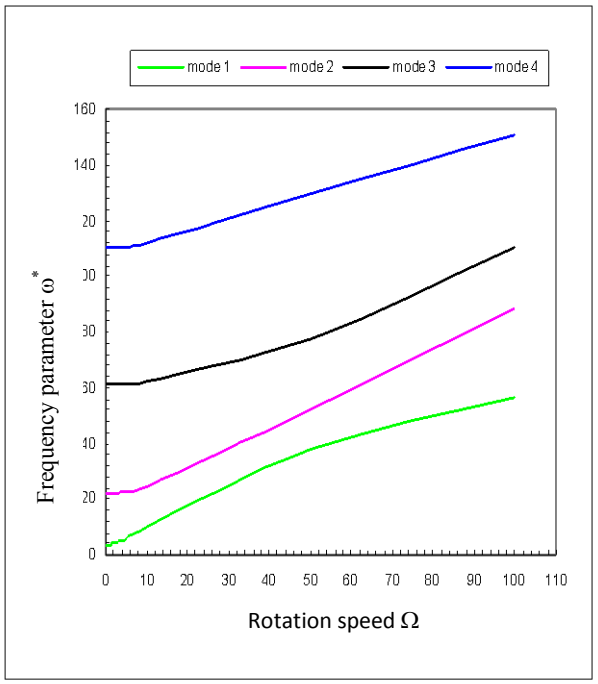

Figure 4 : Chart of the influence speed Ω on the parameter of frequencies ω* in the band [θ110]

IV. Conclusion

In this work, a modeling of the cutting tool by the hierarchical finite element method was the object to determine the Eigen frequencies. The latter has an important influence on the tolerances of manufacture and the surface quality. The found results ensure convergence in the stationary case (rest) and moving, the compared errors are almost the same ones with [13] In all the cases, the Eigen frequencies vary almost linearly in the beach of [0,10] and increases with the increase rotational speed. These frequencies enabled us to pose a good design of system of assembly of the cutting tool .

References Références Referencias

1. Bourdim A., Salhi A., Kebdani S., « Approche à l'étude de la stabilité dynamique de coupe », Premier congrès de mécanique, ENIM, Rabat, Avril 1993.
2. Arfaoui A., Fedotov A.I., Chouchane M., « Modélisation des vibrations de l'outil de coupe en tournage », Premier congrès de mécanique, ENIM, Rabat, pp 331-342, Av.93.
3. Bourdim A., Rahmani O., Boutchicha D., « Simulation numérique du phénomène de broutage », Premier congrès de mécanique ENIM, Rabat, pp 22-27,Avril 1993.
4. Wu D.W., Liu C.R. «An analytical model of cutting dynamics. Part1» Model Building",ASME, Journal of engineering for industry, vol 107, pp107- 111,1985.
5. Younes R. "Simulation du broutement sur les machines-outils", Séminaire international de genie mécanique", SIGMA'02, du 28-29 avril 2002, ENSET, Oran, p. 394-403.

6. N. Ouelaa, N. Kribes, A. Rezaiguia, M.A. Yallese« Etude semi-expérimentale du comportement vibratoire de l'outil de coupe lors de l'opération de chariotage », CPI2003, Conception et Production Intégrées ,Maroc.
7. Vincent thevenot lionel arand gille dessein gille cazenave larroche « l'influence de la position de l'outil sur le comportement dynamique en fraisage de parois minces », Mécanique & Industries 6, 403-410 (2005).
8. Babu_ska I, Szab_o B. "On the rates of convergence of the finite element method". Int J Num Meth in Engng 1982;
9. Szab_o B, Babu_ska I. "Finite element analysis". New York: Wiley; 1992.
10. Babu_ska I, Suri M. "The p and h-p version of the finite element method, basic principles and properties". SIAM Rev 1994
11. Youcef A, « vibration libre d'un bras manipulateu » CIP2005, Novembre 2005, Temcen ,Algerie.
12. Kribes N. Etude semi -expérimentale du comportement vibratoire de l'outil de coupe lors de l'opération de chariotage". Thèse de magister, Université de Guelma. Juin 2003.
13. M Geradin -D Rixen , Théorie des vibrations , Paris, Masson, 2002.

Global Journal of researches in engineering
Mechanical and mechanics engineering
Volume 11 Issue 7 Version 1.0 December 2011
Type: Double Blind Peer Reviewed International Research Journal
Publisher: Global Journals Inc. (USA)
Online ISSN: 2249-4596 Print ISSN:0975-5861

Economic Analysis Of The Wind Energy Generated In Cuba, Considering The Turbines Tested In The Country.

By Deivis Avila Prats, Ramón Alesanco García, Juan Veliz Alonso
University of La Laguna.

Abstract - In this study, the results of the analysis carried out about wind energy potentials in the western provinces of Cuba are shown. Wind characteristics were analyzed using the wind speed data collected from four meteorological stations, selecting for this study, the station with the maximum annual mean wind speed. A technical assessment has been made of electricity generation from three wind turbines having a capacity of (275 kW, 750 kW, and 850 kW), respectively. The yearly energy output for three different turbines was calculated, with the wind data of the meteorological station selected. The production cost of the kWh of wind energy generated with the different machines and the economical variables, such as the payback (PBA) and the net present value (NPV), have been determined for each one, taking for this economic analysis two different costs for kW of wind energy installed: national and international average. The conclusions show that, the production costs of the kWh of wind energy generated in this country is expensive, due to its high generation price, since they are conditioned by high installation costs and the use of turbines with low power of generation.

Keywords : *Wind energy; Weibull distribution; Production cost; Payback; Net present value (NPV).*

GJRE-A Classification : *FOR Code: 091305*

Strictly as per the compliance and regulations of:

Economic Analysis Of The Wind Energy Generated In Cuba, Considering The Turbines Tested In The Country.

Deivis Avila Prats[α], Ramón Alesanco García[Ω], Juan Veliz Alonso[β].

Abstract - In this study, the results of the analysis carried out about wind energy potentials in the western provinces of Cuba are shown. Wind characteristics were analyzed using the wind speed data collected from four meteorological stations, selecting for this study, the station with the maximum annual mean wind speed. A technical assessment has been made of electricity generation from three wind turbines having a capacity of (275 kW, 750 kW, and 850 kW), respectively. The yearly energy output for three different turbines was calculated, with the wind data of the meteorological station selected. The production cost of the kWh of wind energy generated with the different machines and the economical variables, such as the payback (PBA) and the net present value (NPV), have been determined for each one, taking for this economic analysis two different costs for kW of wind energy installed: national and international average. The conclusions show that, the production costs of the kWh of wind energy generated in this country is expensive, due to its high generation price, since they are conditioned by high installation costs and the use of turbines with low power of generation.

Keywords : Wind energy; Weibull distribution; Production cost; Payback; Net present value (NPV).

I. Introduction

The electric production coming from the wind has had a significant growth at worldwide level, being wind energy, one of the biggest dynamic growths of all energy in the last years (WWEA, 2011).

Currently, Latin America is one of the regions of smaller development in this field, with only 1078 MW of wind energy installed until the year 2009 (LAWEA, 2010). Cuba is one of the many countries in this area that does not have large reserves of petroleum or natural gas, which poses a serious problem for the country, because the largest percent of the electricity is obtained from power plants, being only the 2% of the total energy produced by renewable energy sources (UNE, 2008). For this reason, the Cuban government considers wind energy the best choice from amongst the renewable energies, taking into account that it is one of the most abundant renewable energy resources of the national territory. The most significant results obtained in this field are the following:

- Inauguration of the first wind farm of Cuba, in the Turiguanó Island in 1999, with two wind turbines of 225 kW (Leiva, 1999).
- Creation of the National Wind Energy Group (GEN) in 2005, with the objective of settling down and to implement all necessary actions for the application of the wind energy in Cuba (GEN, 2007).
- Culmination of the Wind Potential Map of Cuba in 2006. The possible wind energy capacity in the territory of Cuba, could reach up to 3500 MW (Soltura and Roque, 2007).
- Inauguration of the experimental wind farm "Los Canarreos" (February 2007), with six folding wind generators of 275 kW, with an installed power equivalent to 1.65 MW (GEN, 2007).
- Culmination of the third wind farm "Gibara I" in 2008, with a power of 5.1 MW, having six wind turbines of 850 kW (Anon, 2008).
- Installation of small wind generators isolated from the National Electric System (SEN), with a total of 30 kW (Anon, 2008).
- Culmination and inauguration of the wind farm "Gibara II" in 2010, which have six turbines of 750 kW and a total power of 4.5 MW (Reve, 2010).

The potential sites of wind energy generation of Cuba have not been completely investigated in detail yet. The goal of this study is to carry out an economic analysis of the production costs of the wind energy by kWh generated in Cuba, analyzing the wind data of the meteorological stations in the western region of the country, the annual electric power generated by turbines of 275, 750 and 850 kW, and different investment costs by installed kW of wind power.

II. Methodology and Materials

a) Recoverable wind energy

Knowledge of wind speed frequency distribution is a very important factor to evaluate wind potential in windy areas. Wind data obtained with various observation methods has the widest ranges. Therefore, in wind energy analysis, it is necessary to have only a few key parameters that can explain the behaviour of a wide range of wind speed data. The simplest and most practical method for the procedure is to use a probability distribution function. The Weibull distribution

Author [αΩβ] : Engineering Department; Nautical Technical School; University of La Laguna. C/ Padrón Albornoz s/n, P.O. Box 38001, S/C Tenerife, Spain. E-mail : deivisavila@yahoo.es, ralesanco@gmail.com, veliz24@yahoo.es

is the most commonly used statistical distribution for describing wind speed data.

As indicated by Burton, et al. (2001), the Weibull distribution function which is a two-parameter distribution is a special case of generalized gamma distribution for wind speed and is expressed as:

$$f(v)=\frac{k}{c}\cdot\left(\frac{v}{c}\right)^{k-1}\cdot e^{-\left(\frac{v}{c}\right)^{k}} \quad (1)$$

Where, k is the shape factor, c is the scalar factor, and v is the wind speed.

In order to estimate Weibull k and c parameters, numerous methods have been proposed over the last few years. In this study, the two parameters of Weibull are determined by using mean wind speed–standard deviation method (Ucar and Balo, 2008).

The speed at any height can be calculated using the hypothesis of a neuter atmosphere and is given by the expression (Ucar and Balo, 2008; Fawzi, 2009):

$$\frac{v_1}{v_2}=\left(\frac{z_1}{z_2}\right)^{\alpha} \quad (2)$$

Where, v_1 is the actual wind speed measured at a height of z_1; v_2 the wind speed at the required or extrapolated height z_2. The exponent α depends on the surface roughness (z_o).

Another important aspect is to predict the distribution of speeds for any height (z), according to the principle of Weibull distribution, consists of being able to determine the parameters k and c for this height, starting from the knowledge of the parameters of another height, the empiric expression is expressed as follows (Villarrubia, 2004):

$$k_2=k_1\cdot\left[\frac{1-0.088\cdot\ln\left(\frac{z_1}{10}\right)}{1-0.088\cdot\ln\left(\frac{z_2}{10}\right)}\right] \quad (3)$$

$$c_2=c_1\cdot\left(\frac{z_2}{z_1}\right)^{\beta} \quad (4)$$

Where the coefficient β can be expressed as

$$\beta=\frac{0.37-0.088\cdot\ln c_1}{1-0.088\cdot\ln\left(\frac{z_1}{10}\right)} \quad (5)$$

k_1, k_2 are the shape parameters and c_1, c_2 are the scale factor, for the height z_1 y z_2 respectively.

As displayed by Eskin, et al. (2008) and Hau (2006), it is well known that the power of the wind (P_w) that flows at mean wind speed (v_m) through a blade sweep area (A) increases as the cubic of its velocity and is given by using the following equation:

$$P_w=\frac{1}{2}\rho\cdot A\cdot {v_m}^3 \quad (6)$$

Where ρ is mean air density, ${v_m}^3$ is mean value of the third power of the wind speed and A is sweep area.

The average wind power density ($P_{d,w}$) or energy output, based on Weibull probability density function can be expressed as follows:

$$P_{d,w}=\frac{1}{2}T\cdot\rho\cdot C_p\cdot A\cdot\sum_{x=1}^{J}f_{(v)}\cdot {v_x}^3 \quad (7)$$

Where C_p is the capacity factor of the wind generator, T is the time analyzed (one year), v is the wind speed, and J is the class number of the data.

b) Economic evaluation

In spite of the fact that wind energy has one of the biggest dynamic growths of all energy per year, it only represents a small portion of the whole energy that is produced at world level. This is given mainly by their high production costs per kW, which makes the projects unfeasible in much of the cases. A deep economic analysis of all the proposals will be necessary. In order to do so, it can use for them many different criteria as: Unitary cost of electricity production (c_u), Payback (PBA) and Net present value (NPV).

i. *Unitary cost of electricity production*

In an economic study of wind energy systems it is necessary to know the unitary cost of electricity production, as well as their profitability for payment of the generated kWh.

It is possible to determine the unitary production cost of electricity generated with the wind (c_u), updating all costs of the project along their useful life and to add them to the initial investment of the year zero. The quotient among the resulting quantity in constant monetary units of the zero year and the total electric power that will produce the project, allows a reasonable estimate of the unitary cost of production (\$/kWh) (Villarrubia, 2004). In this way, the unitary cost of electricity production (c_u) will be determined according to the formula:

$$c_u=\frac{I-V_R\cdot(1+r)^{-n}+\sum_{j=1}^{n}(OM_j+F_j)\cdot(1+r)^{-j}}{\sum_{j=1}^{n}P_{d,w}} \quad (8)$$

The variables of the expression are:

c_u : unitary production cost of electricity (\$/kWh) in constant monetary units (year 0).

n : lifetime of the system (year).

I : capital cost of the installed wind power system, in the 0 year ($).
$\boldsymbol{V_R}$ **:** residual value of the installation at the end of their useful life ($).
$\boldsymbol{OM_j}$**:** operation and maintenance costs in the j year ($).
$\boldsymbol{F_j}$ **:** financing cost of the j year ($).
$\boldsymbol{P_{d,w}}$ **:** energy output in the year j (kWh/year).
r : market discount rate (includes the inflation effects).

ii. *Payback (PBA) and Net present value (NPV)*

Wind turbine projects are generally characterized by high initial investment and low operating costs. Thus the basic economic problem is one of comparing an initial known investment with estimated future operating savings. Several economic criteria have been proposed for evaluating and optimizing systems, and there is no universal agreement on which should be used (Tsoutsos, et al., 2003). For the needs of the current study, the two following criteria are used:

- payback period (PBA)
- net present value (NPV)

The payback (PBA) is a financial balance inside the horizon of the project (years). It is possible to obtain it through the expression

$$PBA = \frac{\log\left[\frac{I}{E_j}\cdot\frac{i}{100}+1\right]}{\log\left[1+\frac{i}{100}\right]} \qquad (9)$$

Where I: capital cost of the installed wind power system ($); i: energy inflation (the change of energy prices relative to general inflation), E_j: energy saving ($/yr).

The net present value (NPV) in dollars ($) units, is a sequence of cash flows take as input the cash flows and a discount rate or discount curve and outputs a price.

$$NPV = Y\frac{1}{r-i}\left[1-\frac{1+i}{1+r}\right]^n - I \qquad (10)$$

Where Y: yearly benefits ($/yr), r: market discount rate, i: energy inflation, n: lifetime (yr), I: capital cost of the installed wind power system ($).
The yearly benefits (Y) represent an expression of the annual costs for any system, wind power or non-wind power systems to meet energy needs.

Economic assumptions

The basic assumptions made during the economic evaluation are:

- cost by kW of wind energy installed equal to 1000 $/kW or 1400 $/kW
- operation and maintenance costs (OM_j): 3% of the capital cost.
- lifetime of the system (n): 20 yr.
- market discount rate (r): 7 %
- energy inflation (i): 3%
- residual value of the installation at the end of their useful life (V_R): not considered.
- financing cost:5%

The determination of the capital cost, or total investment, generally involves the cost of the wind turbines and the cost of the remaining installation (Manwel and Rogers, 2009). In relation to the criteria used in this study, the average value cost per kW of wind energy installed in Cuba (1400 $/kW) (Leiva, 1999; UNE, 2008; INEL Project, 2009) and the average cost in the world (1000 $/kW) (Villarrubia, 2004) are used.

The operation cost can include a cost of insurance of the wind turbine, taxes, and the land rental cost, while the maintenance cost can include the following typical components: routine checks, periodic maintenance, periodic testing, blade cleaning, electrical equipment maintenance, and unscheduled maintenance cost (Manwel and Rogers, 2009).

c) Acquisition of wind speed data.

In the study, wind speed data are obtained from four of the meteorological stations placed by the Institute of Meteorology of Cuba (INSMET), for the estimate of the wind energy resource under different physical-geographical conditions of the Cuban archipelago (Roque, et al., 2009). The meteorological stations are located in the western region of Cuba; the more industrialized and inhabited regions of the country.

Table 1 shows the geographical coordinates of the meteorological station and the height level over floor (HLF) of the four stations used in the study. Fig. 1 samples the geographical localization of the studied meteorological stations and the wind farms of the island.

Table 1 : Geographical coordinates of the meteorological stations used in the study (Source: Roque, et al., 2009).

Stations	**Longitude** (deg)	**Latitude** (deg)	**(HLF)** [(1)] (m)
Guanito TV	83° 46' 54"	22° 27' 08"	75
S/C del Norte	81° 55' 58"	23° 09' 00"	60
Jagüey	81° 05´44"	22° 33´39´´	50
El Brinco	81° 03'14"	22° 04' 18"	50

(1) (HLF) - height level over floor (m)

Table 2 shows some parameters of the meteorological stations mentioned before, as power of wind per unit area (P_u), parameters k, c of the Weibull distribution and the mean wind speed (v_m).

Fig. 1 : Distribution of the meteorological stations used in the study. Localization of the wind farms of Cuba.

Table 2 : Wind data of the stations used in the study. (Source: Roque, et al., 2009).

Stations	Weibull parameters *k, c*	Mean wind speed. v_m (m/s)	Power of wind (P_u) (W/m^2)
Guanito TV	*k* =2.55 *c*=6.4	5.7	175
S/C de l Norte	*k* =2.29 *c* =7.4	6.6	292
Jagüey	*k* =2.81 *c*=5.8	5.2	124
El Brinco	*k* =2.63 *c*=6.7	6.0	197

III. Results and Discussion

a) Selection of the optimum location

To compare the wind energy potentials of the different meteorological stations that appear in Table 2, can introduce errors in the analysis, because measurement of wind speed has been carried out at different heights over the floor level. Given these circumstances, the parameters of wind speed of all stations are extrapolated to a height of 55 meters over the floor level (HLF), predetermined study height. The obtained values are shown in Table 3.

Table 3 : Wind data of the stations used in the study, 55 meters high over the floor level.

Stations	Weibull parameters *k, c*	Mean wind speed v_m (m/s)	Power of wind (P_u) (W/m^2)
Guanito TV	*k*=2.47 *c*=5.92	5.46	141
S/C de l Norte	*k* =2.27 *c*=7.25	6.5	276
Jagüey	*k*=2.84 *c* = 5.94	5.27	132
El Brinco	*k*=2.66 *c* =6.85	6.1	209

The obtained results show that the power exerted by the wind per square meter in the four stations to a height of 55 meters over the floor level, is between 132 and 276 W/m^2, being Santa Cruz del Norte, in Havana, the station with the biggest potentials. Fig. 2 samples the probability of Weibull distribution of wind speeds analyzed in the period of one year in the four meteorological stations studied at this height.

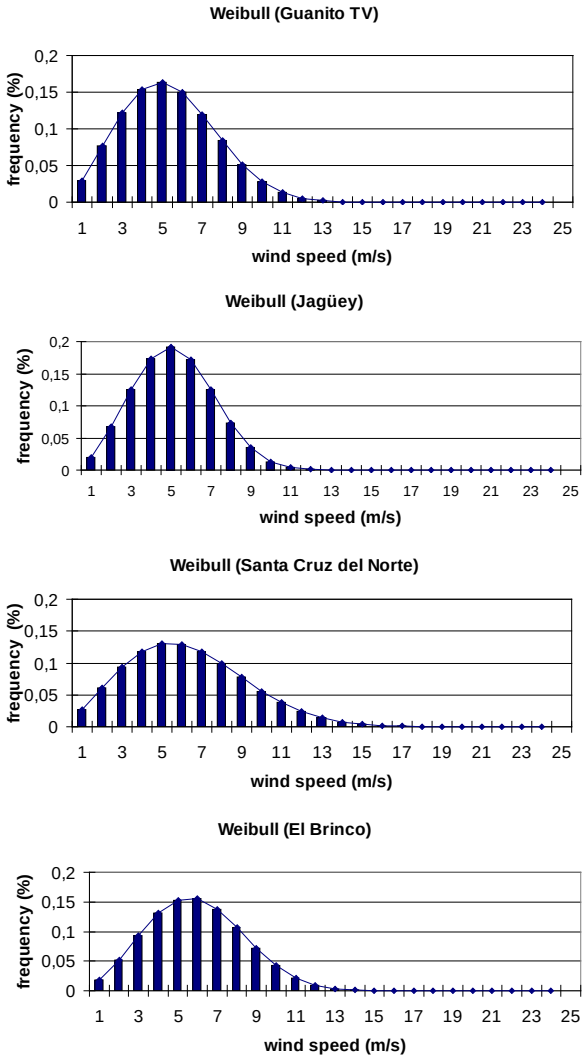

Fig. 2 : Weibull distribution of the analyzed wind speeds, in the meteorological stations studied at a height of 55 meters over floor level.

Known the wind energy potentials of the different meteorological stations analyzed, Santa Cruz del Norte is selected as the best candidate for the study, for its wind potentials, as well as for its climatic and infrastructure conditions.

The area where the meteorological station is located one characterized by mountainous elevations, with a very low occurrence probability of severe meteorological events (hurricanes, tornados and storms, etc) (Limia and Pérez, 1999) and located near ports, electricity transmission grids, industrial centres and good roads.

b) Production of energy by wind turbines

The characteristics of the selected wind turbines are shown in Table 4. The selection of the different machines is based on the wind turbine technologies used in the different wind farms (Los Canarreos, Gibara I, Gibara II) in Cuba. The power curves of turbines with different rated power are shown in Fig. 3. The rated powers of these turbines were 275 kW, 750 kW and 850 kW, respectively. The annual electric power and the annual equivalent hours obtained in the modelling of the wind speeds in the meteorological station of Santa Cruz del Norte, is shown in Table 5.

Table 4 : Main characteristics of three different wind turbines.

Characteristics	GEV-MP275	G52-850	S50/750
Rated P ower (kW)	275	850	750
Hub height (m)	55	55	55
Diameter (m)	32	52	48.4
Sept area (m^2)	805	2 124	1 840
Cut-in wind speed (m/s)	4	4	4
Cut-off w ind speed (m/s)	20	25	25

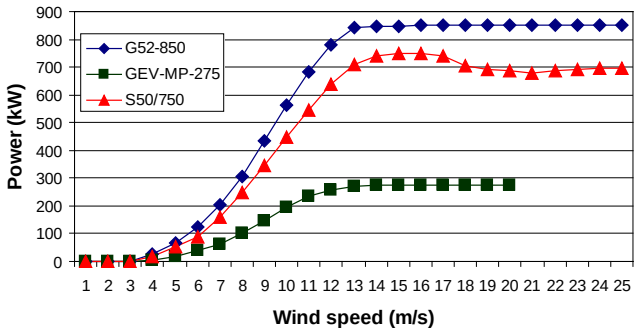

Fig. 3 : Power curves of the selected wind turbines.

Table 5 : Energy generated by the wind in one year.

Turbines.	Rated Power (kW)	Annual power (kW h/ yr)	Annual equivalent hours (h/ yr)
GEV-MP275	275	644 803	2 345
G52-850	850	1 976 090	2 325
S48/750	750	1 574 448	2 100

The annual energy output of the different wind turbines changes due to the capacity of each one. In the case of wind turbines with a capacity of 275 kW the annual energy output is 644 803 kW h/year, with 2 345 equivalent hours. The annual energy generated by a wind turbine of 750 kW is 1574448 kW h/year and 2 100 equivalent hours. The wind turbine of 850 kW is the maximum producer, with 1976090 kW h/year and 2 325 equivalent hours.

c) The wind farms

Currently wind farms are the more viable options for the reception of wind energy and, from the technical point of view, as economic. This is due to the fact that the connection of a group of wind turbines, reduces maintenance expenses, simplifies the requirements for interconnection and compensates the interruptions caused by local fluctuations in the speed of the wind.

Taking as reference the proposition of the Cuban Electric Union (UNE) to develop 10 MW from wind energy power in the western region of Cuba (UNE, 2008), the number of the necessary wind generators to cover this power with a wind farm have been calculated, always in excess, as it is shown in Table 6 .

Table 6 : Number of wind generators by wind farms.

Variants	Turbine	Rated Power (kW)	Nº of turbines	Wind farm Power(MW)
1	GEV-MP275	275	37	10.175
2	G52-850	850	12	10.2
3	S50/750	750	14	10.5

The number of wind turbines by wind farms goes from 37 machines necessary to produce 10.175 MW, with turbines of 275 kW, up to 14 machines of 750 kW necessary to produce 10.5 MW and the 12 of 850 kW required to generate 10.2 MW.

With the obtained wind farm proposals an economic analysis will be developed with the aim of determining the production cost of the kW of wind energy that is supposedly generated in each one. Other criteria (payback, net present value) will be used too to determine the viability of the projects.

d) Economic analysis

The economic analysis of the different wind farm propositions with different wind turbines models will be carried out following these two investments:

1. Cost per kW of wind energy installed equal to 1400 $/kW (average value for kW of wind energy installed in Cuba, it can be bigger in some cases) (Leiva, 1999; UNE, 2008; INEL Project, 2009).
2. Cost per kW of wind energy installed equal to 1000 $/kW (average value for kW of wind energy installed in the world) (Villarrubia, 2004).

i. *First investment*

The economic variables that appear in Table 7 have been obtained establishing a cost per kW of wind energy installed equal to 1400 dollars. The reckoning is carried out from an initial investment in the wind farm, to which are added the costs in which the project incurs in the analyzed period (20 years). In this way the cost of production of the wind energy kW for the different proposals is obtained.

The values of production costs per kW of energy generated in the wind farms (different wind turbines models) are between 5.8 and 6.34 c$/kW. It is assumed as a possible price to pay for the generated electricity a value equal to 7 c$/kW.

It is calculated the payback (PBA) and the net present value (NPV) in this first investment proposition of all turbines. The economic curves for the three turbines with different rated power are shown in Fig. 4.

Table 7 : Production cost of the kW of wind energy (with a cost per kW of wind energy installed equal to 1400 dollars).

Variable	Wind farm with GEV-MP275	Wind farm with G52-850	Wind farm with S48/750
Initial investment ($)	14 245 000	14 280 000	14 700 000
Production cost (c$/kW)	6.34	5.8	6.3

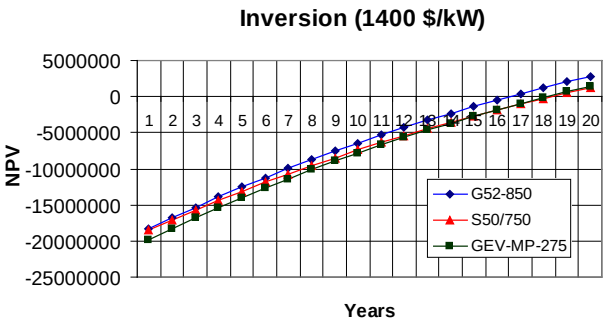

Fig. 4 : Net present value (NPV) with a cost by kW of wind energy installed equal to 1400 $/kW.

The first wind farm that begins to recover the investment is the one calculated with the machines of 850 kW, which begins to the 16 years and seven months, with a net present value of 2 814 985 dollars. The wind farm with the wind turbines of 275 kW begins to recover the investment to the 18 years and two months with NPV of 1 480 030 dollars. The last one in recovering the investment would be the proposal with the turbines of 750 kW, which would begin the recovery in 18 years and five months. The values obtained in the analysis with 1400 $/kW of wind energy installed and a payment of 7 c$/kW by wind energy generated, are not considered a good economic option.

ii. *Second investment*

In this second investment proposition, the data will be processed with a cost for kW of wind energy installed equal to 1000 dollars, the calculations were carried out in the same way that in the first proposal, the obtained results are shown in Table 8.

The production costs per kW of energy generated with the wind in different wind farms, taking as reference the data of wind speed from the station of Santa Cruz del Norte and an investment of 1000 $/kW of installed wind energy, are between the 4.15 and the 4.52 c$/kW. The money pay by the generated wind energy will remain equal in this second proposition, 7 c$/kW. The economic curves are shown in Fig. 5

Table 8 : Production cost of the kW of wind energy (with a cost per kW of wind energy installed equal 1000 dollars).

Variable	Wind farm with GEV-MP 275	Wind farm with G52-850	Wind farm with S48/750
Initial investment ($)	10 175 000	10 200 000	10 500 000
Production cost (c$/kW)	4.52	4.15	4.5

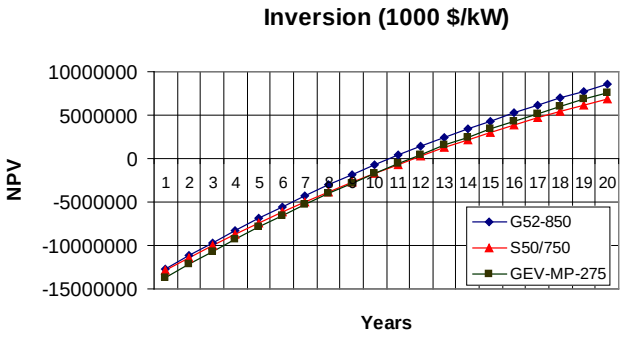

Fig. 5 : Net present value (NPV) with a cost by kW of wind energy installed equal to 1000 $/kW.

With an investment of 1000 $/kW and a payment by the produced electricity equal to 7 c$/kW, the results show that the first wind farm begin to recover the investment is that of the wind turbines of 850 kW in 10 years and eight months with a net present value of 8 523 080 dollars, followed by the wind farm with machines of 275 kW, which take around 11 years and seven months to recover their investment (having a NPV of 7 646 700 dollars). The last one to recover the investment is the wind farm with turbine of 750 kW, which takes one month more than the previous one in recovering the investment, 11 years and eight months with a NPV of 6 903 870 dollars.

IV. Conclusions

Taking in consideration all aspects analyzed in the study of the wind energy potentials in the western region of Cuba, have been reached the following conclusions:

1. The meteorological station located in the region of Santa Cruz del Norte, Havana, has the biggest power mean of wind by square meter in the four stations analyzed in the western region of Cuba, with a value of 276 W/m2 at height of 55 meters over the floor.

2. The biggest electricity production obtained with the analyzed wind turbines is obtained with a machine of 850 kW of power, with 1 976 090 kWh/year, to a hub height of 55 meters and 2 325 annual equivalent hours.
3. The production cost of the kW of wind energy generated in the different wind farms with an investment of 1400 $/kW of wind energy installed is between 5.8 and 6.34 dollar cent, being smaller the costs of the wind farm with turbines of 850 kW of power.
4. The production costs of the kW of wind energy generated in the different wind farms with an investment of 1000 $/kW of wind energy installed is between 4.15 and 4.52 dollar cent, being smaller the costs of the wind farm with machines of 850 kW of nominal power.
5. Taking an investment of 1400 $/kW of wind energy installed and with a payment for the generated electricity of 7 c$/kW, the results show that the wind farm that first begins to recover the investment is the one with turbines of 850 kW, which begins the 16 years and seven months, with a net present value (NPV) of 2 814 985 dollars.
6. With an investment of 1000 $/kW for wind energy installed and with a payment for the generated electricity of 7 c$/kW, the first wind farm that begins to recover the investment is the proposition with turbines of 850 kW, which begins the 11 years and seven months, with a NPV of 7 636 875 dollars.
7. The wind energy is not economically viable in Cuba, due to its high generation prices, which are conditioned by the high installation costs and the use of turbines with low power of generation.

V. Nomenclature

A	sweep area (m^2)
c	Weibull scale parameter (m/s)
C_p	capacity factor (dimensionless)
C_u	unitary production cost of the electricity ($/kWh)
E_j	energy saving ($/yr)
F_j	financing cost ($)
i	energy inflation (dimensionless)
I	capital cost of the installed wind power system($)
J	class number (dimensionless)
k	Weibull shape parameter (dimensionless)
n	lifetime of the system (years)
NPV	net present value ($)
OM_j	operation and maintenance costs ($)
PBA	payback (years)
P_u	power of wind per unit area (W/m^2)
P_w	power of wind (kW)
$P_{d,w}$	energy output (kW h/ year)
r	market discount rate ($)
T	time (h)
v	wind speed (m/s)
v_m	mean wind speed (m/s)
V_R	residual value of the installation ($)
Y	yearly benefits ($/yr)
z	height (m)
z_o	Surface roughness (m).
ρ	air density (kg/m^3)

References Références Referencias

1. Anon., 2008. Wind farm Gibara 1. Energy & you, January – March, 41. ISSN: 1028-9925.
2. Burton, T. et al., 2001. Wind Energy Handbook. England: John Wiley and Sons Ltd., 617 p. ISBN: 0 471 48997 2.
3. Eskin, N. et al., 2008. Wind energy potential of Gökceada Island in Turkey. Renew Sustain Energy Rev, 12, pp. 839–51.
4. Fawzi, A.L., 2009.Wind power analysis and site matching of wind turbine generators in Kingdom of Bahrain. Apply Energy, 86, pp. 538-45.
5. GEN (National Wind Energy Group), 2007. Ten Questions and Answers about Wind Energy. CUBASOLAR, ISBN: 9789597113379.
6. Hau, E., 2006. Wind Turbine, Fundamentals, Technologies, Application, Economics. Berlin: Springer, pp. 81-88. ISBN: 103540242406.
7. INEL Project, 2009. Wind farm Gibara 2, [online] Available at: <http://www.cdmbazaar.net> [Accessed 5 November 2010].
8. LAWEA (Latin American Wind Energy Association), 2009. Wind energy in Latin America. Infopower, October, 120, pp. 11-16. ISSN: 11385073.
9. Leiva, G., 1999. Wind farm of Turiguanó. Energy & you. April-June, 6. ISSN: 1028-9925.
10. Limia, M.; Vega, R. y Pérez, R., 1999. Climatology of the tropical Hurricanes that have affected Cuba and their provinces. CITMA.
11. Manwel, J. F., Mcgowan, J.G., Rogers, A.L., 2009. Wind energy explained, Theory, Designed and Application. England: John Wiley and Sons Ltd., pp. 506-520. ISBN: 978- 0 -470- 01500-1.
12. Reve, 2010. Wind energy in Cuba - next launch of Gibara II wind farm. [online] Available at: <http://www.evwind.es> [Accessed 10 February 2011].
13. Roque, A. et al., 2009. Network of meteorological towers for the Cuban winds program. VI International workshop of Renewable Energy, Saving Energy and Energy Education, Havana, Cuba.
14. Soltura, R. and Roque, A., 2007. Wind resource map of Cuba. Energy & you, January – February, 37. ISSN: 10289925.
15. Tsoutsos, T. et al., 2003. Solar cooling technologies in Greece. An economic viability analysis. Appl. Therm. Eng. 23, pp.1427-39.

16. Ucar, A. Balo, F., 2008. Evaluation of wind energy potential and electricity generation at six locations in Turkey. Apply Energy, 86, pp. 1864- 72.
17. UNE (Electric Union of Cuba), 2008. Wind Energy Program. [online] Available at: <http://www.energia.inf.cu/eventos/memorias6/pdfs/PROG_EOLIC_JUN08.pdf > [Accessed 22 September 2010].
18. Villarrubia, M., 2004.Wind Energy. Barcelona: CEAC, 322 p. ISBN: 8432910627.
19. WWEA (World Wind Energy Association), 2011.World Wind Energy Report 2010.

Global Journal of researches in engineering
Mechanical and mechanics engineering
Volume 11 Issue 7 Version 1.0 December 2011
Type: Double Blind Peer Reviewed International Research Journal
Publisher: Global Journals Inc. (USA)
Online ISSN: 2249-4596 Print ISSN:0975-5861

Predictive Model of Orthotropic Un-Symmetric Box Cam Based On Deflection And countered by Segments of Circular-Arc Contact Profiles

By Dr. Fathi Al-Shamma, Dr. Louay S. Yousuf
College of Engineering Mech. Eng. Dept.

Abstract - In this paper the principal objective is to find the deflection of orthotropic box cam profile countered by segments of circular-arc due to the effect of contact loading which produce the generate force that induces high contact stress on the cam-surface especially in high-speed machine. In high-speed it can be used the composite cam, since it affects the whole machine performance to improve the wear resistance. Several researchers investigated the effects of cam profile in accuracy and system flexibility on the output motion experimentally; but there is a lake in the theoretical part. The theoretical part has been done with the solution of orthotropic circular plate equation using the harmonic deflection motion of the follower. The cam used in this paper can be seen in composite shifter cam for a motorcycle transmission, composite hollow cam-shafts, the running valve lift with roller followers of a composite cam-shaft, and heavy duty of marine engine. The aim of the present paper is to find the maximum deflection of orthotropic box cam on the boundaries of the three circular-arc contact profiles for flanks and noses of contact follower loadings. The results were arrangement into theoretical part and finite element using software ANSYS 12.1.

Keywords : *Orthotropic Cam, Contact Loading, Circular Plate Equation, ANSYS Software, Un-Symmetric Pressure Angles, Box Cam.*

GJRE-A Classification :

Strictly as per the compliance and regulations of:

Predictive Model of Orthotropic Un-Symmetric Box Cam Based On Deflection And countered by Segments of Circular-Arc Contact Profiles

Dr. Fathi Al-Shamma[α], Dr. Louay S. Yousuf [Ω]

Abstract - In this paper the principal objective is to find the deflection of orthotropic box cam profile countered by segments of circular-arc due to the effect of contact loading which produce the generate force that induces high contact stress on the cam-surface especially in high-speed machine. In high-speed it can be used the composite cam, since it affects the whole machine performance to improve the wear resistance. Several researchers investigated the effects of cam profile in accuracy and system flexibility on the output motion experimentally; but there is a lake in the theoretical part. The theoretical part has been done with the solution of orthotropic circular plate equation using the harmonic deflection motion of the follower. The cam used in this paper can be seen in composite shifter cam for a motorcycle transmission, composite hollow cam-shafts, the running valve lift with roller followers of a composite cam-shaft, and heavy duty of marine engine. The aim of the present paper is to find the maximum deflection of orthotropic box cam on the boundaries of the three circular-arc contact profiles for flanks and noses of contact follower loadings. The results were arrangement into theoretical part and finite element using software ANSYS 12.1.

Keywords : Orthotropic Cam, Contact Loading, Circular Plate Equation, ANSYS Software, Un-Symmetric Pressure Angles, Box Cam.

NOMENCLATURES

Normal Letters		
Symbol	Definition	Unit
a_1	Major distance of ellipse axis	m
b_1	Minor distance of ellipse axis	m
a_2	Difference radius of curvatures between ellipse and semi-circle centers	m
C	Particular solution constant	----------
D_r, D_θ, and $D_{r\theta}$	Radial, tangential, and twisting flexural rigidity	N. m
L	Length of simply-supported beam	M
L_1	Difference length between two points of contact	M
m_1	Single trigonometric of Furrier series	----------
$M_r, M_\theta, \text{and } M_{r\theta}$	Circular plate bending and twisting moment	N.m
P_o	Maximum contact pressure	$\frac{N}{m^2}$
r, andθ	Polar coordinates	m, Degree
r_1	Radius of clamped cam center	M
q	Loading contact per unit length	$\frac{N}{m}$
W	Circular plate deflection	M
x, y	Cartesian coordinates	M

Greek Letters		
Symbol	Definition	Unit
σ_y	Yield Stress	$\frac{N}{m^2}$
π	Constant (3.1416)	---------
θ_1, θ_2	Angles of the beginning and the ending for both flanks and noses	Degree

Author[α]: Asst. Prof, College of Engineering Mech. Eng. Dept. E-mail : fathi_alshamma@yahoo.com
Author[Ω] : Lect., College of Engineering Mech. Eng. Dept. E-mail : louaysabah79@yahoo.com

I. Introduction

A new type of composite cam-shafts that obtain an optimum condition valve lift running with roller followers based on it a new composite function cam profile emphatically is developed, in most cases the lobe profile needs to have a concave form (negative radii in the area of the cam lift profile) to improve fullness coefficient, positive and negative peak acceleration and cam-follower contact stress in cam tip; but at the same time the conventional grinding equipment is to suitable to manufacture this type of cam profile, [1, 2].Moreover the mechanical and microstructure properties of cam-shafts surfaces like Brinell, Rockwell, and Vickers hardness tests of Ti Al N/Al N composite film deposited on the profile surface of cam (made of chilled cast iron 45 steel) experimentally and numerically relating with the Ion Beam sputtering deposition, the solidification, and cooling rate technologies, in which the operation temperature can be controlled below the limitation of phases exchanging or at room temperature to avoid phase exchanging deformation and examined the rapid and slow cooling surfaces, rosette like graphite in pearlitic and low ferrite phase on cam hardness to improve the shape and dimension accuracy, [3, 4].In the other hand the cam material (ferrous P/M materials) of a composite shifter hollow cam-shafts for a sequential transmission includes portions formed of a wear resistant material and portions formed of a light weight material using laser surface quenching and discussed the static joining strength and fatigue strength of cam-shafts with different space between tooth. The destroying torsion of the shifter composite cam structure was (20-30) times as many as its actual work torsion, and its fatigue strength to allow the heavier, wear resistant material durable shifter cam, [5, 6]. It can be studied a composite fabricated cam of Al-Sic using cold isostatic compaction and subsequent sintering die casting with a mixture of four different compositions (10, 20, 25, 30)% of Sic powder mixed with Al powders to obtain a high strength to weight ratio and low coefficient of thermal expansion and measured a cam properties like compressive strength, hardness, density and surface roughness, [7]. The fatigue life and microscopic edge cracks is measured for two open-celled foamed polymers having different densities in compression impact using a cam-driven compound pendulum system and observed that the material measurements at constant incident energy included the static compression modulus and peak dynamic stress, which progressively degraded as the number of impacts approached one million, [8].

II. Box Cam Shape

1. *Plate cam or disk cam*:
   The follower moves in a plane perpendicular to the axis of rotation of the camshaft. A translating or a swing arm follower must be constrained to maintain contact with the cam profile.
2. *Grooved cam or closed cam shown in Fig.(1):*
   This is a plate cam with the follower riding in a groove in the face of the cam.

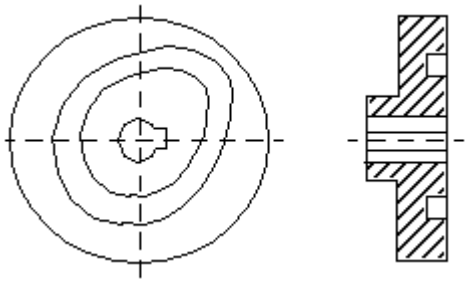

Fig. (1) : Grooved cam.

III. Analytical Procedure

The general circular plate equation as a function of (r, and θ) coordinates is:

$$\left(\frac{\partial^2}{\partial r^2}+\frac{2}{r}\frac{\partial}{\partial r}\right)*M_r+\left(-\frac{1}{r}\frac{\partial}{\partial r}+\frac{1}{r^2}\frac{\partial^2}{\partial \theta^2}\right)*M_\theta+\left(-\frac{2}{r}\frac{\partial^2}{\partial r\,\partial \theta}-\frac{2}{r^2}\frac{\partial}{\partial \theta}\right)*M_{r\theta}+q=0 \quad (1)$$

Where:

For orthotropic plate, the bending and twist moments are:

$$M_r=-[\,D_r*\frac{\partial^2 w}{\partial r^2}+D_1*(\frac{1}{r}\frac{\partial w}{\partial r}+\frac{1}{r^2}\frac{\partial^2 w}{\partial \theta^2})]$$

$$M_\theta=-[D_\theta\left(\frac{1}{r}\frac{\partial w}{\partial r}+\frac{1}{r^2}\frac{\partial^2 w}{\partial \theta^2}\right)+D_1*\frac{\partial^2 w}{\partial r^2}] \quad (2)$$

$$M_{r\theta}=2*\left[\frac{1}{r}\frac{\partial^2 w}{\partial r\,\partial \theta}-\frac{1}{r^2}\frac{\partial w}{\partial \theta}\right]*D_{r\theta}$$

And;

$$D_r = \frac{E_r * t^3}{12*(\nu_{r\theta} * \nu_{\theta r})}$$

$$D_\theta = \frac{E_\theta * t^3}{12*(\nu_{r\theta} * \nu_{\theta r})}$$

$$D_1 = \frac{\nu_{r\theta} * E_\theta * t^3}{12*(\nu_{r\theta} * \nu_{\theta r})} = \frac{\nu_{\theta r} * E_r * t^3}{12*(\nu_{r\theta} * \nu_{\theta r})}$$

$$D_{r\theta} = \frac{\sqrt{D_r * D_\theta} * (1 - \sqrt{\nu_{r\theta} * \nu_{\theta r}})}{2}$$

The value of first term of eq. (1) is:

$$\left(\frac{\partial^2}{\partial r^2} + \frac{2}{r}\frac{\partial}{\partial r}\right) * M_r = -(D_r * \frac{\partial^4 w}{\partial r^4} + \frac{D_1}{r}\frac{\partial^3 w}{\partial r^3} + \frac{D_1}{r^2}\frac{\partial^4 w}{\partial r^2 \partial \theta^2} - \frac{2*D_1}{r^3}\frac{\partial^3 w}{\partial r \partial \theta^2} + \frac{2*D_1}{r^4}\frac{\partial^2 w}{\partial \theta^2} + \frac{2* D_r}{r}\frac{\partial^3 w}{\partial r^3})$$

And the value of second term of eq. (1) is:

$$\left(-\frac{1}{r}\frac{\partial}{\partial r} + \frac{1}{r^2}\frac{\partial^2}{\partial \theta^2}\right) * M_\theta = -(-\frac{D_\theta}{r^2}\frac{\partial^2 w}{\partial r^2} + \frac{D_\theta}{r^3}\frac{\partial w}{\partial r} + \frac{2*D_\theta}{r^4}\frac{\partial^2 w}{\partial \theta^2} - \frac{D_1}{r}\frac{\partial^3 w}{\partial r^3} + \frac{D_\theta}{r^4}\frac{\partial^4 w}{\partial \theta^4} + \frac{D_1}{r^2}\frac{\partial^4 w}{\partial r^2 \partial \theta^2})$$

Also the value of third term of eq. (1) is:

$$\left(-\frac{2}{r}\frac{\partial^2}{\partial r \partial \theta} - \frac{2}{r^2}\frac{\partial}{\partial \theta}\right) * M_{r\theta} = 2 * D_{r\theta}(-\frac{2}{r^2}\frac{\partial^4 w}{\partial r^2 \partial \theta^2} + \frac{2}{r^3}\frac{\partial^3 w}{\partial r \partial \theta^2} - \frac{2}{r^4}\frac{\partial^2 w}{\partial \theta^2})$$

It can be put the three terms derived above in eq. (1) to obtain:

$$D_r * \frac{\partial^4 w}{\partial r^4} + \frac{2* D_r}{r}\frac{\partial^3 w}{\partial r^3} - \frac{D_\theta}{r^2}\frac{\partial^2 w}{\partial r^2} + \frac{D_\theta}{r^3}\frac{\partial w}{\partial r} + \frac{2*(D_1+2*D_{r\theta})}{r^2}\frac{\partial^4 w}{\partial r^2 \partial \theta^2} - \frac{2*(D_1+2*D_{r\theta})}{r^3}\frac{\partial^3 w}{\partial r \partial \theta^2} + \frac{2*(D_1+D_\theta+2*D_{r\theta})}{r^4}\frac{\partial^2 w}{\partial \theta^2} + \frac{D_\theta}{r^4}\frac{\partial^4 w}{\partial \theta^4} = q \quad (3)$$

The homogenous solution of eq. (1) is as follows:

$$w(r,\theta)_H = A * \sin(r * \theta) + B * \cos(r * \theta) \quad (4)$$

Where:

A and B are constants.

It can be derived the homogenous solution (1, 2, 3, 4) times with respect to r and θ to obtain:

$$\frac{\partial w}{\partial r} = A * \theta * \cos(r * \theta) - B * \theta * \sin(r * \theta)$$

$$\frac{\partial^2 w}{\partial r^2} = -A * \theta^2 * \sin(r * \theta) - B * \theta^2 * \cos(r * \theta)$$

$$\frac{\partial^3 w}{\partial r^3} = -A * \theta^3 * \cos(r * \theta) + B * \theta^3 * \sin(r * \theta)$$

$$\frac{\partial^4 w}{\partial r^4} = A * \theta^4 * \sin(r * \theta) + B * \theta^4 * \cos(r * \theta)$$

$$\frac{\partial^4 w}{\partial r^2\,\partial\theta^2} = -A*\left(-\theta^2*r^2*\sin(r*\theta)+4*\theta*r*\cos(r*\theta)+2*\sin(r*\theta)\right)-B*(-\theta^2*r^2*\cos(r*\theta)-4*\theta*r*\sin(r*\theta)+2*\cos(r*\theta))$$

$$\frac{\partial^3 w}{\partial r\,\partial\theta^2} = A*(-\theta*r^2*\cos(r*\theta)-2*r*\sin(r*\theta))-B*(-\theta*r^2*\sin(r*\theta)+2*r*\cos(r*\theta))$$

$$\frac{\partial^2 w}{\partial\theta^2} = -A*r^2*\sin(r*\theta)-B*r^2*\cos(r*\theta)$$

$$\frac{\partial^4 w}{\partial\theta^4} = A*r^4*\sin(r*\theta)+B*r^4*\cos(r*\theta)$$

After putting the above derivatives in eq. (1) and after simplification to obtain:

$$w(r,\theta)_H = \frac{(2*D_r*\theta^3*r^2+6*D_1*r^2*\theta+12*D_{r\theta}*r^2*\theta-D_\theta*\theta)}{(D_r*\theta^4*r^3+D_\theta*\theta^2*r+2*D_1*r^3*\theta^2+4*D_{r\theta}*r^3*\theta^2-2*D_1*r-2*D_\theta*r-4*D_{r\theta}*r+r^3)}*A*\cos(r*\theta)-\frac{(2*D_r*\theta^3*r^2+6*D_1*r^2*\theta+12*D_{r\theta}*r^2*\theta-D_\theta*\theta)}{(D_r*\theta^4*r^3+D_\theta*\theta^2*r+2*D_1*r^3*\theta^2+4*D_{r\theta}*r^3*\theta^2-2*D_1*r-2*D_\theta*r-4*D_{r\theta}*r+r^3)}*B*\sin(r*\theta) \quad (5)$$

And the particular solution is:

$$w(r,\theta)_P = C*r*\theta \quad (6)$$

Put eq. (6) in plate equation eq. (1) and find the value of constant (C):

$$C = \frac{q*r^3}{\theta*D_\theta}$$

$$w(r,\theta)_P = \frac{q*r^4}{D_\theta} \quad (7)$$

The complementary solution of deflection is as below:

$$w(r,\theta) = w(r,\theta)_H + w(r,\theta)_P$$

$$w(r,\theta) = \frac{(2*D_r*\theta^3*r^2+6*D_1*r^2*\theta+12*D_{r\theta}*r^2*\theta-D_\theta*\theta)}{(D_r*\theta^4*r^3+D_\theta*\theta^2*r+2*D_1*r^3*\theta^2+4*D_{r\theta}*r^3*\theta^2-2*D_1*r-2*D_\theta*r-4*D_{r\theta}*r+r^3)}*A*\cos(r*\theta)-\frac{(2*D_r*\theta^3*r^2+6*D_1*r^2*\theta+12*D_{r\theta}*r^2*\theta-D_\theta*\theta)}{(D_r*\theta^4*r^3+D_\theta*\theta^2*r+2*D_1*r^3*\theta^2+4*D_{r\theta}*r^3*\theta^2-2*D_1*r-2*D_\theta*r-4*D_{r\theta}*r+r^3)}*B*\sin(r*\theta)+\frac{q*r^4}{D_\theta} \quad (8)$$

It can be applied the boundary conditions on eq. (8) to obtain the constants (A and B):

$$At\, r = r_1 = 2.5\text{ cm}, \theta = \theta_1, w(r,\theta) = 0$$

$$At\, r = r_1 = 2.5\text{ cm}, \theta = \theta_2, w(r,\theta) = 0$$

Where: θ_1 and θ_2 vary along each flank and nose profile as shown in Fig.(2).

Then;

$$A = \frac{C_1*C_3*\sec(r_1*\theta_2)*\cos(r_1*\theta_1)*\tan(r_1*\theta_2)-C_2*C_3*\tan(r_1*\theta_2)}{C_1*C_2*(\tan(r_1*\theta_2)*\cos(r_1*\theta_1)-\sin(r_1*\theta_1))} - \frac{C_3*\sec(r_1*\theta_2)}{C_2}$$

$$B = \frac{C_1*C_3*\sec(r_1*\theta_2)*\cos(r_1*\theta_1)-C_2*C_3}{C_1*C_2*(\tan(r_1*\theta_2)*\cos(r_1*\theta_1)-\sin(r_1*\theta_1))}$$

Where:

$$C_1 = \frac{2*D_r*\theta_1^3*r_1^2+6*D_1*r_1^2*\theta_1+12*D_{r\theta}*r_1^2*\theta_1-D_\theta*\theta_1}{D_r*\theta_1^4*r_1^3+D_\theta*\theta_1^2*r_1+2*D_1*r_1^3*\theta_1^2+4*D_{r\theta}*r_1^3*\theta_1^2-2*D_1*r_1-2*D_\theta*r_1-4*D_{r\theta}*r_1+r_1^3}$$

$$C_2 = \frac{2*D_r*\theta_2^3*r_1^2+6*D_1*r_1^2*\theta_2+12*D_{r\theta}*r_1^2*\theta_2-D_\theta*\theta_2}{D_r*\theta_2^4*r_1^3+D_\theta*\theta_2^2*r_1+2*D_1*r_1^3*\theta_2^2+4*D_{r\theta}*r_1^3*\theta_2^2-2*D_1*r_1-2*D_\theta*r_1-4*D_{r\theta}*r_1+r_1^3}$$

$$C_3 = \frac{q*r_1^4}{D_\theta}$$

$$\therefore w(r,\theta) = \frac{(2*D_r*\theta^3*r^2+6*D_1*r^2*\theta+12*D_{r\theta}*r^2*\theta-D_\theta*\theta)}{(D_r*\theta^4*r^3+D_\theta*\theta^2*r+2*D_1*r^3*\theta^2+4*D_{r\theta}*r^3*\theta^2-2*D_1*r-2*D_\theta*r-4*D_{r\theta}*r+r^3)} * \left[\frac{C_1*C_3*\sec(r_1*\theta_2)*\cos(r_1*\theta_1)*\tan(r_1*\theta_2)-C_2*C_3*\tan(r_1*\theta_2)}{C_1*C_2*(\tan(r_1*\theta_2)*\cos(r_1*\theta_1)-\sin(r_1*\theta_1))} - \frac{C_3*\sec(r_1*\theta_2)}{C_2}\right] * \cos(r*\theta) - \frac{(2*D_r*\theta^3*r^2+6*D_1*r^2*\theta+12*D_{r\theta}*r^2*\theta-D_\theta*\theta)}{(D_r*\theta^4*r^3+D_\theta*\theta^2*r+2*D_1*r^3*\theta^2+4*D_{r\theta}*r^3*\theta^2-2*D_1*r-2*D_\theta*r-4*D_{r\theta}*r+r^3)} * \left[\frac{C_1*C_3*\sec(r_1*\theta_2)*\cos(r_1*\theta_1)-C_2*C_3}{C_1*C_2*(\tan(r_1*\theta_2)*\cos(r_1*\theta_1)-\sin(r_1*\theta_1))}\right] * \sin(r*\theta) + \frac{q*r^4}{D_\theta} \quad (9)$$

It can be assumed that the two points of contact load are as the simply-supported beam subjected to distributed load (P_o) per unit length of point loading using superposition theory as illustrated in Fig.(3), [9]:

$$P_o = 0.6 * \sigma_y$$

$$q = P_o * \frac{2*\pi}{3} * \frac{L^2}{8} * \frac{1}{L_1} * \upsilon_F \quad (10)$$

Where:

L: is the length of simply-supported beam.

L_1:is the difference length between two points of contact.

υ_F: is the fiber volume fraction ($\upsilon_F = 0.3$)

The elliptic equation is, [10]:

$$w(x,y) = \frac{q*(\frac{x^2}{a_1^2}+\frac{y^2}{b_1^2}-1)^2}{(\frac{24*D_r}{a_1^4}+\frac{16*H}{a_1^2*b_1^2}+\frac{24*D_\theta}{b_1^4})} \quad (11)$$

Where: a_1 and $b_1$is the major and minor distance axis of ellipse.

And; $H = D_1 + 2 * D_{r\theta}$

And the semi-circle equation is, [10]:

$$w(r,\theta) = \sum_{m_1=1,3,5}^{\infty}\left[\frac{4*q*r^4}{\pi*m_1*(16-m_1^2)*(4-m_1^2)*D_r} + A_{1m_1} * r^{m_1} + A_{3m_1} * r^{m_1+2}\right] * \sin(m_1 * \theta) \qquad (12)$$

Where:

$$A_{1m_1} = \frac{-2*q*(m_1+1)*a_2^{4-m_1}}{\pi*m_1*(16-m_1^2)*(4-m_1^2)*D_r}$$

$$A_{3m_1} = \frac{2*q*(m_1-1)*a_2^{2-m_1}}{\pi*m_1*(16-m_1^2)*(4-m_1^2)*D_r}$$

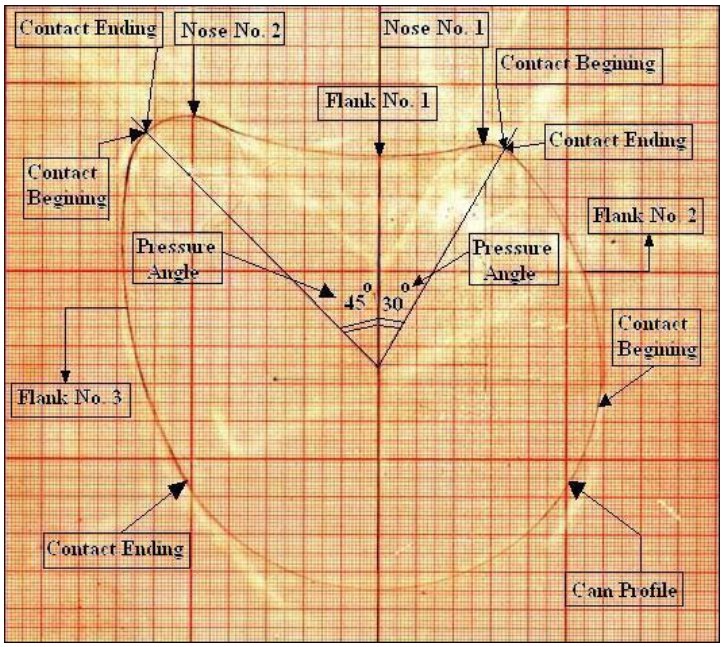

Fig. (2) : Cam Profile Specifications, [11].

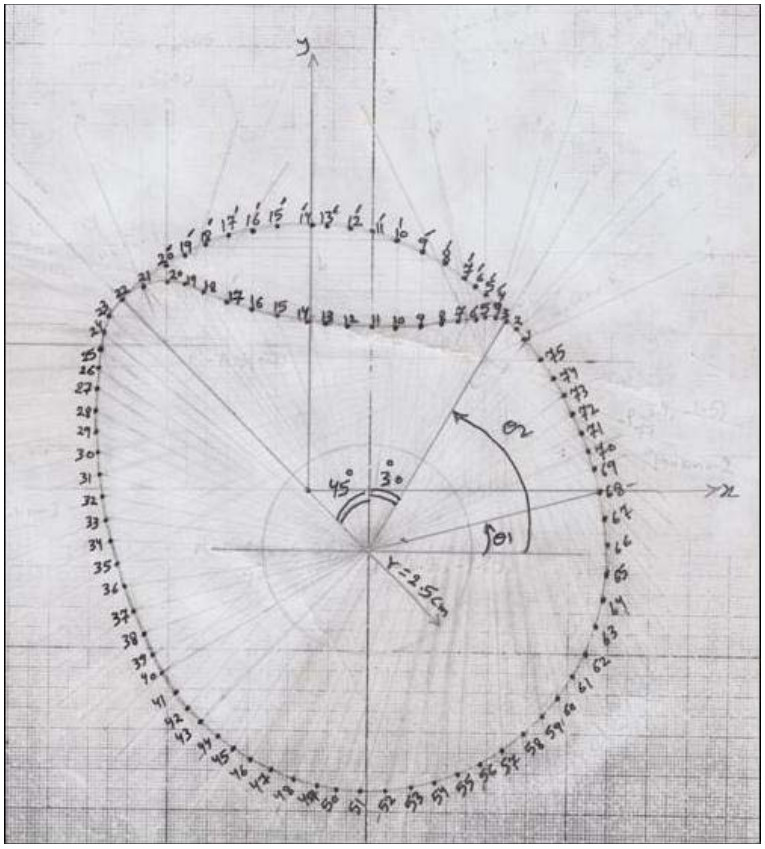

Fig.(3) : The Points of Cam Profile.

IV. Numerical Procedure

For this problem, the (SHELL 99)element is used in this paper for the two-dimensional modeling of orthotropic un-symmetric cam shell structure carried out with ANSYS 12.1 program software and is defined byeight nodes having six degrees of freedom at each node: translations in the nodal x, y, and z directions and rotations about the nodal x, y, and z axes to find the maximum deflection on cam boundaries. The mesh generation of box cam can be indicated in Fig. (4).

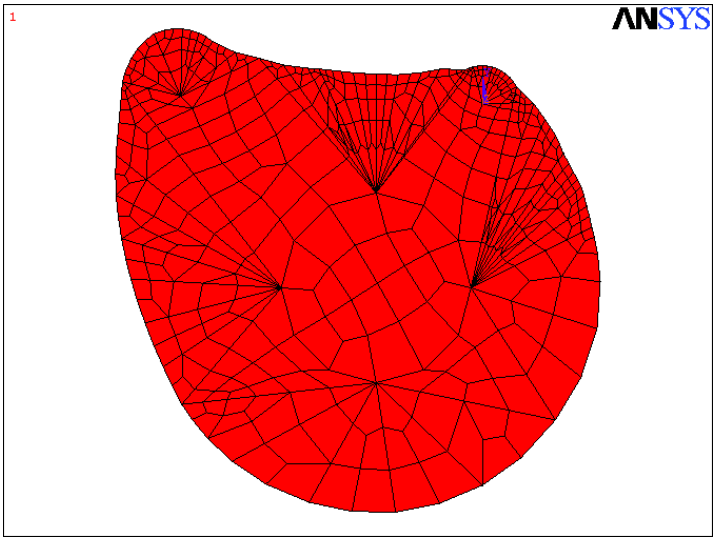

Fig. (4) : The mesh generation of cam un-symmetric cam profile.

V. Results

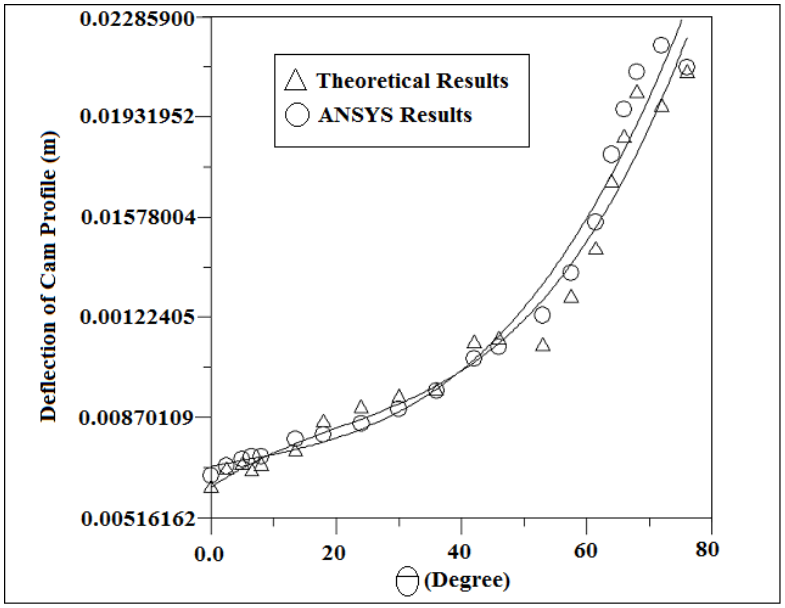

Fig. (5) : Deflection of cam profile against angle of contact for nose no. 1, flank no.1, and nose no. 2.

Fig. (5) shows the deflection of cam profile against angle of contact for nose no. 1, flank no.1, and nose no. 2. The deflection of cam profile increase exponantially with the increasingof the angle of contact for orthotropic cam. The percentage error between theoretical and ANSYS results is closely because the curve degree of orthotropic cam profile is very high.

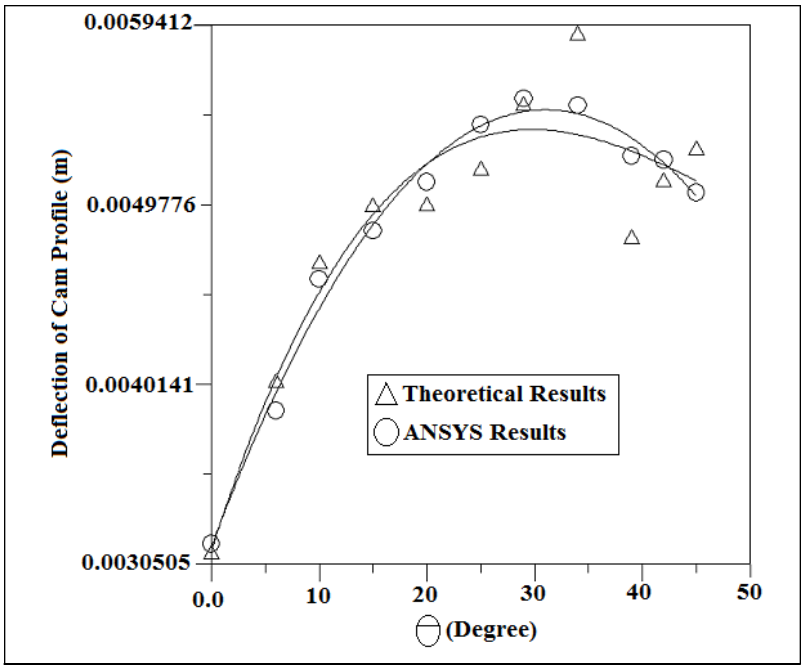

Fig. (6) : Deflection of cam profile against angle of contact for flank no. 2 and nose no. 1.

Fig. (6) shows the deflection of cam profile against angle of contact for flank no. 2 and nose no. 1. The deflection of cam profile vary transiently with the angle of contact for flank no. 2 and nose no. 1 for orthotropic cam. The percentage error between theoretical and ANSYS results is lower than in Fig. (5) because the difference length value between two points of contact (L_1) is accurate.

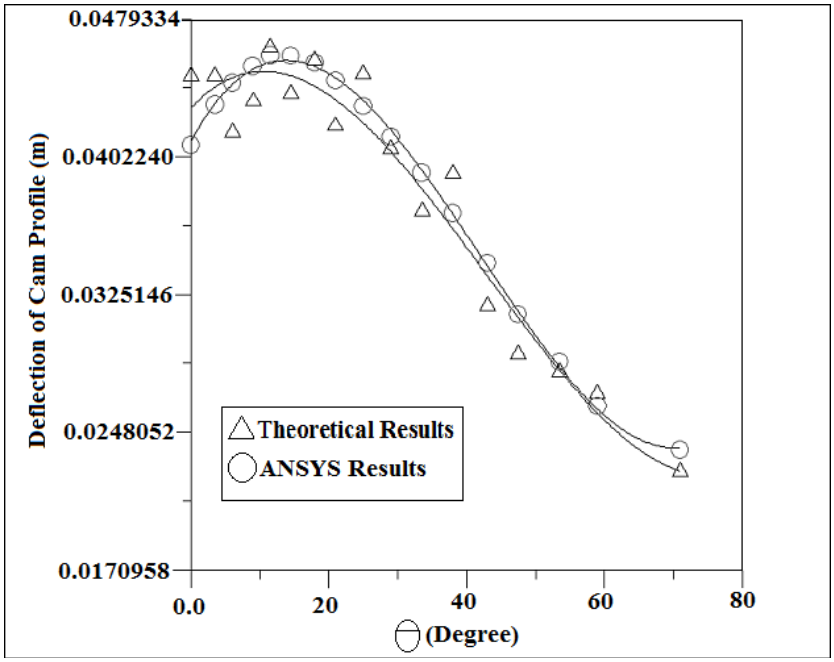

Fig. (7) : Deflection of cam profile against angle of contact for nose no. 2 and flank no. 3.

Fig. (7) shows the deflection of cam profile against angle of contact for nose no. 2 and flank no. 3.The value of deflection decreased sinusoid ally with the increasing of the angle of contact because the contact loading in some locations is small or nearly constant.

Table (1) : Theoretical and ANSYS results for deflection vary with point's numberofnose no. 1, flank no.1, and nose no. 2.

Points Number	Theoretical Results	ANSYS Results	Error (%)
3	0.005161615	0.0056644	8.876%
4	0.0058861	0.006051	2.725%
5	0.00606744	0.0063089	3.827%
6	0.00582013	0.0064287	9.466%
7	0.0060445	0.006436	6.083%
8	0.00661729	0.0071268	7.149%
9	0.00778991	0.0073008	6.278%
10	0.0083432	0.0077435	7.187%
11	0.00878378	0.0083321	5.142%
12	0.00903007	0.0090455	0.17%
13	0.0109305	0.010322	5.566%
14	0.0110767	0.010799	2.507%
15	0.0108222	0.012067	10.31%
16	0.0127715	0.01377	7.251%
17	0.01467905	0.015786	7.012%
18	0.0173589	0.018493	6.132%
19	0.01916212	0.020308	5.642%
20	0.0209437	0.021801	3.932%
21	0.0203995	0.022859	10.76%
22	0.0217526	0.021979	1.03%

Table (1) shows the theoretical and ANSYS results for deflection vary with point's number of nose no. 1, flank no.1, and nose no. 2. The deflection of cam boundary profile increased exponentially with the increasing of point's number on orthotropic cam boundaries because increasing the angle of contact at these points from the point of beginning at nose no.1 to the point of ending at nose no. 2.

Table (2) : Theoretical and ANSYS results for deflection vary with point's number of flank no. 2 and nose no. 1.

Points Number	Theoretical Results	ANSYS Results	Error (%)
68	0.0030505	0.0031101	1.916%
69	0.004008805	0.0038517	3.918%
70	0.00466814	0.0045842	1.798%
71	0.004986	0.0048537	2.653%
72	0.0049904	0.0051238	2.603%
73	0.00519162	0.0054449	4.651%
74	0.0055525	0.0055893	0.658%
75	0.00594125	0.005553	6.691%
1	0.00480574	0.0052705	8.818%
2	0.005125194	0.0052481	2.342%
3	0.005301403	0.0050653	4.453%

Table (2) shows the theoretical and ANSYS results for deflection vary with point's number of flank no. 2 and nose no. 1. The deflection of cam boundary profile increased sinusoid ally with the increasing of point's numbers on orthotropic cam boundaries and the deflection for nose no. (1) is larger than the deflection of flank no. (1) because the effect of the radius of curvaturesfrom the point of beginning at flank no. 2 to the point of ending at nose no. 1.

Table (3) : Theoretical and ANSYS results for deflection vary with point's number of nose no. 2 and flank no. 3.

Points Number	Theoretical Results	ANSYS Results	Error (%)
22	0.0458897	0.040823	11.041%
23	0.0458858	0.043772	4.606%
24	0.0418067	0.045346	7.805%
25	0.0440422	0.046558	5.403%
26	0.0479334	0.047361	1.194%
27	0.04459053	0.047317	5.762%
28	0.0470031	0.046831	0.3661%
29	0.04224056	0.045533	7.231%
30	0.0460082	0.043685	5.049%
31	0.0405565	0.041455	2.167%
32	0.0360775	0.038849	7.134%
33	0.0387652	0.035871	7.466%
34	0.029147	0.032265	9.663%
35	0.0256657	0.028528	10.033%
36	0.02435666	0.025104	2.977%
37	0.02280797	0.021889	4.029%
39	0.0170958	0.018668	8.421%

Table (3) shows the theoretical and ANSYS results for deflection vary with point's number of nose no. 2 and flank no. 3. The deflection of cam boundary profile decreased transiently with the increasing of point's number on orthotropic cam boundaries because varying the radius of curvature at these points from the point of beginning at nose no. 2 to the point of ending at flank no. 3.

VI. Conclusions

1) The deflection of orthotropic cam is larger than the deflection in isotropic cam because the modulus of elasticity and Poisson's ratio for orthotropic cam is small for the same contact loading.
2) The maximum deflection occurs at nose no. (2) because the radius of curvature is small.
3) The deflection on noses is larger thanthe deflection of flanks because the effect of the radius of curvatures.

References Références Referencias

1. Harald Müller, MWP Mahle, J. Wizemann, Pleuco GmbH, and Andreas Kaiser, "Composite Camshaft-Avoid Lobe Grinding Using PM Lobes", Journal of SAE, No. 970001, 24-2-2007.
2. kong Fan-feng1, CHU Chao-meil, WANG Bo2, and LI Zhao-jian1, "Design and Study of New Composite Function Cam Profile", Chinese Journal,12-1-2011.
3. LeventCenkKumruoğlu, " Mechanical and Microstructure Properties of Chilled Cast Iron Camshaft: Experimental and Computer Aided Evaluation ", Journal of Materials and Design, No. 33, pp. 927-938, 2009.
4. Pei QuanGuq, ShouRen Wang, and Huan Yong Cui," Microstructure and Properties of Ti Al N/Al N Composite Film Deposited on Cam's Profile by Ion Beam Sputtering Technique", Journal of Key

Engineering Materials, Vol. 443, pp. 465-468, June 2010.
5. ZHANG Chi, LI Yue-ying, YANG Shen-hua, and LIU Yong-bing, “The Study of Cam Materials and Assembling Technology of Composite Hollow Camshafts", Chinese Journal (Material Science and Technology), 3-1-2005.
6. Eric M. Chappelear, and William J.Hacker, “Composite Shifter Cam for A Motorcycle Transmission", Track new patents and Technologies, 2006.
7. R. Purohit, and R. Sagar, "Fabrication of A Cam using Metal Matrix Composites", Journal of Advanced Manufacturing Technology , No. 9, Vol. 17, pp. 644-648, 2001.
8. James F. Wilson, “Impact-Induced Fatigue of Foamed Polymers ", Journal of Impact Engineering, No. 34, pp. 1370-1381, 2007.
9. E. J. Hearn, "Mechanics of Materials", Book of second edition, Volume 2, 1985.
10. Eduard Ventsel, and Theodor Krauthammer, "Thin Plates and Shells", Book of Theory, Analysis and Application, 2001.
11. Yu and H P Lee, "Size Optimization of Cam Mechanisms with Translating Roller Followers", Journal of Mechanical Engineering Science, Vol. 212, No. C5, 1998.

This page is intentionally left blank

Global Journal of researches in engineering
Mechanical and mechanics engineering
Volume 11 Issue 7 Version 1.0 December 2011
Type: Double Blind Peer Reviewed International Research Journal
Publisher: Global Journals Inc. (USA)
Online ISSN: 2249-4596 Print ISSN:0975-5861

A Combined Effect of Elasto-Plasto Hydrodynamic Lubrication in Cold Strip Rolling

By Dr.fathi.a.alshamma
Baghdad University.

Abstract - The aim of this study is to analysis the behavior of lubricants in cold strip rolling. An elastohydrodynamic lubrication analysis which takes account of elastic deformation of the roller while the metal strip deform plastically ,so that a relation between the E.H.L and plastohydrodynamic is used to determine the lubricant film thickness which will entrained in metal rolling operation .The viscosity variation and the variation between the pressure gradient and the speed of the roller with lubricant which is Newtonian up to some critical shear stress and thereafter behaves plastically is derived.The results are compared with the experimental one ,which shows good agreement with it.

Keywords : *Elastohydrodynamic, plastohydrodynamic, cold rolling, viscosity variation*

GJRE-A Classification :

Strictly as per the compliance and regulations of:

A Combined Effect of Elasto-Plasto Hydrodynamic Lubrication in Cold Strip Rolling

Dr.fathi.a.alshamma

Abstract - The aim of this study is to analysis the behavior of lubricants in cold strip rolling. An elastohydrodynamic lubrication analysis which takes account of elastic deformation of the roller while the metal strip deform plastically ,so that a relation between the E.H.L and plastohydrodynamic is used to determine the lubricant film thickness which will entrained in metal rolling operation .The viscosity variation and the variation between the pressure gradient and the speed of the roller with lubricant which is Newtonian up to some critical shear stress and thereafter behaves plastically is derived.The results are compared with the experimental one ,which shows good agreement with it.

Keyword: Elastohydrodynamic, plastohydrodynamic, cold rolling, viscosity variation

Nomenclature

p= pressure	N/m²
x= Dimension along arc of contact	m
μ= Viscosity of lubricant.	N.m/sec
μo= Base viscosity of lubricant at ambient temperature	N.m/sec
γ= Lubricant pressure coefficient of viscosity	
h= Film thickness	m
u1= Rolling speed	m/sec
u2= Strip velocity	m/sec
σ1= Back tension	N/mm²
σo= Front tension	N/mm²
σy= Yield stress of strip material	N/mm²
R= Roll radius	m
r= Reduction	
y1= Initial strip thickness	mm
τ= Shear stress at the surface	N/mm²
η= Coefficient of friction between roll surface and material	
k= Yield stress with initial speed	N/mm²
k1,ko= Yield stress with inhibited speed at inlet and outlet side	N/mm²
yo= Thickness of strip at exit	mm
yi= Thickness of strip at inlet	mm
α= Angular coordinates radius	

I. Introduction

In the lubrication of cold metal forming such as rolling drawing, and extrusion, lubricant films are entrained by wedge action in nominally steady processes. The pressure of the film thickness can vary from atmospheric to the order of yield stress of the work piece.

Author : Prof. Assistant, Mechanical engineering Department, Baghdad University.

In cold rolling as strip is reduced and elongated it changes speed relative to roll speed and must slide against the roll surfaces .The resultant friction produces forces ,which tend to retain the strip in the roll bite ,roll force and torque increasing with increase in friction. A decreases in (μ), the coefficient of friction, is thus desirable to reduce power consumption and roll loads and to obtain increased strip reduction. The latter is of particular importance in the rolling of thin plate where the high loads required because considerable roll flattening. This increases frictional forces until a point is reached at which no further reduction of the strip can occur. Further increase in load merely cause further roll flattening. If (μ) could be reduced by improved lubrication, the value of this limiting reduction would be increased enabling thinner strip to be rolled.

consequently the roll gap will increase during the rolling, as well as being increased slightly by the elastic roll-flattening already exist under very high loading and the mill "spring back", which is the deformation will be elastic-plastic of the mill, it is an important factor which must be taken into account when setting the roll gap for a given pass .Some reheological model was used by (Grubin and Vinogradova, [9] and Dowson and Higginson, [6] such as the ones used in elastohydrodynamic lubrication (Cheng, [4], (Wilson and Walowit, [13] in their plasto- hydrodynamic analysis of the strip rolling,(Aggarwal and Wilson,[1],[2] solved numerically the equations which includes the permissible velocity profiles against various relevant flow.Their results can provide neither the local variation of flow properties nor the global behavior in any real metal forming lubrication since the continuity equation has not been incorporated in their analysis. (Yuan and Chern, [14] developed a theoretical hydrodynamic lubrication analysis which takes account of temperature dependent viscosity variation along as well as across the film thickness. (Kuniaki and zhrgaug,[8] carried out a series of experiments using a rolling type tirbo meter to investigate the frictional dependence on the average velocity of the lubricant V at the contact zone inlet and the relative sliding velocity ΔV between the roll and the work piece during deformation .

In this research undertake to gain further knowledge of the mechanism of lubrication in the roll gap by taking a model of lubricant entrainment under very high pressure using E.H.L. theory with the effect of elasto-plastic behavior of metal rolling strip which

prompted to develop an improved model. The theoretical results give good agreement when compared with an experimental one done by the previous workers.

II. Analysis

1. The Reynolds equation, which take into consideration, the isoviscous properties of the lubricant and the boundary conditions at the surfaces as derived by (Wilson and Aggarwal,1987):-

From equilibrium considerations the local velocity (u) is given by:-

$$u = \frac{1}{\mu}\left(\frac{z^2}{2}\frac{\partial p}{\partial x} - c_1 z + c_2\right) \quad \text{.....(1)}$$

The values of c_1 and c_2 could be obtained by taking (z=0),(u=u_1) and(z=h),(u=u_2). Then eq. (1) becomes:-

$$u = u_1 + \frac{(u_2 - u_1)z}{h} + \frac{\partial p/\partial x}{2\mu}(z^2 - h^2)$$

.....(2)

The volume flow rate per unit width (Q) is given by :-

$$Q = \int_0^h u\partial z \quad \text{.....(3)}$$

Substituting eq.(2) into (3) gives :-

$$\frac{h^3}{12}\mu\frac{dp}{dx} = \bar{u}.h - Q \quad \text{.....(4)}$$

Where:

$$\bar{u} = (u_1 + u_2)/2$$

$$\mu = \mu_0 e^{\gamma p}$$

2. The film thickness of the lubricant in eq.(4) can be represented as :

h total = h (elastic of the roller) + h (elastic-plastic deformation of the strip) .....(5)

h (elastic of the roller) could be delivered from E.H.L. theory :-

$$h_{elastic} = \frac{x^2}{2R} - \frac{1}{\pi E}\int p(s)\ln(x-s)^2.ds$$

.....(6)

note that in eq.(6) we have just the elastic deformation of one surface roller.

h (elastic-plastic deformation) could be obtained as :-

$$d \in ij = (d \in ij)_e + (d \in ij)_p \quad \text{.....(7)}$$

where

$$(d \in ij)_e = \frac{d\sigma_{ij}'}{2G} + \frac{(1-2\nu)}{E}\delta_{ij}d\sigma_{kk} \quad \text{.....(8)}$$

σij'=deviatric stress

G= modulus of rigidity

E= young modulus

ν =poisons ratio

δij dσkk= the component of mean stresses

Also the plastic strain is:-

$$(d \in ij)_p = d\lambda\frac{dQ}{d\sigma_{ij}} \quad \text{.....(9)}$$

Where

dλ=proportionality constant termed the plastic multiplier.

$\frac{\partial Q}{\partial \sigma_{ij}}$ = Plastic potential flow rate after yielding =σij`

$$\therefore (d \in ij)_p = d\lambda\,\sigma ij` \quad \text{.....(10)}$$

So that it can be seen that the total elastic-plastic strain for the strip is:

$$d \in ij = \frac{d\sigma_{ij}}{2G} + \frac{(1-2\nu)}{E}\delta_{ij}d\sigma_{kk} + d\lambda\sigma_{ij}'$$

.....(11)

Where

dεij = $\frac{\Delta h(i)}{hi}$ for the deformation of the strip.

Knowing that the value of dλ are variable for each element which is dependent on the strip flow rate Q and can be obtained as in the numerical method.

III. Theoretical Solution

1. assume the pressure distribution in the work zone as in (Bland and Ford,1948)

$$p^+ = \frac{k.y}{y_o}\left[1 - \frac{\sigma_o}{k_o}\right]e^{\eta.H} \quad \text{.....(12)}$$

$$P^- = \frac{k.y}{y_o}\left[1 - \frac{\sigma_i}{k_o}\right]e^{\eta.H} \quad \text{.....(13)}$$

Where η= the coefficient of friction between roll surface and Material.

2. Substitute the pressure distribution in the total film thickness equation h(total)
3. The values of h(i) and p(i) that obtained from steps(1) and (2) are substituted in eq.(4) and new values of u(i) and new position of (αn) .
4. The new values of h(i) are substituted in Reynolds equation to Finding a new pressure distribution p(i) in the work zone.
5. These new pressure values compared with the old

one so that the convergence criterion must be less than (.005).

$$\sum \left| p_{new} - p_{old} \right| / \sum p_{new} \le 0.005 \quad \text{.....(14)}$$

6. If the convergence criterion > 0.005 the new values of p(i) are Obtained from:

pnew(i) = wp(pnew(i) – pold(i)) + pold (i) .....(15)

Where WP: Relaxation factor.

7. These new values of p(i) are substituted in step (2) to find new values of film thickness.
8. Then we check the new value of p(i) at the edge of work zone with The yield stress of the material, if they are not equal then we take the new value of p(i) as :

p(i) = (p(i) – σy) /2 – pnew .....(16)

and then we return to step (2) to find new h(i).

IV. Numerical Method

The multilevel technique which have been used by (Lubrecht, Tennapel and Bosma, [10], (Conry and Cusano, [5], (Venner and Tennapel, [12] is used in solving this problem by dividing the work zone into 120 nodes with equal mesh size (Δ) where (Δ) = α(i+1) – αi .This mesh size is used in discretization of Reynolds equation.

The elastic film thickness is discredited as :

$$(hi)\ \text{elastic} = \left(\frac{xi^2}{2}\right) + \left(\frac{1}{\pi}\sum_{j=1}^{n} k_{ij}\, p_j\right) \quad \text{.....(17)}$$

where:

k(i,j) = (i – j + 1/2)Δ(ln| i – j + ½ Δ) – 1 – (i – j – ½)Δ(ln|i – j – 1/2|.Δ) – 1)

Mixed hardening

To cope with the directional change of friction at the neutral point (or region), the relative velocity Δ v of the roll to the strip (see Fig.1) is approximated by:

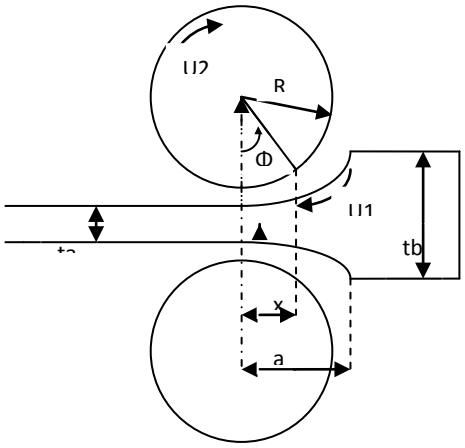

fig (1) : shows the strip rolling with lubrication

$$\Delta v = \sqrt{\left(\frac{1}{2}[(U_h)^2 + (V_h)^2 + (U_{h+1})^2 + (V_{h+1})^2]\right)}$$

$$U_h = u_h + R\omega \sin \alpha_h$$

$$V_h = v_h - R\omega \cos \alpha_h$$

$$U_{h+1} = u_{h+1} + R\omega \sin \alpha_{h+1}$$

$$V_{h+1} = v_{h+1} - R\omega \cos \alpha_{h+1}$$

so that the direction of the frictional shear stress need not prescribed , because the relative velocity Δv is always positive over the roll surface and the position of the neutral point (or region) is determined as a result of minimization of the functional.

The hardening behavior of most materials seems to be a combination of both isotropic and kinematics type of hardening .Sanda c.t,[11] used in his paper the effect of mixed hardening results in a modification of the yield surface which is written as :

$$f(\sigma_{ij} - \sigma_{ij}^{\ b}) - \sigma_y(\kappa) = 0 \quad \text{.....(18)}$$

The terms and dk are respectively obtained by assuming a kinematics hardening law.

For eq(11) it can be immediately written as :

$$d\in = [D]^{-1}.d\sigma + d\lambda \frac{df}{d\sigma} \quad \text{.....(19)}$$

where D is the usual matrix of elastic constants

$$d\lambda = \frac{1}{\left[A + a^T D_a\right]} a^T dD.d\in \quad \text{.....(20)}$$

$$a^T = \frac{df}{d\sigma_{ij}} = \left[\frac{\partial f}{\partial \sigma_x}\ \frac{\partial f}{\partial \sigma_y}\ \frac{\partial f}{\partial \sigma_z}\ \frac{\partial f}{\partial \tau_{yz}}\ \frac{\partial f}{\partial \tau_{zx}}\ \frac{\partial f}{\partial \tau_{xy}}\right]$$

,A=H which is the hardness function of the strip material.

V. Results and Discussion

In Fig.(3-a) shows the distribution of the pressure along the contact zone for (14%) percent reduction of steel strip using oil H (see table 1), v = 1.64 m/s , h = 5.75 mm, R = 0.14 m, t/σ1 = 0.024.In this figure there will be a comparison between theoretical and experimental result (done by Dow ,Kannel , and Bupava, 1975) which show some agreement between them . The elastic strain of the elasto-plastic material causes in the entering a decrease in the pressure and the stresses can be felt downstream a distance related to the relaxation time of the material and the velocity Δv while in the next region in the work zone before reaching the neutral point the value of Δv will be decreased and the plastic deformation begin causes very high pressure and the elastic deformation of the roller which introduced in the E.H.L. equations gives the fluctuating

of the pressure in this zone . After the neutral point to the exit region the pressure will be dropped to some value and then returned to increase and this is because Δv will be increased also causes the elastic part of the metal strip decreases the pressure roll.

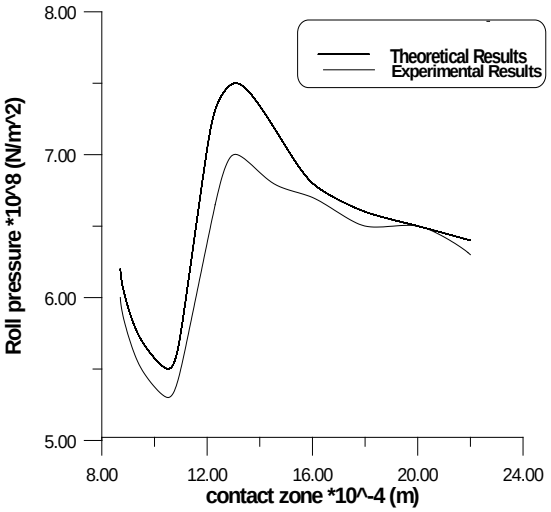

Fig.(3-a) Theoretical and experimental pressure distribution for 14 percent reduction of steel strip using oil H , V=1.64 m/s, R=.14m

In Fig (3-b) shows the variation of film thickness along the contact zone. In the region between(8-11)* m the film thickness increased with decreasing in the pressure then it full very rabidly with increasing the pressure and then increased after the neutral point and then decreases.

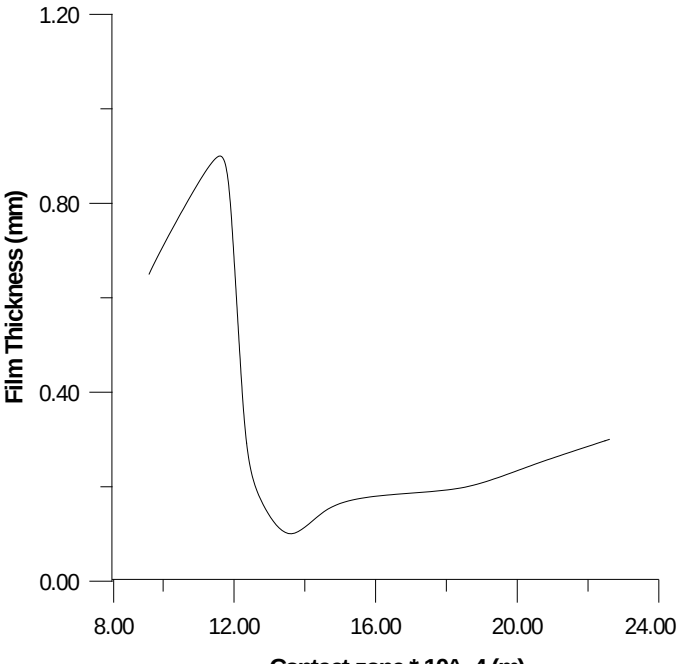

Fig. (3-b) Variation of film thickness with contact zone

The agreement between the practical and theoretical results is more pronounced in Fig .(4-a) which could be shown that at high reduction (30 percent) of steel strip by using oil c give a decrease in the pressure at point (30* m) and a sudden increases in the film thickness as shown in Fig (4-b) . This mean that at high reduction the using of elasto-plastic model with E.H.L. condition affect the pressure distribution and give more accurate results.

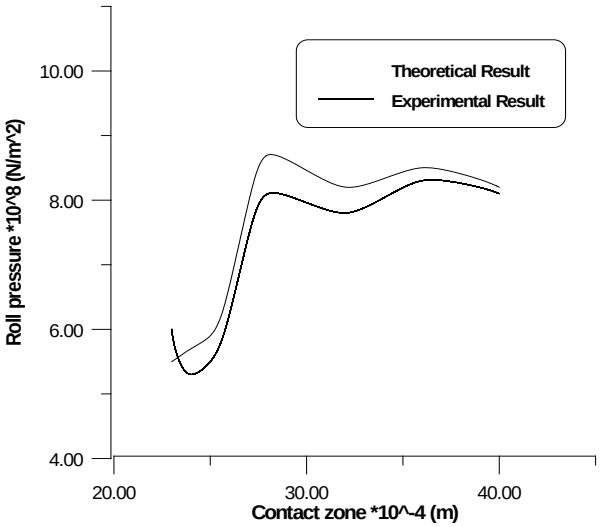

Fig.(4-a) Theoretical and experimental pressure distribution for 30 percent reduction of steel strip using oil C , V=1.65 m/s, R=.3m

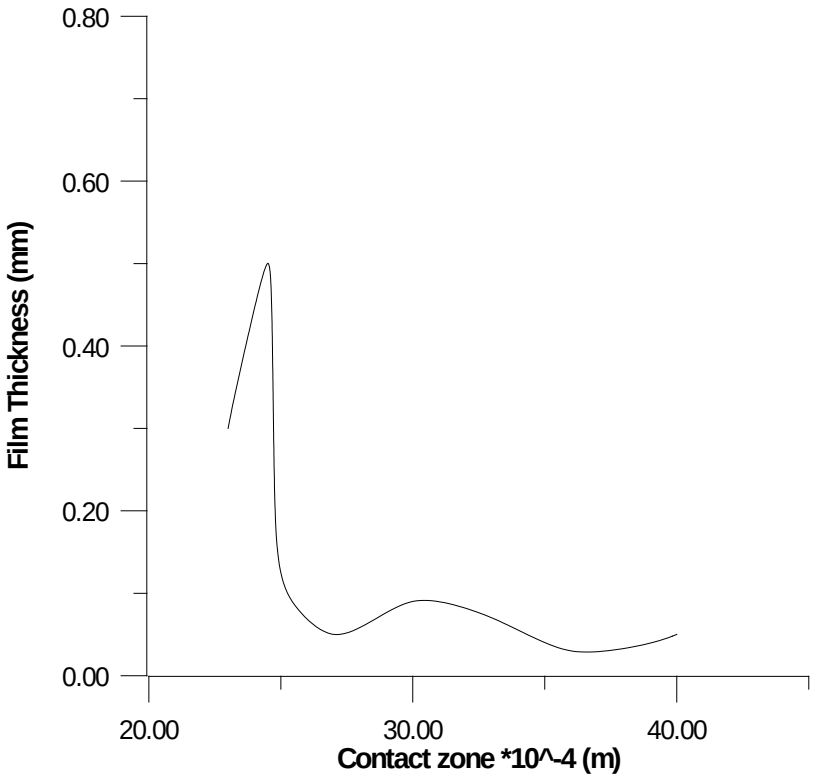

Fig (4-b) Variation of film thickness with contact zone.

In Fig.(5) it shows the relationship between the coefficient of friction and the speed of rolling at high reduction (30 percent) by using oil H and C. The coefficient of friction decreases with increasing the roll speed for values between 17-19 m/min and then will increased. This is because the effect of the relative speed on the pressure distribution and then on the viscosity of the lubricant in the contact zone.

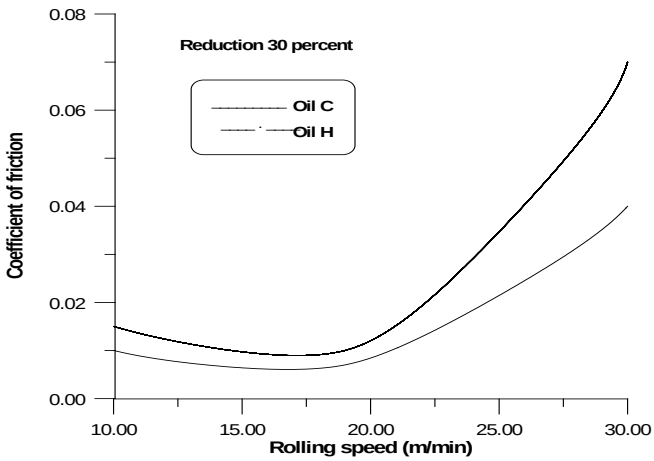

Fig (5) relationship between coefficient of friction and the Rolling speed.

VI. Conclusions

1. The aim of this research is to used the E.H.D lubrication with plastohydrodynamic of cold sheet rolling for determining the effect of lubrication on the pressure distribution and film thickness along the contacts zone .
2. The varaiation of the relative velocity Δv that have been calculated along the contact region give the position of the neutral point which variuas with the percent reduction of the strip and the viscosity of the oil .
3. The results shows that for heavy viscosity and low percent reduction of strip , the pressure distribution and film thickness along the contact region will be agreement with an experimental one for plasto-hydrodynamic lubrication while for high reduction and low viscosity the mixed theory of E.H.L and plasto-hydrodynamic lubrication be more accurate .
4. The effect of speed of the roller with lubricant on the coefficient of friction and then on the critical shear stress under plastic deformation of the strip have been investigated .

References Références Referencias

1. Aggarwal, B.B and Wilson, W.R.D.,(1980) "Improved thermal Reynolds equations" Proc. Leeds- Lyon symp. On Tribology , inst.Mech.Engrs. pp.152-161
2. Aggarwal, B.B and Wilson, W.R.D, (1987) " Thermal effects in hydro-dynamically lubricated strip rolling" Proc. .Leeds-lyon symp. On Tribology , Inst.Mech.Engr.pp.351-359
3. Bland, D.R. and Hug Ford, (1948) " The calculation of Roll force and torque in cold strip rolling with tensions" Proc.Inst.Mech.engrs.159.
4. Cheng .H.s.,(1966) " Plastohy-drodynamic

lubrication " , friction and lubrication in processing , ASME, NEWYORK.
5. Conry and Cusano, (1992) "Numerical method in the effect of an E.H.L. line contact " J. of Tribology , vol.114, pp.616.
6. Dowson and Higginson , (1976) "Elastohydrodynamic Lubrication ", Pergamon, Oxford.
7. Dow.T.A. Kannel, J.W. and Bupara.S.S., (1975) "A hydrodynamic lubrication theory for strip rolling including thermal effect" ASME journal of lubrication Technology, Vol.97 , pp.4-13
8. Dohda kuniaki , Wang zhrgang (1998) " Effects of average lubricant velocity and sliding velocity on friction behavior in mild steel sheet forming" , Journal of Tribology , Vol .120,pp724.
9. Grubin ,A.N. and Vinogradova ,I.E., (1949)"Investigation of the contact of machine components" TSNITMASH (Moscow), 30 (DSIR, London,Transl.337)
10. Lubrecht, Tennaple and Bosma, (1991) "Numerical simulation of the overall rolling of a surface feature in an E.H.L., line contact".J. of Tribology, Vol.113,pp777.
11. Sanda cleja-Tigoiu , (2002) "Small elastic strains in finite elasto-plastic materials with continuously distributed dislocations ", J.of.Theoretical and applied mechanics , vol. 28-29, pp.93-112.Belgrade.
12. 12- Venner and tennapel, (1990) " Advanced multilevel solution of the E.H.L. line contact problem " J of Tribology , Vol.112 , PP.426
13. Wilson, W.R.D. and Walwit, J.A, (1971) "An isothermal hydrodynamic lubrication theory for strip rolling with front and back tension " , In Tribology convection , I.Mech.E.London, pp.169-172.
14. Yuan. k and Chern.B.c (1990) " A thermal hydrodynamic lubrication analysis for entrained film thickness in cold strip rolling "Journal of tribology vol 112.pp.128.

Fig (2) table (1) properties of lubricants

Lubricant	Type of lubrication	Base viscosity (C.P.)	Temperature (1/K)	Coefficient of viscosity
C	Anaphthenic industrial oil fully formulated	93	0.0625	2.9
B	Heavy viscosity Anaphthenic industrial oil fully formulated	3738	0.107	2.5

Global Journal of researches in engineering
Mechanical and mechanics engineering
Volume 11 Issue 7 Version 1.0 December 2011
Type: Double Blind Peer Reviewed International Research Journal
Publisher: Global Journals Inc. (USA)
Online ISSN: 2249-4596 Print ISSN:0975-5861

"A Study of the Effect of Surface Defect Caused By Impact Load from Shock Wave on Wing Design in Transonic Speeds Using Classical Plate Theory"

By Dr.Fathi Alshamma, assma Hassan
Baghdad University.

Abstract - In this research the aerodynamic load have been determined in critical transonic speeds taking into consideration the shock wave effect along X-29 aircraft wing , first by using computational fluid dynamics in fluent program, then taking these results as an applied loads in the classical plate theory (c.p.t) to estimate these stresses depending on time and speeds of impact load as a major parameter, and a numerical method using F.E.M (Ansys 10) for confirming the results that obtained from analytical solution. Results shows that the value of pressure coefficient along the wing using (c.p.t) is higher then the experimental one which is more save in design for transonic flow and its appeared that the position of maximum effect of shock wave on wing section depends on angle of attack , sweep angle and duration time of the shock wave load .

Keywords : *shock wave , impact , classical plate theory , fluent program, ANSYS 10 .*

GJRE-A Classification :

A STUDY OF THE EFFECT OF SURFACE DEFECT CAUSED BY IMPACT LOAD FROM SHOCK WAVE ON WING DESIGN IN TRANSONIC SPEEDS USING CLASSICAL PLATE THEORY

Strictly as per the compliance and regulations of:

"A Study of the Effect of Surface Defect Caused By Impact Load from Shock Wave on Wing Design in Transonic Speeds Using Classical Plate Theory"

Dr.Fathi Alshamma[α], assma Hassan[Ω]

Abstract - In this research the aerodynamic load have been determined in critical transonic speeds taking into consideration the shock wave effect along X-29 aircraft wing , first by using computational fluid dynamics in fluent program, then taking these results as an applied loads in the classical plate theory (c.p.t) to estimate these stresses depending on time and speeds of impact load as a major parameter, and a numerical method using F.E.M (Ansys 10) for confirming the results that obtained from analytical solution. Results shows that the value of pressure coefficient along the wing using (c.p.t) is higher then the experimental one which is more save in design for transonic flow and its appeared that the position of maximum effect of shock wave on wing section depends on angle of attack , sweep angle and duration time of the shock wave load .

Keyword : shock wave , impact , classical plate theory , fluent program, ANSYS 10 .

I. Introduction

In many modern design of aircraft it was needed for operational efficiency to develop a complex process of determining the local mach number along the wing taking into consideration the unsteady aerodynamic phenomena in the context of nonlinear flow behavior for transonic flow which is terminated by a shock wave allowing the flow to slow down to subsonic speeds .This causes the shock wave to be propagated from leading edge to the trailing edge so a complicated in the analytical analysis specially with free stream mach numbers from M = 0.6 to M = 1.4 which must airplane kept flying fast enough to encounter transonic flow. This required that the viscous effect and incompressibility must be taken into consideration .

The loads are caused by aerodynamic forces and interacted with elastic forces which have been taken as a static or steady state systems knowing that aero elasticity, R.Duvigneau [1] have been solved this problem taking into consideration the aerodynamic shape optimization with uncertain operating conditions is addressed in this paper, a two-level modeling strategy is proposed, that relies on the use of CFD simulations in conjunction with metamodels. Also Andrey M.Shevchenko (etal) [2] compute the transonic flows over a complex 3D aircraft configuration, a viscous/in viscid interaction method is developed by coupling an integral boundary-layer solver with an Euler solver, showing results in good agreement with the wind tunnel data The object of this contribution is to introduce an efficient interactive boundary-layer method. Another object of this paper is to present a far-field drag prediction technique.

While for dynamic aero elasticity Gareth A.Vio (etal) [3] taken the main objective of the work is the characterization of the dynamic response of aeroelastic models resulting from coupled Computational Fluid Dynamic and Finite Element .At higher free stream Mach numbers the shock wave has moved all the way to the trailing edge at steady-state conditions and zero angle of attack and cannot move any further, despite the bending and twisting motion. Consequently, the aero elastic instability disappears and the system becomes stable again.

Atef. Alshabu etal [4] taken into consideration the preliminary experimental and numerical investigation of wave processes taking place in the flow field on a supercritical airfoil in a defined Mach and Reynolds number range. Time-resolved pressure measurements performed, reveal the unsteady behavior of these waves, the experimental and numerical results are in good agreement. some researchers using a numerical study for shock wave oscillations Akira oyama (etal) [5] have been obtained a method to understand Mach number effect on flow field over a delta wing with blunt leading edge in supersonic and high angle of attack region .The present results indicate that a delta wing with blunt leading edge can be mixed flow of two different types of flow structure in supersonic and high angle of attack flow region and the location of the boundary of the two types of flow moves toward the apex of the wing as the free-stream Mach number increases.

Author[α] : Assistant.proff, Department of mechanical Engineering, Baghdad university , Iraq
Author[Ω] : Licture, Department of mechanical Engineering, Baghdad university , Iraq

Mylene thiery and Eric coustols[6] have been deals with recent numerical results from ongoing research conducted at ONERA/DMAE regarding the prediction of transonic flows ,simulation was performed to demonstrated the real impact of all lateral wind – tunnel walls on such a flow . Also R.Bur etal [7] investigate and analyses the response of a transonic channel flow when the shock wave is subjected to a periodic motion at a well defined and controlled frequency in the shock oscillation region. The good agreement between the evolutions of the measured and computed fluctuating quantities which is part of a study investigating the prediction of the aero elastic behavior of aircraft subjected to non-linear aerodynamic forces .
Antony Jamson [8] examines the use of computational fluid dynamics as a tool for aircraft design . the paper discusses the use of techniques drawn from control theory to determine optimal aerodynamic shapes . Essential elements of algorithm design are discussed in detail with unified approach to the design of shock capturing schemes .

The geometry and the swept angle affect the design of the wing as in P.C Steimle etal [9] Wind tunnel tests with force and pressure measurements have been performed using an oscillating rigid swept wing to investigate unsteady aerodynamic phenomena in the context of non-linear flow behavior and the development of aero elastic instabilities in the transonic flight regime. V.N.Zudov and E.A.Pimonov [10] investigated an external flow around supersonic airplanes with a large swept wing and low aspect ratio . experimental investigation indicate that at some interaction regimes of the stream wise vortex with shock wave , a vortex explosion arises to model with different types of the stream wise vortex with the inclined shock wave using three dimensional non stationary Eulers equations .

In this research two things have been taken to be investigated, the first one is to modify the Mach number which consist the effect of shock wave position on the wing surface for mediums that comes in transonic flow on the stress distribution along the shell of the wing as an low impact velocity load in the mach number and then substituted in classical plate theory for finding the deflection and the pressure coefficients distribution. The second one is using ANSYS 10 as a finite element method for determining the position of the shock wave pressure value which depends on the Mach number for transonic flow.

II. Analytical Solution

In this section the analysis of the wing as a thin elastic , isotropic , homogeneous , clamped rectangular plate of uniform thickness h with sides a and b based on the Levey hypothesis .
The governing equation of the subject plate is derived by utilizing the Hamiltons principle :

$$\delta \int_{t_1}^{t_2} (T - U - V)dt = 0 \cdots\cdots (1)$$

Where T=the kinetic energy , U= the strain energy , V= the potential energy produced by external loads and δ=the first variation operator .

The strain energy U is given by :

$$U = W \cdot \tfrac{1}{2} \int_0^a \int_0^b \left(M_x k_x + M_y k_y + 2M_{xy} k_{xy}\right) d_x d_y \ldots\ldots (2)$$

Where k_x , k_y and k_{xy} = the curvatures and twist of the middle surface respectively . k_x = -w,xx , k_y = -w,yy , k_{xy} =-w,xy and w(x,y,t)= the deflection

M_x = the bending moment per unit width =

$$-Dd(x,y)\left(w_{,xx} + \mu w_{,yy}\right) \cdots\cdots (3)$$

M_y = the bending moment per unit width =

$$-Dd(x,y)\left(w_{,yy} + \mu w_{,xx}\right) \cdots\cdots (4)$$

M_{xy} = the twisting moment =

$$-(1-\mu)Dd(x,y) - w_{xy} \cdots\cdots\cdots (5)$$

Where D = the flexural rigidity of the plate = $Eh^3 / 12(1-\mu^2)$

E= young modulus and μ = poisons ratio

The strain energy becomes :

$$U = \frac{1}{2}\int_0^a\int_0^b D \cdot d(x,y) \cdot \left[(k_x)^2 + (k_y)^2 + 2\mu k_x k_y + 2(1-\mu)(k_{xy})^2\right] dxdy \ldots\ldots(6)$$

Now the variation of potential energy can be expressed as :

$$V = \iint_{00}^{ab} (p.w - \rho.g.h.Y)dxdy + \int_0^b (M_o)_x.w_{,x}dy + \int_0^a (M_o)_y.w_{,y}dx$$

……..(7)

Where Y= the variation in the altitude of the airplane
P = external forces prescribed from boundary edges

$(M_o)_{x,y}$ = the aerodynamic pitching moment of the aircraft in the x , y direction respectively
The kinetic energy can be written as :

$$T = \frac{1}{2}\rho \cdot h\int_0^a\int_0^b (v^2 + (w^{\bullet})^2 dxdy \ldots\ldots(8)$$

Where v= the free stream speed of the airplane

From compressibility effect in aerodynamic flow causes change in the density and this will lead to pressure change especially when the Mach number is greater than 1 , various types of waves can form in the flow

So that in equation (8) the value of v can be substituted as :

$$v^2 = \frac{p - p_{\infty}}{\frac{1}{2}\rho c_p} \ldots\ldots\ldots(9)$$

Where $p - p_{\infty}$ is the gauge pressure which is various along the airfoil , c_p is the pressure coefficient along the airfoil and its value depend on the magnitude of the mach number . the transonic problem is difficult because it is inherently nonlinear , and the steady solution changes math type , being elliptic in the subsonic portion of the flow and hyperbolic in the supersonic part of the flow .

So the value of c_p can found by substitute eq (6) ~ eq(9) into eq (1) and the differential equation of motion can be obtained associated with the following boundary conditions :-

$$(w)_{x=0} = 0 \ , \ (\frac{\partial w}{\partial x})_{x=0} = 0 \ldots\ldots\ldots(10)$$

$$(M_X)_{X=0} = (\frac{\partial^2 w}{\partial x^2} + \mu\frac{\partial^2 w}{\partial y^2})_{x=0} = 0 \ldots\ldots(11)$$

$Dd\left(\frac{\partial^2 w}{\partial x^2} + v\frac{\partial^2 w}{\partial y^2}\right) = m_x$ along the edge x=a …….. (12)

The similar boundary conditions can be written along the edges y=0 and y=b .

III. The Shock Wave Effect on The Boundary Condition in Transonic Flow

The load applied on the wing consider as a subsonic condition depending on the value of the pressure coefficient c_p that obtained from the solution of the above equation of motion .

Adding to the boundary conditions that the value of c_p in transonic flow have a value at a point on the airfoil a critical value indicate that the region where the flow is locally supersonic or isentropic flow and the good basic formula for compressible flow is :-

$$c_{p_{crit}} = -\frac{2}{\gamma M_{\infty}^2\left[1 - \left\{\frac{2}{\gamma+1} + \frac{\gamma-1}{\gamma+1}M_{\infty}^2\right\}^{\frac{\gamma}{\gamma-1}}\right]} \ldots\ldots\ldots (13)$$

So that the pressure coefficient obtained from plate theorem compared with the $c_{p_{crit}}$ if it reach this value then the load at this region have been taken as shock wave load and the behavior of the load with time as an low velocity impact with the following assumption [11] :-

$$P = P_o(1 - \frac{\tau}{t})\exp(-\alpha\frac{\tau}{t}) \ldots\ldots\ldots(14)$$

Where p_o = the max load per unit width .

t = the time duration of the shock wave .

τ = the period of time duration of the shock wave .

α= critical damping coefficient ranges between 2 to 20 %

while below the $c_{p_{crit}}$ value the load assumed to be represent as p(x ,y) by a Fourier series as :-

$$p(x,y) = \sum_{m=1}^{\infty}\sum_{n=1}^{\infty} a_{mn} \sin\frac{m\pi x}{a}\sin\frac{n\pi y}{b} \dots\dots\dots\dots (15)$$

And this will effect on the pressure distribution and the value of the locally much number along the wing cord .

IV. The Effect of The Defects on The Pressure Coefficient

In the surface of the wing there will be some defects which come from the metal working of the shell that covers the reinforced beams of the wing or from the cycling aerodynamic pressure under shock waves that causes a surface crack initiation in the region of high local mach number value along the wing . this defects can be detected in this analysis in the region of high shock waves by taking the variation of the thickness of the plate and the depth of the surface crack as a percentage of the plate thickness along the defect. This will cause decrease in the value of the flexural rigidity of the plate D and the pressure coefficient c_p leading to increase the value of the stresses around the crack causes the stress intensity factor increased and the defect will be start to propagate .

It must be noticed that the stress intensity factor have been determined from the max principal stress which cab calculated by the equation :-

$$\sigma_{1,2} = \frac{\sigma_x + \sigma_y}{2} \pm \sqrt{\left(\frac{\sigma_x - \sigma_y}{2}\right)^2 + \tau_{xy}^2} \cdots\cdots (16)$$

And the angle inclined of the crack with the principle axis can be calculated by the equation :

$$\alpha = \frac{1}{2}\tan^{-1}\left(\frac{2\tau_{xy}}{\sigma_x - \sigma_y}\right) \cdots\cdots\cdots (17)$$

So the elastic stress for a point located a distance r and θ from the crack tip is given by :-

$$\sigma_x = \frac{KI}{\sqrt{2\pi r}}\cos\frac{\theta}{2}\left[1 - \sin\frac{\theta}{2}\sin\frac{3\theta}{2}\right] - \frac{KII}{\sqrt{2\pi r}}\sin\frac{\theta}{2}\left[2 + \cos\frac{\theta}{2}\cos\frac{3\theta}{2}\right] + (\sigma_1 - \sigma_2)\cos 2\alpha \dots\dots (18)$$

$$\sigma_y = \frac{KI}{\sqrt{2\pi r}}\cos\frac{\theta}{2}\left[1 + \sin\frac{\theta}{2}\sin\frac{3\theta}{2}\right] + \frac{KII}{\sqrt{2\pi r}}\sin\frac{\theta}{2}\left[\sin\frac{\theta}{2}\cos\frac{\theta}{2}\cos\frac{3\theta}{2}\right] \dots\dots (19)$$

$$\tau_{xy} = \frac{KI}{\sqrt{2\pi r}}\left[\sin\frac{\theta}{2}\cos\frac{\theta}{2}\cos\frac{3\theta}{2}\right] + \frac{KII}{\sqrt{2\pi r}}\cos\frac{\theta}{2}\left[1 - \sin\frac{\theta}{2}\sin\frac{3\theta}{2}\right] \dots\dots (20)$$

$$KI = \frac{\sigma_1\sqrt{\pi a}}{2\left[\left(1 + \frac{\sigma_2}{\sigma_1}\right) + \left(1 - \frac{\sigma_2}{\sigma_1}\right)\cos 2\propto\right]} \dots\dots\dots (21)$$

$$KII = \frac{\sigma_1\sqrt{\pi a}}{2\left[\left(1 - \frac{\sigma_2}{\sigma_1}\right)\sin 2\propto\right]} \dots\dots\dots (22)$$

And these stresses have been calculated for a specific angle of attack and swept angle , also it must be noticed that this solution is valid only for surface crack less than 0.5h because the classical plate theory assumed that the middle line along the thickness of the plate will remain straight and its position in the z direction will changed with the varying thickness .

V. Numerical Analysis

In this research FLUENT software and ANSYS software had been used.

First FLUENT program part:

The X- 29 aircraft wing had been taken with NACA0004

The two dimensional model drawn in many sections in GAMBIT program as shown in Fig (1) .

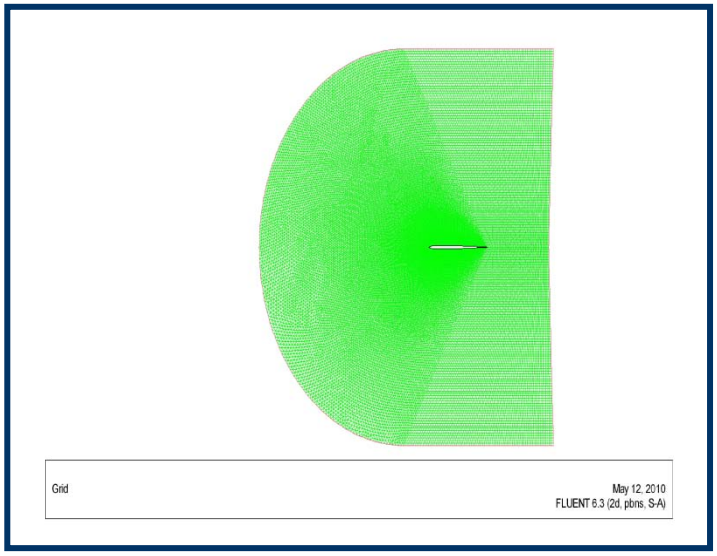

Figure (1) : mesh in Gambit

the mesh have done using quadrilateral element, boundary conditions were , 1) airfoil surface as wall 2) circumference about airfoil are all pressure far field type . Airflow applied on airfoil sections in FLUENT in order to obtain pressure distribution on wing body. Specifications had been used are: Pressure based, two dimensional, implicit formulation, steady time, absolute velocity, Green - Gauss cell - based solver option. Air properties; Ideal-gas, Sutherland viscosity (as shown in Fig 2), solution controls; modified turbulent viscosity, standard pressure, second order density, momentum, viscosity ,For Mach number from (.8, 1, 1.2, and 1.6) iteration has been done and pressure distribution for five sections on wing in order to find average resultant pressure on wing for each Mach number.

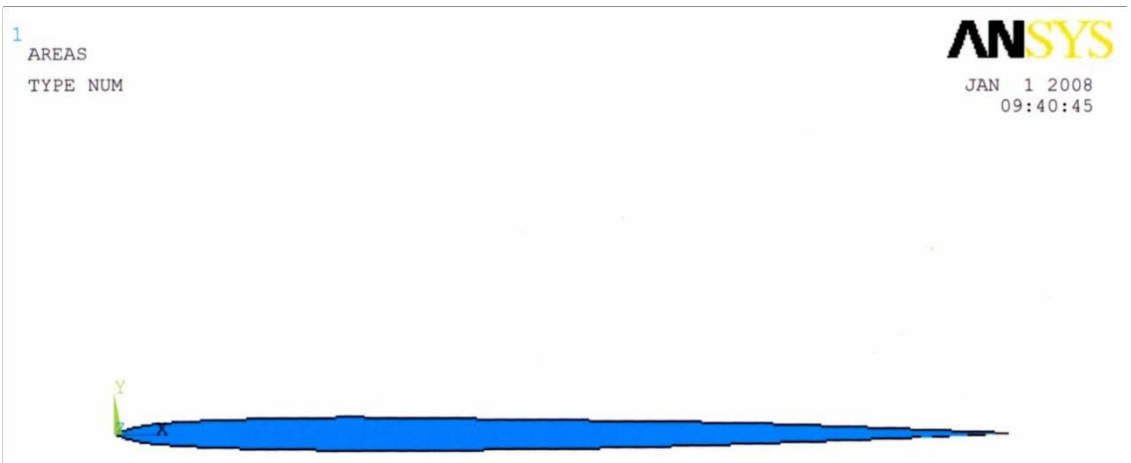

Fig (2) : the profile of airfoil and the origin of the axis.

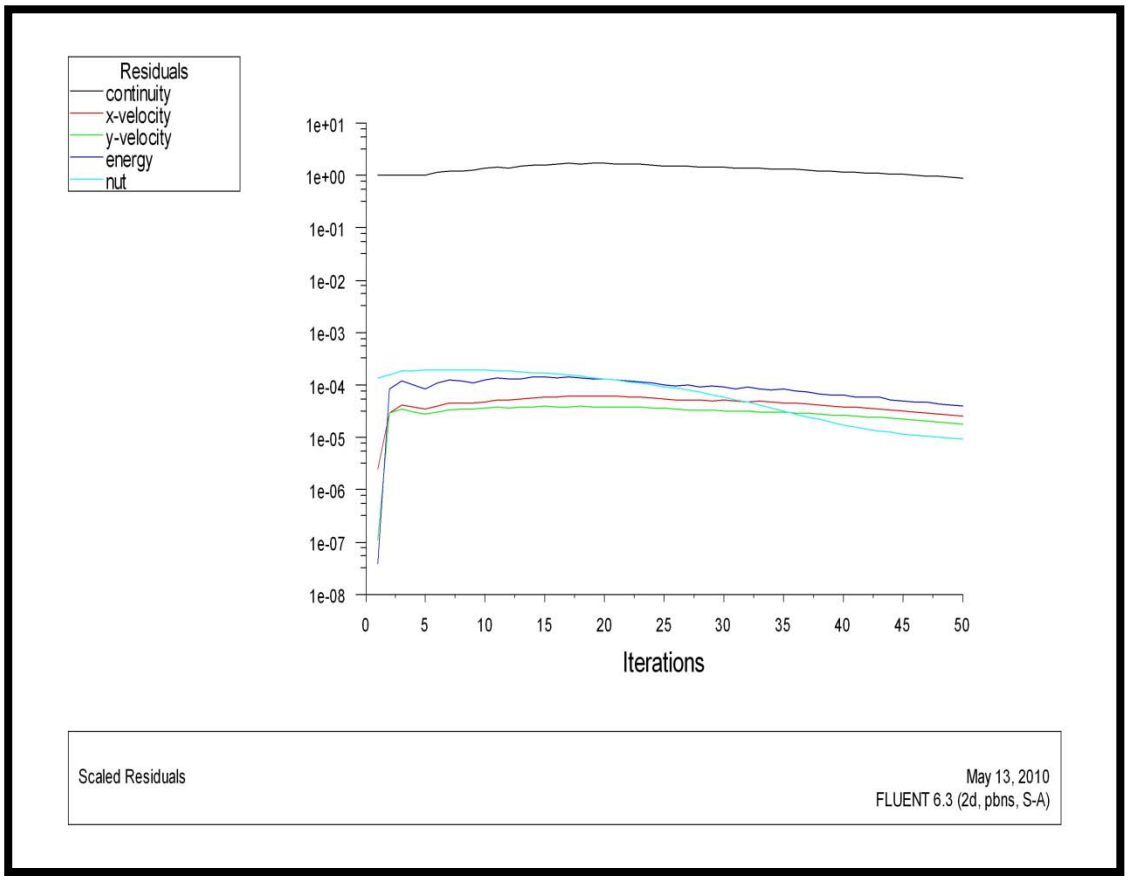

Figure (3) : iterations of solver

ANSYS program first the full X-29 aircraft wing drawn with section NACA0004 but only a skin (shell element) Second part; structural analysis in ANSYS program Shell thickness (0.01m) material used (aluminum) young modulus 70e9 Pascal, Poisson ratio 0.3 density 2800 kg/m3 element type was shell 63 for isotropic type material as shown in Fig (4).

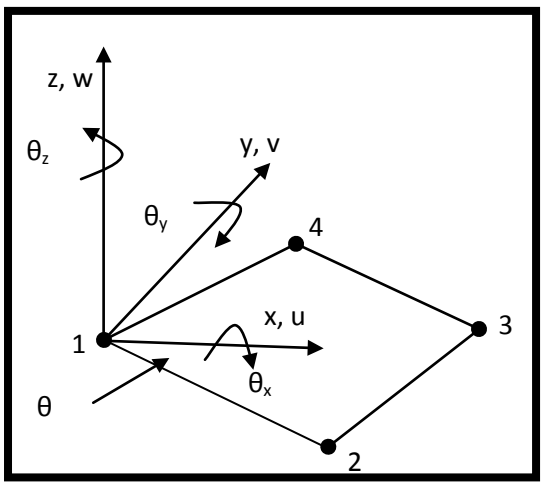

Figure (4) : shell 63 element

The boundary conditions taken are clamped from wing root and free for all other points like cantilever beam as shown in fig (5a,b,c), the pressure distributed on the wing area for example at Mach = 0.8 average pressure then static analysis have been done to obtain stress distribution and deflection distribution on the wing ,each velocity of air generates a different value of pressure on the other hand , the dynamic load function applied (exponential relationship) with time to find pressure change with time , so we take deferent times (0 to 1) and calculate pressure at each time and apply that pressure on wing area in ANSYS also to get stress and deflection distribution at each value to compare stress values and the position of maximum stress for times and velocities of air changes .

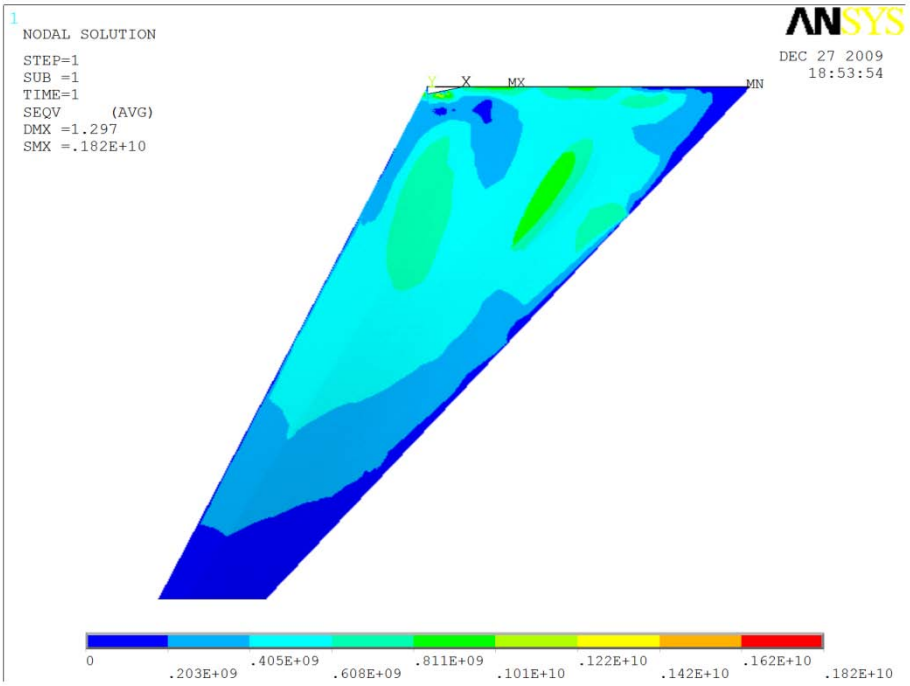

Fig (5-a) : the pressure distribution at mach number 0.6

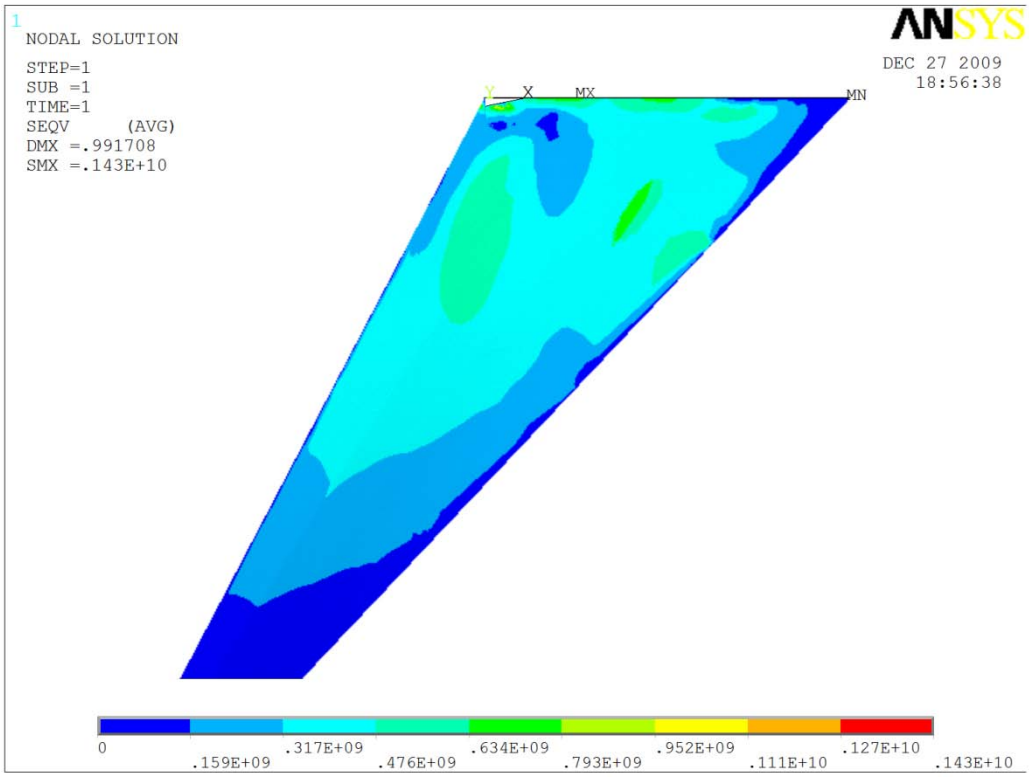

Fig (5-b) : the pressure distribution at mach number 0.8

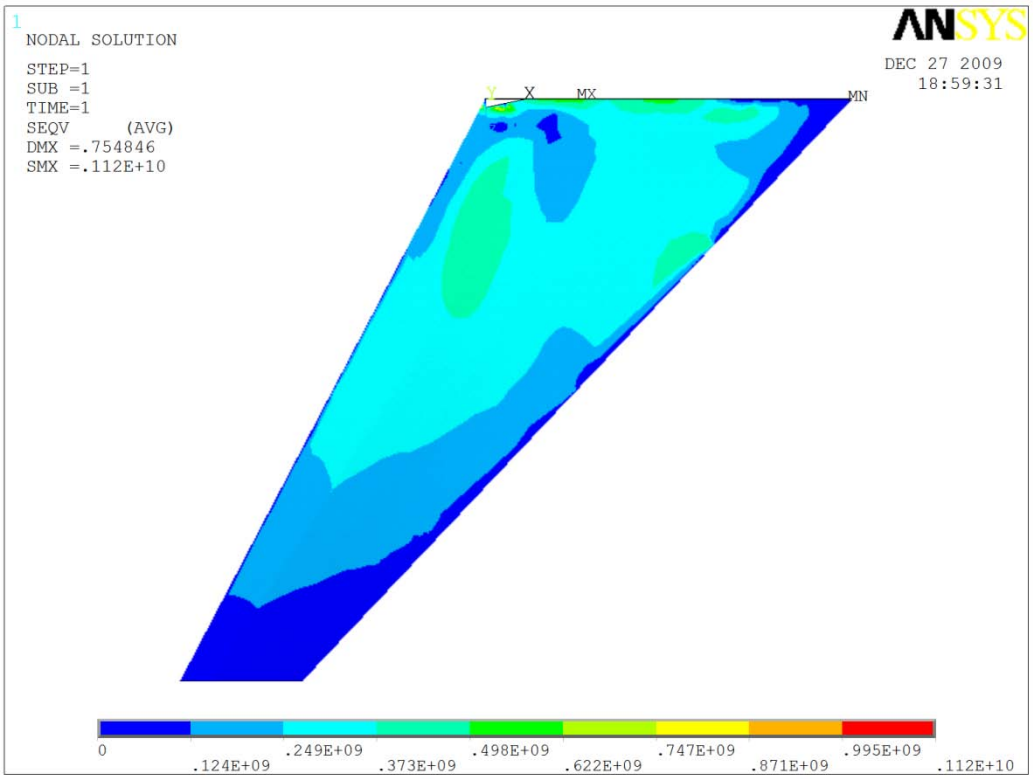

Fig (5-c) : the pressure distribution at mach number 1.0

VI. Model Generation by Ansys10

The ultimate purpose of a finite element analysis is to re-create mathematically the behavior of an actual engineering system . In other words, the analysis must be an accurate mathematical model of a physical prototype . In the broadest sense, the model comprises all the nodes, elements, material properties, real constants, boundary conditions and the other features that used to represent the physical system. In ANSYS10 terminology, the term model generation usually takes on the narrower meaning of generating the nodes and elements that represent the special volume and connectivity of the actual system. Thus, model generation in this study will mean the process of defining the geometric configuration of the model's nodes and elements. The program offers the following approaches to model generation :(a) Creating a solid model , (b) Using direct generation and (c) Importing a model created in a computer-aided design CAD system. The method used in this research to generate a model is solid model. In solid modeling some one can be described the boundaries of the model, establish controls over the size and desired shape elements automatically, i.e. drawing the three dimensional model and meshing using meshtool. Solid modeling is usually more powerful and versatile than other modeling, and is commonly the preferred method for generation models. The one Dimension model is done by drawing and dragging to get three dimension model then meshing with element shell63 .

Procedure is presented for modeling of wing skin shell with stiffeners by ANSYS10 software by using solid-modeling approach method. Hence the following is the program of modeling the characteristics of wing skin shell in APDL (ANSYS Parametric Design Language). (in the end of this file)

VII. Shell 63

SHELL63 has both bending and membrane capabilities. Both in-plane and normal loads are permitted. The element has six degrees of freedom at each node: translations in the nodal x, y, and z directions and rotations about the nodal x, y , and z-axes. Stress stiffening and large deflection capabilities are included. A consistent tangent stiffness matrix option is available for use in large deflection (finite rotation) analyses. Other elements are SHELL181 (plastic capability) and SHELL281 (midside node capability) .

SHELL63 Assumptions and Restrictions

- Zero area elements are not allowed. This occurs most often whenever the elements are not numbered properly.
- Zero thickness elements or elements tapering down to a zero thickness at any corner are not allowed.
- The applied transverse thermal gradient is assumed to vary linearly through the thickness and vary bilinearly over the shell surface.
- An assemblage of flat shell elements can produce a good approximation of a curved shell surface

provided that each flat element does not extend over more than a 15° arc. If an elastic foundation stiffness is input, one-fourth of the total is applied at each node. Shear deflection is not included in this thin-shell element.

- A triangular element may be formed by defining duplicate K and L node numbers as described in Triangle, Prism, and Tetrahedral Elements. The extra shapes are automatically deleted for triangular elements so that the membrane stiffness reduces to a constant strain formulation. For large deflection analyses, if KEYOPT(1) = 1 (membrane stiffness only), the element must be triangular.
- For KEYOPT(1) = 0 or 2, the four nodes defining the element should lie as close as possible to a flat plane (for maximum accuracy), but a moderate amount of warping is permitted. For KEYOPT(1) = 1, the warping limit is very restrictive. In either case, an excessively warped element may produce a warning or error message. In the case of warping errors, triangular elements should be used (see Triangle, Prism, and Tetrahedral Elements).

VIII. Analytical and Numerical Results

From numerical analysis of distribution the pressure along the wing cord , it can be found that the peak pressure coefficient is not affected by changing mach number from (0.6) to (1.4) as shown in figure (6) while when using these values of the leading edge of the wing in the main equation of the analytical solution of this research and finding the value of c_p along the rectangular plate as shown in figure (7) , it can be seen that for mach number below 1 , the theoretical results is the same when compared with the numerical one and this is because the value of c_p is not reach the critical value .

When using much number greater than 1 the numerical results shows different behavior then the theoretical results and this is because the value of c_p at some regions become greater than the critical value and the load substituted as an impact load and its value taken from eq (14) so that the effect of shock wave have been pronounced and its peak values increased with increasing the mach number when its position become nearer to the trailing edge in the x direction . also in the y direction on the face of the airfoil the effect of aerodynamic pitching , yawing and rolling moments increased the potential energy non linearly causes a fluctuating of the value of c_p higher than the experimental values from previous researches which give more safety in the design and must be avoided in the design of air craft wing as shown in Fig (8).

In fig (9) it can be shown using the analytical solution that the behavior of pressure coefficient c_p will be changed along the plate when there is defect of length 4 mm with different surface depth of (0.1) of thickness h and there will be many asperities of shock waves and are much higher than the plate without defect causes sudden change in the aerodynamic pressure and this is because the variation of the stress intensity factor at the edge of the crack along the time of impact of shock wave in period time τ =(0.25 , 0.5 , 0.75) of the total impact time t so that it must be avoided in the design of airfoil for specified angle of attack and swept angle . It can be seen from Fig (10) the percentage of increasing the pressure coefficient and locally mach number will be max at 0.5 t with sudden drop at the end of 0.75 t .

IX. Conclusion

A new method have been used in this research for calculating the stress distribution on a surface of wing for a specific angle of attack and swept angle by using classical plate theory combined with numerical results by ansys10 .

Also the effect of the defects at the surface of the wing on the pressure coefficient c_p and the values of stress intensity factor at the edge of the crack tip have been studied during the time of shock wave in transonic flow .

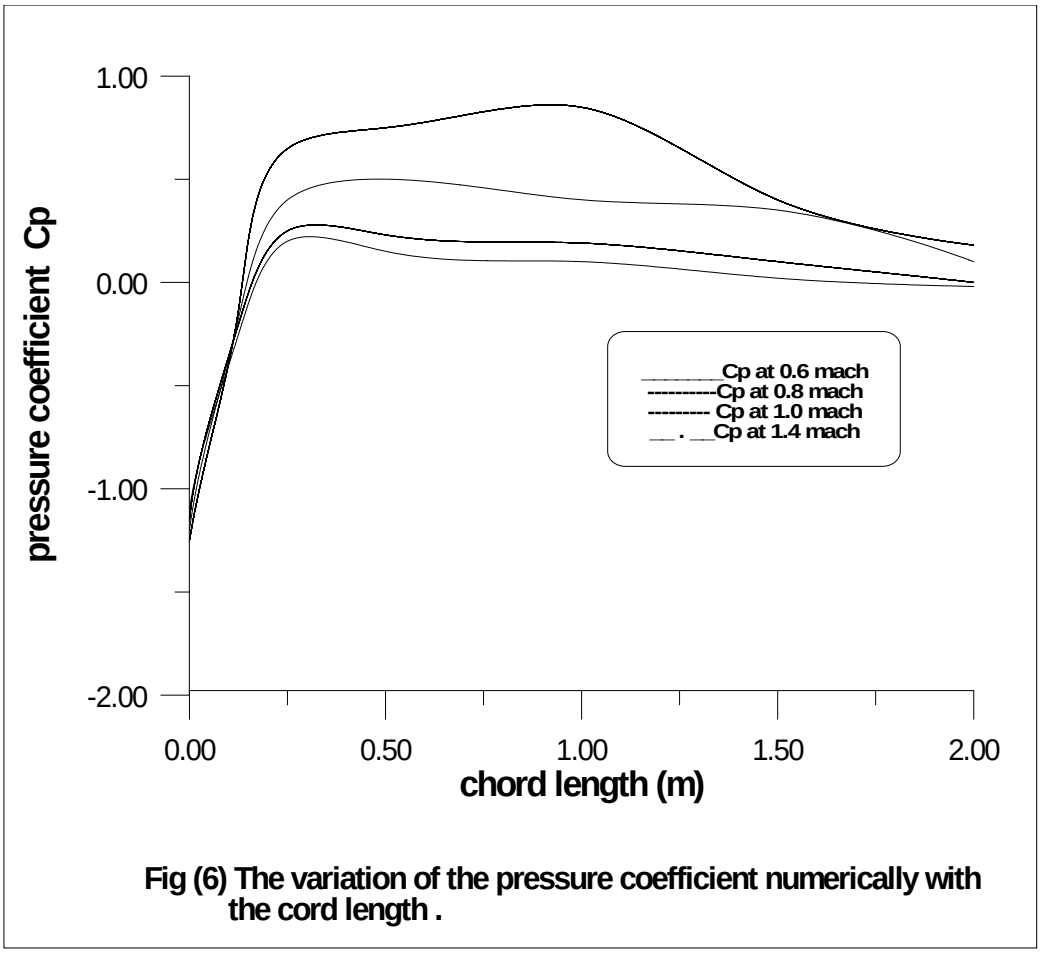

Fig (6) The variation of the pressure coefficient numerically with the cord length .

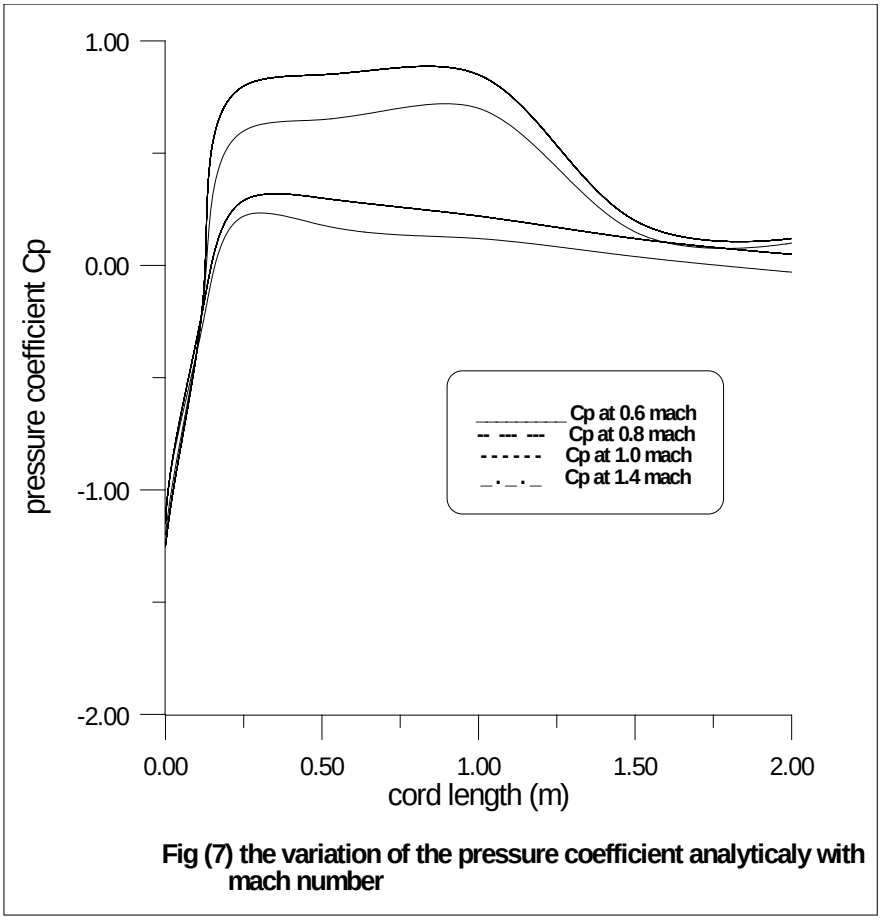

Fig (7) the variation of the pressure coefficient analyticaly with mach number

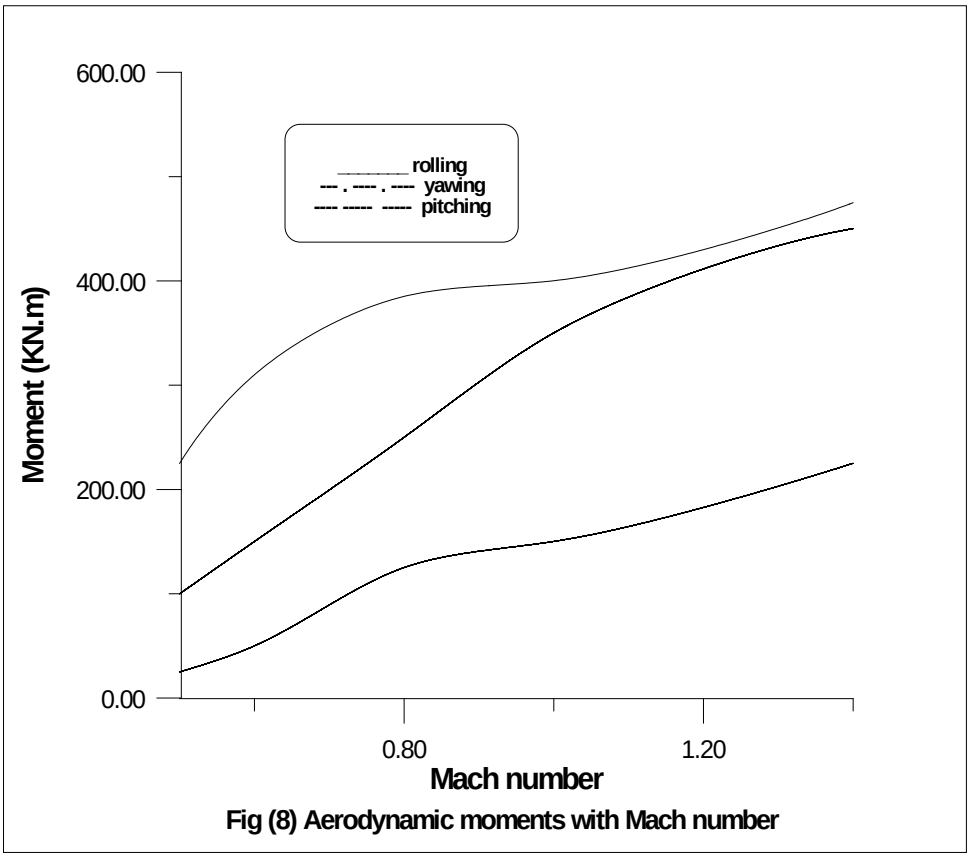

Fig (8) Aerodynamic moments with Mach number

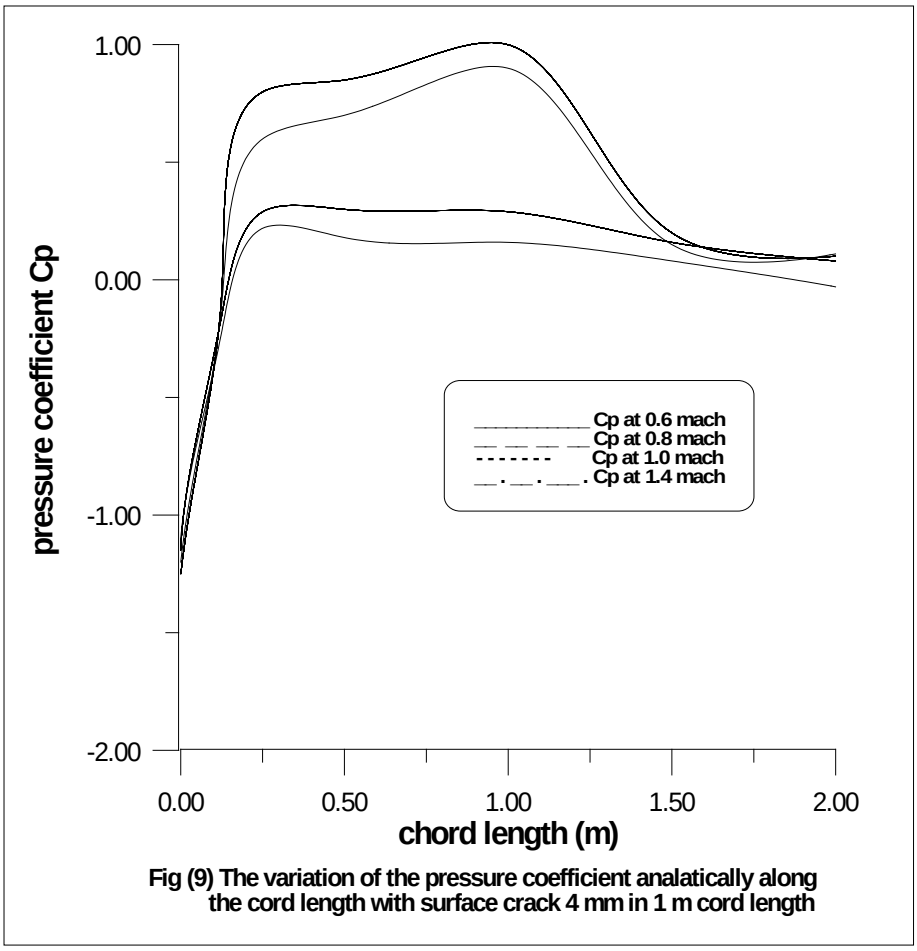

Fig (9) The variation of the pressure coefficient analatically along the cord length with surface crack 4 mm in 1 m cord length

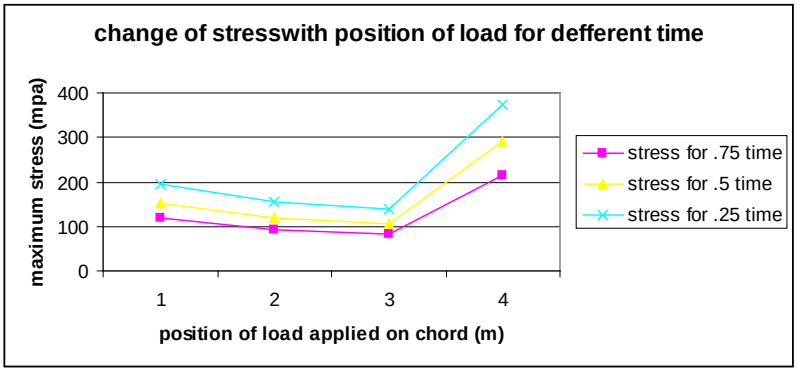

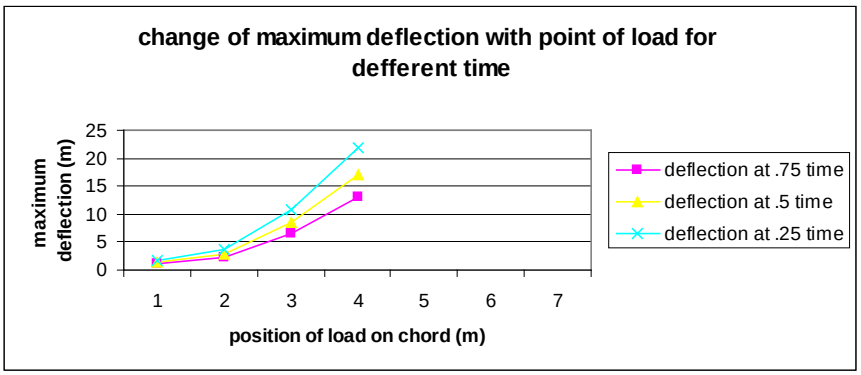

Fig (10) : the variation of the stress and deflection with impact time .

References Références Referencias

1. R. Duvigneau " Robust design of a transonic wing with un- certain Mach number " , J. Evolutionary methods for design optimization and control , Espain , 2007 .
2. Andrey.M . shevchenko , Ivan . Nkavun , Alexender . A . Pavlov and Valery. I. Zapryogave , "
3. Gareth.A.Vio , Grigorios Dimitriadis , E. cooper , Ken .Badcock , Mark . A . Woodgate and Abdul . M . Rampurawalc " Aero elastic system identification using transonic CFD data for a wing /store configuration " Aerospace science and technology ,vol 11 , issus 2-3 , p. 146-154 , 2007
4. Atef Alshabu , Herbert Olivier and Kliout chlnikov " Investigation of upstream moving pressure waves on a supercritical airfoil " , Aero space science and technology , vol 10 , issue 6 , p.465 – 473 , 2006
5. Akira oyama , masato Ito , Genta Imai , sejji Tsutsami , Nobuo Amitani and Kozo Fujji " Mach number effect on flow field over a delta wing in supersonic region " ,American institute of aeronautics and astronautics , 2008 .
6. Mylene Thiery and Eric coustols " Numerical prediction of shock induced oscillations over a 2D airfoil influence of turbulence modeling and test section wall " , International journal of heat and fluid flow , vol 27 , issue 4 , p. 661 – 670 , 2006 .
7. R.Bur , R. Benary , A . Galli and P. Berthouze " Experimental and numerical study of forced shock wave oscillations in a transonic channel " Aero space science and technology , vol 10 . issu 4 , p. 265 – 278 , 2006 .
8. Antony jamson " A perspective on computational algorithms for aerodynamic analysis and design " , 2001
9. P.C.Steimle , W.Schroder , W. Limberg and W.Althaus " Unsteady pressure measurement on an osillaating swept wing in transonic flow " , xx1 ICTAM ,15 – 21 august , Warsaw , Poland .
10. V.N Zudov and E.A.Pimonov " Study of interaction of stream wise vortex with a shock wave " Institute of theoretical and applied mechanics , SBRAS , Russia.
11. Loke Sworapa and R. Dharni " Laminated Architectural glass subjected to blast impact loading " 2005 .

This page is intentionally left blank

Global Journal of researches in engineering
Mechanical and mechanics engineering
Volume 11 Issue 7 Version 1.0 December 2011
Type: Double Blind Peer Reviewed International Research Journal
Publisher: Global Journals Inc. (USA)
Online ISSN: 2249-4596 Print ISSN:0975-5861

Investigating The Effect Of Valve Submersion Depth On The Flow Rate Of Sonic Pump

By Ivan A. Loukanov, Jacek Uziak
University of Botswana, Botswana.

Abstract - This paper investigates the effect of the valve submersion depth under the water level in the well on the flow rate of a sonic pump furnished with a spring loaded poppet valve. An equation governing the retardation of water column (WC) in terms of valve head losses, valve submersion depth and the depth of pumping is derived and analyzed. Graphs showing the WC retardation in terms of these parameters are presented. It is found that the above parameters have considerable effect on the flow rate of the pump when operating on shallow wells. In order to improve the flow rate when pumping from such wells, valves with low head losses have to be used and submersed at a depth of 3 - 4m. It is also found that the above results do not apply to pumps operating on deep wells because the WC retardation attains the gravitational acceleration and the flow rate improvement become negligible.

Keywords : *spring loaded poppet valve, depth of pumping, valve head losses, valve parameters.*

GJRE-A Classification :

Strictly as per the compliance and regulations of:

Investigating The Effect Of Valve Submersion Depth On The Flow Rate Of Sonic Pump

Ivan A. Loukanov[α], Jacek Uziak[Ω]

Abstract - This paper investigates the effect of the valve submersion depth under the water level in the well on the flow rate of a sonic pump furnished with a spring loaded poppet valve. An equation governing the retardation of water column (*WC*) in terms of valve head losses, valve submersion depth and the depth of pumping is derived and analyzed. Graphs showing the WC retardation in terms of these parameters are presented. It is found that the above parameters have considerable effect on the flow rate of the pump when operating on shallow wells. In order to improve the flow rate when pumping from such wells, valves with low head losses have to be used and submersed at a depth of 3 - 4m. It is also found that the above results do not apply to pumps operating on deep wells because the *WC* retardation attains the gravitational acceleration and the flow rate improvement become negligible.

Keywords : spring loaded poppet valve, depth of pumping, valve head losses, valve parameters.

I. Introduction

The major pumping elements used in sonic pumps are one-way valves of various designs. For shallow wells up to 30 m and pump resonance frequency up to 20 Hz one valve is usually used, while for deep wells and operating frequency of 20 to 50 Hz, the number of valves may be increased to seven (Usakovskii, 1973). Such arrangement reduces the static and dynamic loads on each valve and increases the flow rate and pressure developed by the pump. Since valves are the only mechanical elements involved in the pumping process the valve design is of great importance for the performance of sonic pumps (Usakovskii, 1973; Virnovskii & Tzinkova, 1966; Loukanov, 2007). In the above studies it is observed that the valve design and valve parameters determine the pump performance. However, in the research of Usakovskii (1973) and Virnovskii & Tzinkova (1966), old valve designs were employed. Since spring loaded poppet valves are readily available today it is therefore required to investigate the suitability of these valves for sonic pump applications. Therefore the objective of this paper is to investigate the effect of the valve submersion depth below the water level in the well on the flow rate of a sonic pump taking into account the valve head losses, the depth of pumping and the valve design parameters.

Author [α] : Department of Mechanical Engineering, University of Botswana, Botswana. (Telephone: +267 3554356
E-mail : loukanov@mopipi.ub.bw.com)
Author [Ω] : Department of Mechanical Engineering, University of Botswana, Botswana.(Telephone: +2673554304
E-mail : uziak@mopipi.ub.bw)

II. Material and Methods

The design schematic of a spring loaded poppet valve is shown in Fig. 1.

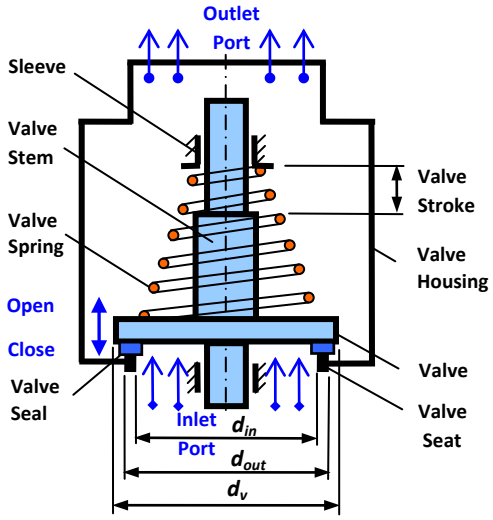

Fig.1 : Schematic of spring loaded poppet valve

In this design water enters through the inlet port, passes through the valve housing and around the valve and leaves from the outlet port towards the oscillating pipe (Fig. 2). As the name of the valve suggests the valve itself is kept generally closed by a preloaded helical compression spring. When the valve opens water flows around the valve through the valve housing experiencing some head losses due to sudden change of the interior cross section as well as due to vortices around the housing corners and the spring. When a poppet valve is employed in a sonic pump it oscillates together with the pipe as shown in Fig. 2. During this process the valve is subjected to a number of forces; some of them are pushing the valve to open while others are assisting it to close. According to Loukanov (2010) the major design parameters of a spring loaded poppet valve are: valve diameters (inlet - d_{in} and outlet - d_{out}), valve stroke (s), valve spring constant (k_v), spring preload (Δ), valve mass (m_v), valve body inlet area (A_{in}), maximum stroke limiting area ($A_{max,\ s}$) and valve body limited area ($A_{v,b}$). Depending upon the size of the valve these parameters vary considerably and determine the performance ability of the poppet valve.

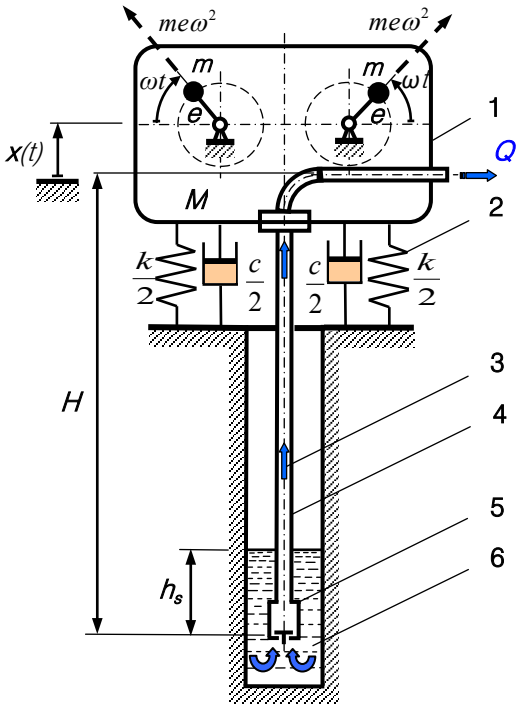

Fig.2 : The dynamic model of a sonic pump: 1 – dual shaft shaker, 2 – spring suspension system, 3 – water column (*WC*) in the pipes 4, 5 – spring loaded poppet valve, and 6 – aquifer of the well

In this study the dynamic model of a sonic pump is presented in order to understand the behaviour of the spring loaded poppet valve as well as the effects of valve head losses and valve submersion depth on the pump flow rate.

Fig. 2 shows the dynamic model of a low frequency sonic pump furnished with one spring loaded poppet valve. The valve is attached to the bottom end of the oscillating pipe and submersed at a depth h_s under the water level in the well. The pump is modelled as one degree-of-freedom oscillating system and for simplicity of the analysis it is assumed that both the pipe and the water column (*WC*) in the pipe are solid bodies. Therefore, the compressibility of *WC* and the elastic properties of the pipe are neglected. In addition to that, the valve itself could move together with the valve housing that is with the pipe as well as relative to the pipe and relative to the *WC*.

In Fig. 2, the following nomenclature is introduced:

- *x(t)* - denotes the absolute displacement of the oscillating system of mass *M*, which includes the masses of shaker, pipes, valve housing and the mass of *WC* in the pipes;
- *H* – is the depth of pumping being equal to the height of *WC,* assuming that water is discharged at the upper end of the well;
- h_s – stands for the depth of valve submersion below the water level in the well;

Since the pipes, valve housing and the shaker are connected together they undergo the same displacement, velocity and acceleration.

The equations governing the resonance vibrations of the oscillating system for one period, such as pipe (valve) displacement, velocity and acceleration are found to be (Loukanov, 2007):

$$x_p(t) = X_{\max} \sin \omega t,$$
$$\dot{x}_p(t) = \omega X_{\max} \cos \omega t = V_{\max} \cos \omega t \quad , \qquad (1)$$
$$\ddot{x}_p(t) = -\omega^2 X_{\max} \sin \omega t = -a_{\max} \sin \omega t$$

where

$x_p(t) = x(t)$, $a_{\max} = \omega^2 X_{\max}$ and $V_{\max} = \omega X_{\max}$ are the absolute displacement, maximum acceleration, and the maximum velocity respectively. The expression $X_{\max} = \dfrac{me}{2M\varsigma\sqrt{1-\varsigma^2}}$ gives the resonance amplitude and the parameter ς denotes the damping factor of the oscillating system.

The equations governing the absolute motion of the *WC* when it is controlled by the gravitational acceleration are as follows

$$x_{wc}(t) = -\frac{gt^2}{2} + V_s t + X_s,$$
$$\dot{x}_{wc}(t) = -gt + V_s, \qquad (2)$$
$$\ddot{x}_{wc}(t) = -g.$$

where

$$V_s = \dot{x}_p(t_s) = V_{\max} \cos \omega t_s = \frac{a_{\max}}{\omega} \cos \omega t_s \qquad (2a)$$

is the velocity of the *WC* at the point of separation *S* (Fig. 3), and

$$X_s = \delta_{st} = \frac{g}{\omega^2} \qquad (2b)$$

is the static spring deflection of the suspension system.

In Eq. (2a), the variable t_s is the time taken by the oscillating system to move from equilibrium position to the point of separation located in Phase 2 (Fig. 3) and is given by

$$t_s = \frac{1}{\omega} \sin^{-1}\left(\frac{g}{a_{\max}}\right). \qquad (3)$$

According to Loukanov (2007) in deriving the equation for the theoretical flow rate of the pump it is assumed that the absolute motion of the *WC* after the point of separation is governed only by the gravitational acceleration, *g* neglecting the losses in the valve and the pipe as well as neglecting the effect of the valve submersion depth under the water level in the well. Under these conditions the equation for the theoretically predicted flow rate of the pump is found to be

$$Q = 250\pi\, d_{in}^2\, x_r\, n \quad [\ell/\text{min}], \tag{4}$$

where

d_{in} - is the valve inlet diameter [m], as per Fig. 1

$$x_r = h_{\max} - x_p(t_p) \tag{4a}$$

is the relative distance between the valve seat and the bottom end of the *WC*, where

$$h_{\max} = \frac{V_s^2}{2g} + X_s \tag{4b}$$

is the maximum height attained by the *WC*, [m] as seen in Fig. 3; $x_p(t_p)$ is the pipe (valve) coordinate at the time when *WC* is at maximum height, [m], g=9.81 m/s^2 and n is the shaker resonance speed [rev/min].

According to Loukanov (2007) four distinguished phases are identified in the motion of the pipe (valve). Fig. 3 illustrates the phases of the pumping process, the motion of the oscillating pipe (valve) and the motion of the *WC*. Since the resonance vibrations of the system are periodic the investigation is carried out for one period of pipe oscillations. The abbreviations in Fig. 3 *"pipe-TDP"* and *"pipe-BDP"* mean "Pipe Top Dead Position" and "Pipe Bottom Dead Position" respectively. Fig. 3 also shows the method of determination of the relative distance x_r, used in Eq. (4). During operation the valve could be either closed or opened. When closed the valve is moving together with the pipe and the *WC* and when opened it moves relative to the pipe and relative to the *WC*. Previously it was found (Loukanov, 2007) that during the suction period taking place in Phases 2, 3 and 4 the valve relative motion is affected by the water stream passing through the valve housing. Since the valve mass, valve spring constant and the valve spring preload are negligibly small as compared to the comparable parameters of the oscillating system the effect of valve relative motion to the pipe (valve) is neglected in this analysis. Also after separating from the valve *WC* initiates independent upward motion interacting with the valve mainly through the suction effect produced, causing the water flow to blow onto the valve bottom face. The above interactions have significant influence on both the valve relative motion to the pipe and valve relative motion to the *WC* but will be neglected in this study.

To determine when the valve opens and closes during one period of pipe oscillations and what forces are acting upon it, both static and dynamic loading conditions on the valve will be investigated taking into account the valve submersion depth, valve head losses and the depth of pumping. It was previously found that for values of $a_{max} \leq 4.04 \times g$ the valve is closed during Phase 1 and moves together with the pipe. At the same time *WC* is retarding with progressively decreasing acceleration directed towards the equilibrium position (Loukanov, 2007).

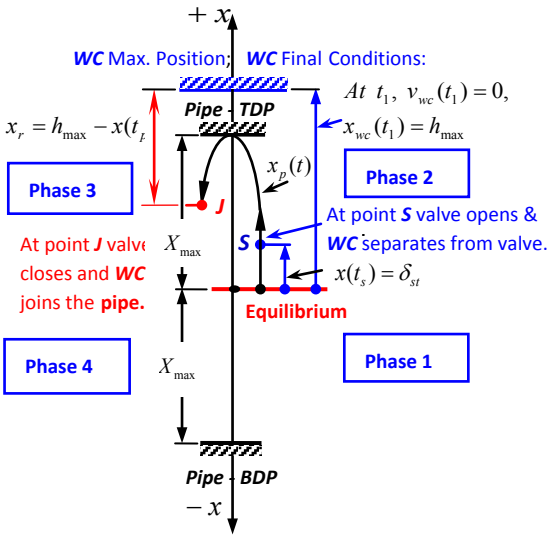

Fig.3 : Phases of the pumping process

During Phase 1 forces acted upon the valve are:

- $G_{wc} = (\rho g H + p_{atm}) A_{out}$, [N] - the combined force of the weight of *WC* and the force due to atmospheric pressure acting upon the upper face of the valve, where A_{out} is the upper area of the valve corresponding to a diameter – d_{out}, and ρ is the density of water.
- $G_v = m_v g$, [N] - the weight of the valve, where m_v is the mass of the valve itself along with half of the mass of the valve spring,
- $F_{pl} = k_v \Delta$, [N] - the valve spring preload, where k_v is the valve spring constant and Δ is the primary spring deflection generated during the initial installation of the valve and the spring in the housing,
- $F_{h-st} = (\rho g h_s + p_{atm}) A_{in}$, [N] - the combined hydrostatic and atmospheric force acting on the bottom face of the valve, A_{in} is the inlet area of the valve corresponding to the diameter - d_{in},
- $\phi_{wc} = m_{wc}\, \ddot{x}_p(t)$, [N] - the inertia force of *WC* acting downwards on the valve upper face,
- $\phi_v = m_v\, \ddot{x}_p(t)$, [N] - the inertia force of valve acting also downwards, which appears to be negligible as compared to ϕ_{wc}, because of the huge mass difference $m_{wc} >> m_v$, and
- R, [N] – is the reaction of the valve seat acting on the valve.

It should be noted that forces ϕ_{wc} and ϕ_v are alternating in accordance with the direction of pipe acceleration $\ddot{x}_p(t)$. As long as the reaction R is not zero the valve is closed and moves together with the rest of oscillating parts. Subsequently all the forces acting on the valve are in dynamic equilibrium according to the equation

$$F_{h-st} + R - G_{wc} - G_v - F_{pl} - \phi_{wc} - \phi_v = 0 \tag{5}$$

Consider now the upward motion of the oscillating system from equilibrium position towards the point of separation - *S*, as shown in Fig. 3. After passing the equilibrium position the pipe acceleration changes its direction becoming retardation. Then the inertia forces acting on the valve, pipe, shaker and the *WC* change their directions accordingly. On the other hand the resonance amplitude X_{max} of the oscillating system may be considered very small as compared to the depth of submersion ($X_{max} << h_s$), and so it can be assumed with negligible error that the hydrostatic component of the force $F_{h\text{-}st}$ does not vary appreciably.

As long as the reaction *R* of the valve seat exists the valve would be closed and moving together with the pipe. Also it should be mentioned that the inertia forces ϕ_{wc} and ϕ_v are progressively increasing due to an increase in the pipe acceleration $\ddot{x}_p(t)$. It is important to point out that the acceleration of the oscillating pipe is zero at equilibrium and maximum at both *TDP* and *BDP*, being always directed towards the equilibrium. To achieve pumping action the maximum pipe acceleration must be larger than the gravitational acceleration, i.e. $a_{p,max} > g$. At the point of separation *S*, when $t=t_s$ the reaction *R* of the valve seat nullifies and the *WC* begins an independent upward motion in the pipe with constant retardation equal to the gravitational acceleration (Loukanov, 2007). In the interim the pipe is moving up with increasing retardation and when reaching *TDP* it instantly stops and changes its direction of motion towards the equilibrium. After that *WC* reaches its maximum height h_{max} a bit later than the pipe reaches its *TDP* because after the point of separation the pipe's retardation is always larger than the gravitational acceleration $a_p(t)_{retard} > g$. After *WC* attains maximum height it initiates free fall towards the equilibrium with constant acceleration *g*. It should be noted that in the above analysis the effects of valve submersion depth and valve head losses are not taken into consideration.

To summarize, the motion of the pipe (valve) from equilibrium position towards the *TDP* is retarding and takes place in Phase-2, then from *TDP* towards equilibrium (Phase-3) – is accelerating, from equilibrium position towards *BDP* (Phase-4) – is retarding and from *BDP* towards equilibrium position (Phase-1) - is accelerating. In all phases the pipe acceleration is variable, increasing in the directions of *TDP* and *BDP*, and decreasing toward the equilibrium position. It nullifies at the equilibrium position of the system and then changes its direction but it is always directed towards the equilibrium position.

Under these conditions, after the point of separation, there will be two possible interactions between *WC* and the valve. These are:

- *WC* is moving up (Phase-2) acting as a long piston in a cylinder (the pipe) creating a suction force on the upper face of the valve and hence forcing it to open,
- *WC* is moving down (Phase-3 and 4) pushing the valve to close.

The above interactions are to a large extent dependent upon the motion of the pipe and *WC*, and the balance of forces acting upon the valve. Therefore the valve will be either temporarily opened or closed within one oscillating cycle depending upon the balance of forces acting on it. The free motion of *WC* is initiated at the point of separation *S* in Phase 2, as shown in Fig. 3, where the static deflection of the spring suspension system becomes $\delta_{st} = 0$ (Loukanov, 2007).

At this point *WC* separates from the valve and its mass is no longer part of the total oscillating mass *M* of the system. It could be expected that instantaneous change of the total oscillating mass would trigger an immediate change of the resonance frequency of the pipe and consequently change of the resonance amplitudes. But these transformations do not occur since the resonance amplitudes are time dependent and to change them time interval longer than several periods is required.

In the following analysis it is assumed that both the upper end of the pipe and the well are connected to the atmosphere and so the atmospheric pressure acting on both ends of *WC* cancels. Also, the fluid friction between *WC* and the pipe is neglected and the cross sectional area of the pipe is assumed to be equal to the inlet area of the valve. In addition it is considered that water is discharged at the top end of the well and therefore the depth of pumping *H* equals the height of *WC*. Under the above assumptions the equation governing the absolute motion of *WC* is found to be

$$m_{wc}\ddot{x}_{wc} = \rho g h_s A_{in} - m_{wc} g - \rho g h_v A_{in} \qquad (6)$$

The parameters involved in Eq. (6) are as follows:

$\ddot{x}_{wc}$ - acceleration of *WC*, with the +*x*-axis directed up as shown in Fig. 3, [m/s^2];

$m_{wc} = \rho H A_{in}$ - mass of the *WC*, [kg];

ρ - density of water, [kg/m^3];

h_s - valve submersion depth as shown in Fig. 2, [m];

$F_{res} = \rho g h_v A_{in}$ - resisting force due to head losses in the valve housing, [N];

h_v - head losses in the valve housing, measured in meters water head, and

A_{in} - valve inlet area, [m^2].

Upon substitution in Eq. (6) and rearrangement of terms yields

$$\ddot{x}_{wc} = -g\left(1 + \frac{h_v - h_s}{H}\right) = g_1 . \qquad (7)$$

Eq. (7) suggests that the absolute upward motion of the *WC* is retarding with acceleration g_1. The analysis of this equation reveals that the sign of the expression in the parentheses depends upon the difference (h_v –h_s) and the depth of pumping *H*.

Accordingly there are four important cases for the practice depending upon the combination of magnitudes of the above parameters.

Case 1: When $(h_v - h_s) < 0$, that is $(h_v < h_s)$, as a result

$$0 < \left(1 + \frac{h_v - h_s}{H}\right) < 1,$$

and therefore *WC* will retard with acceleration smaller than the gravitational acceleration. Then, in accordance with Eq. (2), Eq. (4b) and Fig. 3 the *WC* will attain greater height h_{max}. As a result the relative distance between the bottom end of *WC* and the valve seat will increase and Eq. (4) would yield larger flow rate. In this case the pump performance is improved and to achieve that it requires developing valves with low head losses. The reason is that practically the valve submersion depth is limited to a maximum of 3 – 4 m due to an increased damping effect on the oscillating system (Usakovskii, 1973). It should be noted that the parameter h_s may also vary in case when the well capacity is smaller than the pump capacity. Then the water level in the well would gradually drop to a lower level until a suitable well and pump capacity balance is obtained. As a result the valve submersion depth would also drop although it may become zero when the well and pumping capacity balance is not reached. This would ultimately cease the pumping until water level in the well is recovered.

Case 2: When $(h_v - h_s) > 0$ or $(h_v > h_s)$, then under these conditions

$$\left(1 + \frac{h_v - h_s}{H}\right) > 1.$$

Then *WC* would retard with acceleration greater than the gravitational acceleration. This implies that it would attain smaller maximum height h_{max} and consequently smaller relative distance x_r would be obtained from Eq. (2). Accordingly Eq. (4) would give a smaller flow rate and therefore the flow rate would depreciate. Obviously the above effect becomes insignificant when the depth of pumping *H* is increased considerably. However, when pumping from shallow to medium depth wells (20-60 m) it has to be accounted for. This situation was observed during experiments with a model resonance pump (Loukanov, 2007). The pump was tested with a 55-mm spring loaded poppet valve having head losses h_v=0.43 m and operated at resonance frequency of 5.37 Hz. The oscillating system was subjected to acceleration $a_{max} = 2.0 \times g$, pumping water from *H*=1.65 m at valve submersion depth h_s=0.25 m. Subsequently the flow rate was measured to be *Q* = 5.28 ℓ/min while the calculated one was *Q* = 5.77 ℓ/min.

Now employing Eq. (7) and substituting the values for h_v and h_s the *WC* retardation is found to be

$$\ddot{x}_{wc} = -g\left(1 + \frac{0.43 - 0.25}{1.65}\right) = -1.11g = -10.9\ \text{m/s}^2.$$

Accordingly *WC* attained lesser height h_{max} resulting in a smaller flow rate being calculated from Eq. (4).

Case 3: When $h_v = h_s$, then for any value of *H*,

$$\left(1 + \frac{h_v - h_s}{H}\right) = 1.$$

Under this condition *WC* would retard with acceleration equal to the gravitational acceleration. This is exactly the case described by Eqs. (2), (3), and (4), which do not account for the valve head losses and the submersion depth.

Case 4: When $h_v > h_s$ and $h_s > H$, then the expression in the parentheses become negative

$$\left(1 + \frac{h_v - h_s}{H}\right) < 0.$$

Under these conditions *WC* would be subjected to acceleration larger than the gravitational acceleration and hence would be accelerated contrary to the three cases already discussed. In fact, this case describes the well known principle of the siphon, which is not applicable to sonic pumps since always $H >> h_s$.

Based on the above analysis it is proposed to replace the gravitational acceleration in Eq. (2) and Eq. (4b), with the values of g_1 calculated from Eq. (7) corresponding to the values of h_s, h_v, and *H*, then to determine h_{max}, $x_p(t_p)$ and x_r, and finally to calculate the theoretical flow rate from Eq. (4).

III. Results and Discussion

The variations of *WC* retardation in terms of parameters involved in Eq. (7) are shown in Figs. 4, 5 and 6, where the gravitational acceleration is included for comparison. All graphs are plotted for valve head losses (h_v) varying from 0 to 1 m, valve submersion depth (h_s) under the water level in the well varying from 0 to 4 m and for three depths of pumping; mainly *H*=1.65 m, *H*=10 m and *H*=20 m.

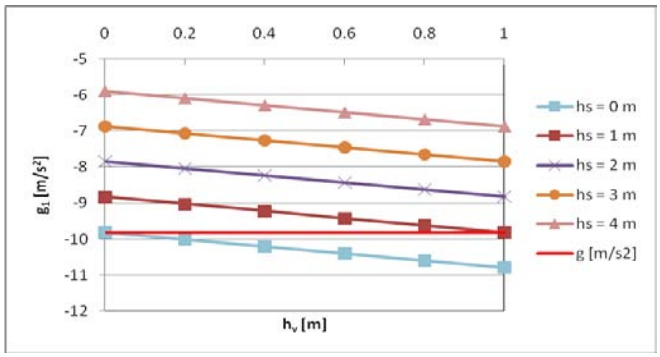

Fig.4 : Retardation of *WC* for *H*=10 m

Fig. 4 illustrates the variation of *WC* retardation (g_1) for depth of pumping *H*=10m. It is observed that the *WC* retardation is linearly dependent upon h_v and h_s.

Values above the line of gravitational acceleration indicate that *WC* would retard with $g_1 < g$, corresponding to Case 1 and for values below the gravitational acceleration line *WC* would retard with $g_1 > g$, as described by Case 2.

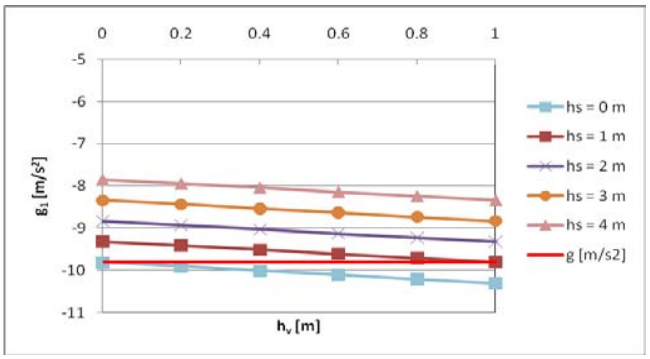

Fig.5 : Retardation of *WC* for *H*=20 m

Fig. 5 shows similar trends of variation of *WC* retardation when plotted for depth of pumping H=20 m. In contrast to Fig. 4 it is seen that the lines become closer to each other and the values of g_1 are grouped within the range of (8.0 – 10.3) m/s^2, while in Fig. 4 these values are within the range (6.0 – 10.4) m/s^2. Also the lines in Fig. 4 are a steeper as compared to the lines in Fig. 5. This indicates that the increased depth of pumping suppresses the effect of valve head losses and valve submersion depth to a large extent forcing the lines to level and approach the line of the gravitational acceleration. The reason being is the term $(h_v-h_s)/H$, which tends to zero when the depth of pumping approaches infinity that is when $H\rightarrow\infty$ then $a_{wc} \rightarrow g$ and *WC* would retard with the gravitational acceleration irrespective of the values of valve head losses and valve submersion depth. Values of the *WC* retardation $g_1 < g$, imply that *WC* would attain greater maximum height (h_{max}) and therefore larger volume of water will be discharged, which is desirable. On the other hand values of *WC* retardation $g_1 > g$, suggest smaller maximum height and therefore lesser flow rate.

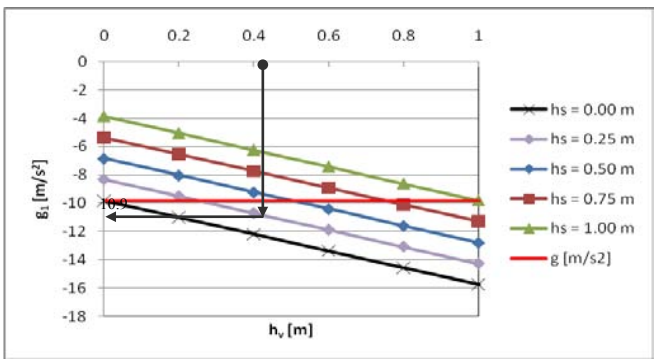

Fig.6 : Retardation of *WC* of model pump for *H*=1.65 m

Fig. 6 depicts the variation of the *WC* retardation of the model pump discussed in Case 2. It is seen from the figure that for the data used (h_s=0.25 m, h_v=0.43 m and *H*=1.65m) in the illustrative example the graph confirms that the *WC* retarded with acceleration larger than the gravity, (a_{max}=10.9 m/s^2), and therefore the pump delivered smaller flow rate as established during the experiments. To obtain better flow rate it necessitates to submerse the valve deeper than 0.43 m so as to achieve ($a_{max}=g_1$) $< g$.

IV. Conclusions

In this paper the effects of valve head losses, valve submersion depth and the depth of pumping on the flow rate of a sonic pump are investigated. An equation relating the above parameters is derived, analyzed and graphs based on it are plotted. It is found from the graphs that the parameters involved in Eq. (7) have significant effect on the flow rate of the pump when pumping from shallow to medium depth wells. To improve the flow rate it is suggested to using valves with small head losses and submersing them to a depth of 3-4 m under the water level in the well. The analysis also revealed that an increase in the depth of pumping reduces the negative effect of valve head losses but also the positive effect of the valve submersion depth on flow rate of the pump. Furthermore the greater the depth of pumping the closer the *WC* retardation become to the gravitational acceleration. So the benefits of using valves of small head losses and submersing them deeper in the well would not contribute towards better flow rate when pumping water from very deep wells. To verify the effect of the phenomena based on Eq. (7) a consistent and precise testing on shallow, medium and deep boreholes is required. Possibly this will be the aim of another investigation where valves with low head losses will be developed and tested on a sonic pump under the recommended submersion depths and determine the effects on the flow rate of a sonic pump.

References Références Referencias

1. Loukanov, I.A. (2007). Investigating the pumping process of a resonance vibrating pump for medium-depth boreholes *Research in Agricultural Engineering*, *53,* 172-181.
2. Loukanov, I.A. (2010). Measuring the Parameters of Foot Valves for Sonic Pumps. *Journal of Emerging Trend in Engineering and Applied Sciences, 1,* 184-189.
3. Virnovskii, A.C. & Tzinkova, O.E. (1965). On the operating cycle of a vibrating pump. *Oil Industry, 10,* 58-60.
4. Usakovskii, V.M. (1973). *Inertia Pumps*. Moscow: Machine-Building Publishing House.

Global Journals Inc. (US) Guidelines Handbook 2011

www.GlobalJournals.org

FELLOW OF ASSOCIATION OF RESEARCH SOCIETY IN ENGINEERING (FARSE)

- 'FARSE' title will be awarded to the person after approval of Editor-in-Chief and Editorial Board. The title 'FARSE" can be added to name in the following manner. eg. Dr. John E. Hall, Ph.D., FARSE or William Walldroff Ph. D., M.S., FARSE
- Being FARSE is a respectful honor. It authenticates your research activities. After becoming FARSE, you can use 'FARSE' title as you use your degree in suffix of your name. This will definitely will enhance and add up your name. You can use it on your Career Counseling Materials/CV/Resume/Visiting Card/Name Plate etc.
- 60% Discount will be provided to FARSE members for publishing research papers in Global Journals Inc., if our Editorial Board and Peer Reviewers accept the paper. For the life time, if you are author/co-author of any paper bill sent to you will automatically be discounted one by 60%
- FARSE will be given a renowned, secure, free professional email address with 100 GB of space eg.johnhall@globaljournals.org. You will be facilitated with Webmail, Spam Assassin, Email Forwarders, Auto-Responders, Email Delivery Route tracing, etc.
- FARSE member is eligible to become paid peer reviewer at Global Journals Inc. to earn up to 15% of realized author charges taken from author of respective paper. After reviewing 5 or more papers you can request to transfer the amount to your bank account or to your PayPal account.
- Eg. If we had taken 420 USD from author, we can send 63 USD to your account.
- FARSE member can apply for free approval, grading and certification of some of their Educational and Institutional Degrees from Global Journals Inc. (US) and Open Association of Research, Society U.S.A.
- After you are FARSE. You can send us scanned copy of all of your documents. We will verify, grade and certify them within a month. It will be based on your academic records, quality of research papers published by you, and 50 more criteria. This is beneficial for your job interviews as recruiting organization need not just rely on you for authenticity and your unknown qualities, you would have authentic ranks of all of your documents. Our scale is unique worldwide.
- FARSE member can proceed to get benefits of free research podcasting in Global Research Radio with their research documents, slides and online movies.
- After your publication anywhere in the world, you can upload you research paper with your recorded voice or you can use our professional RJs to record your paper their voice. We can also stream your conference videos and display your slides online.
- FARSE will be eligible for free application of Standardization of their Researches by Open Scientific Standards. Standardization is next step and level after publishing in a journal. A team of research and professional will work with you to take your research to its next level, which is worldwide open standardization.

- FARSE is eligible to earn from their researches: While publishing his paper with Global Journals Inc. (US), FARSE can decide whether he/she would like to publish his/her research in closed manner. When readers will buy that individual research paper for reading, 80% of its earning by Global Journals Inc. (US) will be transferred to FARSE member's bank account after certain threshold balance. There is no time limit for collection. FARSE member can decide its price and we can help in decision.

MEMBER OF ASSOCIATION OF RESEARCH SOCIETY IN ENGINEERING (MARSE)

- 'MARSE' title will be awarded to the person after approval of Editor-in-Chief and Editorial Board. The title 'MARSE" can be added to name in the following manner. eg. Dr. John E. Hall, Ph.D., MARSE or William Walldroff Ph. D., M.S., MARSE
- Being MARSE is a respectful honor. It authenticates your research activities. After becoming MARSE, you can use 'MARSE' title as you use your degree in suffix of your name. This will definitely will enhance and add up your name. You can use it on your Career Counseling Materials/CV/Resume/Visiting Card/Name Plate etc.
- 40% Discount will be provided to MARSE members for publishing research papers in Global Journals Inc., if our Editorial Board and Peer Reviewers accept the paper. For the life time, if you are author/co-author of any paper bill sent to you will automatically be discounted one by 60%
- MARSE will be given a renowned, secure, free professional email address with 30 GB of space eg.johnhall@globaljournals.org. You will be facilitated with Webmail, SpamAssassin, Email Forwarders, Auto-Responders, Email Delivery Route tracing, etc.
- MARSE member is eligible to become paid peer reviewer at Global Journals Inc. to earn up to 10% of realized author charges taken from author of respective paper. After reviewing 5 or more papers you can request to transfer the amount to your bank account or to your PayPal account.
- MARSE member can apply for free approval, grading and certification of some of their Educational and Institutional Degrees from Global Journals Inc. (US) and Open Association of Research,Society U.S.A.
- MARSE is eligible to earn from their researches: While publishing his paper with Global Journals Inc. (US), MARSE can decide whether he/she would like to publish his/her research in closed manner. When readers will buy that individual research paper for reading, 40% of its earning by Global Journals Inc. (US) will be transferred to MARSE member's bank account after certain threshold balance. There is no time limit for collection. MARSE member can decide its price and we can help in decision.

AUXILIARY MEMBERSHIPS

ANNUAL MEMBER

- Annual Member will be authorized to receive e-Journal GJRE for one year (subscription for one year).
- The member will be allotted free 1 GB Web-space along with subDomain to contribute and participate in our activities.
- A professional email address will be allotted free 500 MB email space.

PAPER PUBLICATION

- The members can publish paper once. The paper will be sent to two-peer reviewer. The paper will be published after the acceptance of peer reviewers and Editorial Board.

Process of submission of Research Paper

The Area or field of specialization may or may not be of any category as mentioned in 'Scope of Journal' menu of the GlobalJournals.org website. There are 37 Research Journal categorized with Six parental Journals GJCST, GJMR, GJRE, GJMBR, GJSFR, GJHSS. For Authors should prefer the mentioned categories. There are three widely used systems UDC, DDC and LCC. The details are available as 'Knowledge Abstract' at Home page. The major advantage of this coding is that, the research work will be exposed to and shared with all over the world as we are being abstracted and indexed worldwide.

The paper should be in proper format. The format can be downloaded from first page of 'Author Guideline' Menu. The Author is expected to follow the general rules as mentioned in this menu. The paper should be written in MS-Word Format (*.DOC,*.DOCX).

The Author can submit the paper either online or offline. The authors should prefer online submission.Online Submission: There are three ways to submit your paper:

(A) (I) First, register yourself using top right corner of Home page then Login. If you are already registered, then login using your username and password.

(II) Choose corresponding Journal.

(III) Click 'Submit Manuscript'. Fill required information and Upload the paper.

(B) If you are using Internet Explorer, then Direct Submission through Homepage is also available.

(C) If these two are not conveninet , and then email the paper directly to dean@globaljournals.org.

Offline Submission: Author can send the typed form of paper by Post. However, online submission should be preferred.

Preferred Author Guidelines

MANUSCRIPT STYLE INSTRUCTION (Must be strictly followed)

Page Size: 8.27" X 11'"

- Left Margin: 0.65
- Right Margin: 0.65
- Top Margin: 0.75
- Bottom Margin: 0.75
- Font type of all text should be Swis 721 Lt BT.
- Paper Title should be of Font Size 24 with one Column section.
- Author Name in Font Size of 11 with one column as of Title.
- Abstract Font size of 9 Bold, "Abstract" word in Italic Bold.
- Main Text: Font size 10 with justified two columns section
- Two Column with Equal Column with of 3.38 and Gaping of .2
- First Character must be three lines Drop capped.
- Paragraph before Spacing of 1 pt and After of 0 pt.
- Line Spacing of 1 pt
- Large Images must be in One Column
- Numbering of First Main Headings (Heading 1) must be in Roman Letters, Capital Letter, and Font Size of 10.
- Numbering of Second Main Headings (Heading 2) must be in Alphabets, Italic, and Font Size of 10.

You can use your own standard format also.
Author Guidelines:

1. General,

2. Ethical Guidelines,

3. Submission of Manuscripts,

4. Manuscript's Category,

5. Structure and Format of Manuscript,

6. After Acceptance.

1. GENERAL

Before submitting your research paper, one is advised to go through the details as mentioned in following heads. It will be beneficial, while peer reviewer justify your paper for publication.

Scope

The Global Journals Inc. (US) welcome the submission of original paper, review paper, survey article relevant to the all the streams of Philosophy and knowledge. The Global Journals Inc. (US) is parental platform for Global Journal of Computer Science and Technology, Researches in Engineering, Medical Research, Science Frontier Research, Human Social Science, Management, and Business organization. The choice of specific field can be done otherwise as following in Abstracting and Indexing Page on this Website. As the all Global

Journals Inc. (US) are being abstracted and indexed (in process) by most of the reputed organizations. Topics of only narrow interest will not be accepted unless they have wider potential or consequences.

2. ETHICAL GUIDELINES

Authors should follow the ethical guidelines as mentioned below for publication of research paper and research activities.

Papers are accepted on strict understanding that the material in whole or in part has not been, nor is being, considered for publication elsewhere. If the paper once accepted by Global Journals Inc. (US) and Editorial Board, will become the copyright of the Global Journals Inc. (US).

Authorship: The authors and coauthors should have active contribution to conception design, analysis and interpretation of findings. They should critically review the contents and drafting of the paper. All should approve the final version of the paper before submission

The Global Journals Inc. (US) follows the definition of authorship set up by the Global Academy of Research and Development. According to the Global Academy of R&D authorship, criteria must be based on:

1) Substantial contributions to conception and acquisition of data, analysis and interpretation of the findings.

2) Drafting the paper and revising it critically regarding important academic content.

3) Final approval of the version of the paper to be published.

All authors should have been credited according to their appropriate contribution in research activity and preparing paper. Contributors who do not match the criteria as authors may be mentioned under Acknowledgement.

Acknowledgements: Contributors to the research other than authors credited should be mentioned under acknowledgement. The specifications of the source of funding for the research if appropriate can be included. Suppliers of resources may be mentioned along with address.

Appeal of Decision: The Editorial Board's decision on publication of the paper is final and cannot be appealed elsewhere.

Permissions: It is the author's responsibility to have prior permission if all or parts of earlier published illustrations are used in this paper.

Please mention proper reference and appropriate acknowledgements wherever expected.

If all or parts of previously published illustrations are used, permission must be taken from the copyright holder concerned. It is the author's responsibility to take these in writing.

Approval for reproduction/modification of any information (including figures and tables) published elsewhere must be obtained by the authors/copyright holders before submission of the manuscript. Contributors (Authors) are responsible for any copyright fee involved.

3. SUBMISSION OF MANUSCRIPTS

Manuscripts should be uploaded via this online submission page. The online submission is most efficient method for submission of papers, as it enables rapid distribution of manuscripts and consequently speeds up the review procedure. It also enables authors to know the status of their own manuscripts by emailing us. Complete instructions for submitting a paper is available below.

Manuscript submission is a systematic procedure and little preparation is required beyond having all parts of your manuscript in a given format and a computer with an Internet connection and a Web browser. Full help and instructions are provided on-screen. As an author, you will be prompted for login and manuscript details as Field of Paper and then to upload your manuscript file(s) according to the instructions.

To avoid postal delays, all transaction is preferred by e-mail. A finished manuscript submission is confirmed by e-mail immediately and your paper enters the editorial process with no postal delays. When a conclusion is made about the publication of your paper by our Editorial Board, revisions can be submitted online with the same procedure, with an occasion to view and respond to all comments.

Complete support for both authors and co-author is provided.

4. MANUSCRIPT'S CATEGORY

Based on potential and nature, the manuscript can be categorized under the following heads:

Original research paper: Such papers are reports of high-level significant original research work.

Review papers: These are concise, significant but helpful and decisive topics for young researchers.

Research articles: These are handled with small investigation and applications

Research letters: The letters are small and concise comments on previously published matters.

5.STRUCTURE AND FORMAT OF MANUSCRIPT

The recommended size of original research paper is less than seven thousand words, review papers fewer than seven thousands words also.Preparation of research paper or how to write research paper, are major hurdle, while writing manuscript. The research articles and research letters should be fewer than three thousand words, the structure original research paper; sometime review paper should be as follows:

Papers: These are reports of significant research (typically less than 7000 words equivalent, including tables, figures, references), and comprise:

(a)Title should be relevant and commensurate with the theme of the paper.

(b) A brief Summary, "Abstract" (less than 150 words) containing the major results and conclusions.

(c) Up to ten keywords, that precisely identifies the paper's subject, purpose, and focus.

(d) An Introduction, giving necessary background excluding subheadings; objectives must be clearly declared.

(e) Resources and techniques with sufficient complete experimental details (wherever possible by reference) to permit repetition; sources of information must be given and numerical methods must be specified by reference, unless non-standard.

(f) Results should be presented concisely, by well-designed tables and/or figures; the same data may not be used in both; suitable statistical data should be given. All data must be obtained with attention to numerical detail in the planning stage. As reproduced design has been recognized to be important to experiments for a considerable time, the Editor has decided that any paper that appears not to have adequate numerical treatments of the data will be returned un-refereed;

(g) Discussion should cover the implications and consequences, not just recapitulating the results; conclusions should be summarizing.

(h) Brief Acknowledgements.

(i) References in the proper form.

Authors should very cautiously consider the preparation of papers to ensure that they communicate efficiently. Papers are much more likely to be accepted, if they are cautiously designed and laid out, contain few or no errors, are summarizing, and be conventional to the approach and instructions. They will in addition, be published with much less delays than those that require much technical and editorial correction.

The Editorial Board reserves the right to make literary corrections and to make suggestions to improve briefness.

It is vital, that authors take care in submitting a manuscript that is written in simple language and adheres to published guidelines.

Format

Language: The language of publication is UK English. Authors, for whom English is a second language, must have their manuscript efficiently edited by an English-speaking person before submission to make sure that, the English is of high excellence. It is preferable, that manuscripts should be professionally edited.

Standard Usage, Abbreviations, and Units: Spelling and hyphenation should be conventional to The Concise Oxford English Dictionary. Statistics and measurements should at all times be given in figures, e.g. 16 min, except for when the number begins a sentence. When the number does not refer to a unit of measurement it should be spelt in full unless, it is 160 or greater.

Abbreviations supposed to be used carefully. The abbreviated name or expression is supposed to be cited in full at first usage, followed by the conventional abbreviation in parentheses.

Metric SI units are supposed to generally be used excluding where they conflict with current practice or are confusing. For illustration, 1.4 l rather than 1.4 × 10-3 m3, or 4 mm somewhat than 4 × 10-3 m. Chemical formula and solutions must identify the form used, e.g. anhydrous or hydrated, and the concentration must be in clearly defined units. Common species names should be followed by underlines at the first mention. For following use the generic name should be constricted to a single letter, if it is clear.

Structure

All manuscripts submitted to Global Journals Inc. (US), ought to include:

Title: The title page must carry an instructive title that reflects the content, a running title (less than 45 characters together with spaces), names of the authors and co-authors, and the place(s) wherever the work was carried out. The full postal address in addition with the e-mail address of related author must be given. Up to eleven keywords or very brief phrases have to be given to help data retrieval, mining and indexing.

Abstract, used in Original Papers and Reviews:

Optimizing Abstract for Search Engines

Many researchers searching for information online will use search engines such as Google, Yahoo or similar. By optimizing your paper for search engines, you will amplify the chance of someone finding it. This in turn will make it more likely to be viewed and/or cited in a further work. Global Journals Inc. (US) have compiled these guidelines to facilitate you to maximize the web-friendliness of the most public part of your paper.

Key Words

A major linchpin in research work for the writing research paper is the keyword search, which one will employ to find both library and Internet resources.

One must be persistent and creative in using keywords. An effective keyword search requires a strategy and planning a list of possible keywords and phrases to try.

Search engines for most searches, use Boolean searching, which is somewhat different from Internet searches. The Boolean search uses "operators," words (and, or, not, and near) that enable you to expand or narrow your affords. Tips for research paper while preparing research paper are very helpful guideline of research paper.

Choice of key words is first tool of tips to write research paper. Research paper writing is an art.A few tips for deciding as strategically as possible about keyword search:

- One should start brainstorming lists of possible keywords before even begin searching. Think about the most important concepts related to research work. Ask, "What words would a source have to include to be truly valuable in research paper?" Then consider synonyms for the important words.
- It may take the discovery of only one relevant paper to let steer in the right keyword direction because in most databases, the keywords under which a research paper is abstracted are listed with the paper.
- One should avoid outdated words.

Keywords are the key that opens a door to research work sources. Keyword searching is an art in which researcher's skills are bound to improve with experience and time.

Numerical Methods: Numerical methods used should be clear and, where appropriate, supported by references.

Acknowledgements: Please make these as concise as possible.

References

References follow the Harvard scheme of referencing. References in the text should cite the authors' names followed by the time of their publication, unless there are three or more authors when simply the first author's name is quoted followed by et al. unpublished work has to only be cited where necessary, and only in the text. Copies of references in press in other journals have to be supplied with submitted typescripts. It is necessary that all citations and references be carefully checked before submission, as mistakes or omissions will cause delays.

References to information on the World Wide Web can be given, but only if the information is available without charge to readers on an official site. Wikipedia and Similar websites are not allowed where anyone can change the information. Authors will be asked to make available electronic copies of the cited information for inclusion on the Global Journals Inc. (US) homepage at the judgment of the Editorial Board.

The Editorial Board and Global Journals Inc. (US) recommend that, citation of online-published papers and other material should be done via a DOI (digital object identifier). If an author cites anything, which does not have a DOI, they run the risk of the cited material not being noticeable.

The Editorial Board and Global Journals Inc. (US) recommend the use of a tool such as Reference Manager for reference management and formatting.

Tables, Figures and Figure Legends

Tables: Tables should be few in number, cautiously designed, uncrowned, and include only essential data. Each must have an Arabic number, e.g. Table 4, a self-explanatory caption and be on a separate sheet. Vertical lines should not be used.

Figures: Figures are supposed to be submitted as separate files. Always take in a citation in the text for each figure using Arabic numbers, e.g. Fig. 4. Artwork must be submitted online in electronic form by e-mailing them.

Preparation of Electronic Figures for Publication

Even though low quality images are sufficient for review purposes, print publication requires high quality images to prevent the final product being blurred or fuzzy. Submit (or e-mail) EPS (line art) or TIFF (halftone/photographs) files only. MS PowerPoint and Word Graphics are unsuitable for printed pictures. Do not use pixel-oriented software. Scans (TIFF only) should have a resolution of at least 350 dpi (halftone) or 700 to 1100 dpi (line drawings) in relation to the imitation size. Please give the data for figures in black and white or submit a Color Work Agreement Form. EPS files must be saved with fonts embedded (and with a TIFF preview, if possible).

For scanned images, the scanning resolution (at final image size) ought to be as follows to ensure good reproduction: line art: >650 dpi; halftones (including gel photographs) : >350 dpi; figures containing both halftone and line images: >650 dpi.

Color Charges: It is the rule of the Global Journals Inc. (US) for authors to pay the full cost for the reproduction of their color artwork. Hence, please note that, if there is color artwork in your manuscript when it is accepted for publication, we would require you to complete and return a color work agreement form before your paper can be published.

Figure Legends: Self-explanatory legends of all figures should be incorporated separately under the heading 'Legends to Figures'. In the full-text online edition of the journal, figure legends may possibly be truncated in abbreviated links to the full screen version. Therefore, the first 100 characters of any legend should notify the reader, about the key aspects of the figure.

6. AFTER ACCEPTANCE

Upon approval of a paper for publication, the manuscript will be forwarded to the dean, who is responsible for the publication of the Global Journals Inc. (US).

6.1 Proof Corrections

The corresponding author will receive an e-mail alert containing a link to a website or will be attached. A working e-mail address must therefore be provided for the related author.

Acrobat Reader will be required in order to read this file. This software can be downloaded

(Free of charge) from the following website:

www.adobe.com/products/acrobat/readstep2.html. This will facilitate the file to be opened, read on screen, and printed out in order for any corrections to be added. Further instructions will be sent with the proof.

Proofs must be returned to the dean at dean@globaljournals.org within three days of receipt.

As changes to proofs are costly, we inquire that you only correct typesetting errors. All illustrations are retained by the publisher. Please note that the authors are responsible for all statements made in their work, including changes made by the copy editor.

6.2 Early View of Global Journals Inc. (US) (Publication Prior to Print)

The Global Journals Inc. (US) are enclosed by our publishing's Early View service. Early View articles are complete full-text articles sent in advance of their publication. Early View articles are absolute and final. They have been completely reviewed, revised and edited for publication, and the authors' final corrections have been incorporated. Because they are in final form, no changes can be made after sending them. The nature of Early View articles means that they do not yet have volume, issue or page numbers, so Early View articles cannot be cited in the conventional way.

6.3 Author Services

Online production tracking is available for your article through Author Services. Author Services enables authors to track their article - once it has been accepted - through the production process to publication online and in print. Authors can check the status of their articles online and choose to receive automated e-mails at key stages of production. The authors will receive an e-mail with a unique link that enables them to register and have their article automatically added to the system. Please ensure that a complete e-mail address is provided when submitting the manuscript.

6.4 Author Material Archive Policy

Please note that if not specifically requested, publisher will dispose off hardcopy & electronic information submitted, after the two months of publication. If you require the return of any information submitted, please inform the Editorial Board or dean as soon as possible.

6.5 Offprint and Extra Copies

A PDF offprint of the online-published article will be provided free of charge to the related author, and may be distributed according to the Publisher's terms and conditions. Additional paper offprint may be ordered by emailing us at: editor@globaljournals.org .

the search? Will I be able to find all information in this field area? If the answer of these types of questions will be "Yes" then you can choose that topic. In most of the cases, you may have to conduct the surveys and have to visit several places because this field is related to Computer Science and Information Technology. Also, you may have to do a lot of work to find all rise and falls regarding the various data of that subject. Sometimes, detailed information plays a vital role, instead of short information.

2. Evaluators are human: First thing to remember that evaluators are also human being. They are not only meant for rejecting a paper. They are here to evaluate your paper. So, present your Best.

3. Think Like Evaluators: If you are in a confusion or getting demotivated that your paper will be accepted by evaluators or not, then think and try to evaluate your paper like an Evaluator. Try to understand that what an evaluator wants in your research paper and automatically you will have your answer.

4. Make blueprints of paper: The outline is the plan or framework that will help you to arrange your thoughts. It will make your paper logical. But remember that all points of your outline must be related to the topic you have chosen.

5. Ask your Guides: If you are having any difficulty in your research, then do not hesitate to share your difficulty to your guide (if you have any). They will surely help you out and resolve your doubts. If you can't clarify what exactly you require for your work then ask the supervisor to help you with the alternative. He might also provide you the list of essential readings.

6. Use of computer is recommended: As you are doing research in the field of Computer Science, then this point is quite obvious.

7. Use right software: Always use good quality software packages. If you are not capable to judge good software then you can lose quality of your paper unknowingly. There are various software programs available to help you, which you can get through Internet.

8. Use the Internet for help: An excellent start for your paper can be by using the Google. It is an excellent search engine, where you can have your doubts resolved. You may also read some answers for the frequent question how to write my research paper or find model research paper. From the internet library you can download books. If you have all required books make important reading selecting and analyzing the specified information. Then put together research paper sketch out.

9. Use and get big pictures: Always use encyclopedias, Wikipedia to get pictures so that you can go into the depth.

10. Bookmarks are useful: When you read any book or magazine, you generally use bookmarks, right! It is a good habit, which helps to not to lose your continuity. You should always use bookmarks while searching on Internet also, which will make your search easier.

11. Revise what you wrote: When you write anything, always read it, summarize it and then finalize it.

12. Make all efforts: Make all efforts to mention what you are going to write in your paper. That means always have a good start. Try to mention everything in introduction, that what is the need of a particular research paper. Polish your work by good skill of writing and always give an evaluator, what he wants.

13. Have backups: When you are going to do any important thing like making research paper, you should always have backup copies of it either in your computer or in paper. This will help you to not to lose any of your important.

14. Produce good diagrams of your own: Always try to include good charts or diagrams in your paper to improve quality. Using several and unnecessary diagrams will degrade the quality of your paper by creating "hotchpotch." So always, try to make and include those diagrams, which are made by your own to improve readability and understandability of your paper.

15. Use of direct quotes: When you do research relevant to literature, history or current affairs then use of quotes become essential but if study is relevant to science then use of quotes is not preferable.

16. Use proper verb tense: Use proper verb tenses in your paper. Use past tense, to present those events that happened. Use present tense to indicate events that are going on. Use future tense to indicate future happening events. Use of improper and wrong tenses will confuse the evaluator. Avoid the sentences that are incomplete.

17. Never use online paper: If you are getting any paper on Internet, then never use it as your research paper because it might be possible that evaluator has already seen it or maybe it is outdated version.

18. **Pick a good study spot:** To do your research studies always try to pick a spot, which is quiet. Every spot is not for studies. Spot that suits you choose it and proceed further.

19. Know what you know: Always try to know, what you know by making objectives. Else, you will be confused and cannot achieve your target.

20. Use good quality grammar: Always use a good quality grammar and use words that will throw positive impact on evaluator. Use of good quality grammar does not mean to use tough words, that for each word the evaluator has to go through dictionary. Do not start sentence with a conjunction. Do not fragment sentences. Eliminate one-word sentences. Ignore passive voice. Do not ever use a big word when a diminutive one would suffice. Verbs have to be in agreement with their subjects. Prepositions are not expressions to finish sentences with. It is incorrect to ever divide an infinitive. Avoid clichés like the disease. Also, always shun irritating alliteration. Use language that is simple and straight forward. put together a neat summary.

21. Arrangement of information: Each section of the main body should start with an opening sentence and there should be a changeover at the end of the section. Give only valid and powerful arguments to your topic. You may also maintain your arguments with records.

22. Never start in last minute: Always start at right time and give enough time to research work. Leaving everything to the last minute will degrade your paper and spoil your work.

23. Multitasking in research is not good: Doing several things at the same time proves bad habit in case of research activity. Research is an area, where everything has a particular time slot. Divide your research work in parts and do particular part in particular time slot.

24. Never copy others' work: Never copy others' work and give it your name because if evaluator has seen it anywhere you will be in trouble.

25. Take proper rest and food: No matter how many hours you spend for your research activity, if you are not taking care of your health then all your efforts will be in vain. For a quality research, study is must, and this can be done by taking proper rest and food.

26. Go for seminars: Attend seminars if the topic is relevant to your research area. Utilize all your resources.

27. Refresh your mind after intervals: Try to give rest to your mind by listening to soft music or by sleeping in intervals. This will also improve your memory.

28. Make colleagues: Always try to make colleagues. No matter how sharper or intelligent you are, if you make colleagues you can have several ideas, which will be helpful for your research.

29. **Think technically:** Always think technically. If anything happens, then search its reasons, its benefits, and demerits.

30. Think and then print: When you will go to print your paper, notice that tables are not be split, headings are not detached from their descriptions, and page sequence is maintained.

31. Adding unnecessary information: Do not add unnecessary information, like, I have used MS Excel to draw graph. Do not add irrelevant and inappropriate material. These all will create superfluous. Foreign terminology and phrases are not apropos. One should NEVER take a broad view. Analogy in script is like feathers on a snake. Not at all use a large word when a very small one would be

sufficient. Use words properly, regardless of how others use them. Remove quotations. Puns are for kids, not grunt readers. Amplification is a billion times of inferior quality than sarcasm.

32. Never oversimplify everything: To add material in your research paper, never go for oversimplification. This will definitely irritate the evaluator. Be more or less specific. Also too, by no means, ever use rhythmic redundancies. Contractions aren't essential and shouldn't be there used. Comparisons are as terrible as clichés. Give up ampersands and abbreviations, and so on. Remove commas, that are, not necessary. Parenthetical words however should be together with this in commas. Understatement is all the time the complete best way to put onward earth-shaking thoughts. Give a detailed literary review.

33. Report concluded results: Use concluded results. From raw data, filter the results and then conclude your studies based on measurements and observations taken. Significant figures and appropriate number of decimal places should be used. Parenthetical remarks are prohibitive. Proofread carefully at final stage. In the end give outline to your arguments. Spot out perspectives of further study of this subject. Justify your conclusion by at the bottom of them with sufficient justifications and examples.

34. After conclusion: Once you have concluded your research, the next most important step is to present your findings. Presentation is extremely important as it is the definite medium though which your research is going to be in print to the rest of the crowd. Care should be taken to categorize your thoughts well and present them in a logical and neat manner. A good quality research paper format is essential because it serves to highlight your research paper and bring to light all necessary aspects in your research.

Informal Guidelines of Research Paper Writing

Key points to remember:

- Submit all work in its final form.
- Write your paper in the form, which is presented in the guidelines using the template.
- Please note the criterion for grading the final paper by peer-reviewers.

Final Points:

A purpose of organizing a research paper is to let people to interpret your effort selectively. The journal requires the following sections, submitted in the order listed, each section to start on a new page.

The introduction will be compiled from reference matter and will reflect the design processes or outline of basis that direct you to make study. As you will carry out the process of study, the method and process section will be constructed as like that. The result segment will show related statistics in nearly sequential order and will direct the reviewers next to the similar intellectual paths throughout the data that you took to carry out your study. The discussion section will provide understanding of the data and projections as to the implication of the results. The use of good quality references all through the paper will give the effort trustworthiness by representing an alertness of prior workings.

Writing a research paper is not an easy job no matter how trouble-free the actual research or concept. Practice, excellent preparation, and controlled record keeping are the only means to make straightforward the progression.

General style:

Specific editorial column necessities for compliance of a manuscript will always take over from directions in these general guidelines.

To make a paper clear

· Adhere to recommended page limits

Mistakes to evade

- Insertion a title at the foot of a page with the subsequent text on the next page

- Separating a table/chart or figure - impound each figure/table to a single page
- Submitting a manuscript with pages out of sequence

In every sections of your document

· Use standard writing style including articles ("a", "the," etc.)

· Keep on paying attention on the research topic of the paper

· Use paragraphs to split each significant point (excluding for the abstract)

· Align the primary line of each section

· Present your points in sound order

· Use present tense to report well accepted

· Use past tense to describe specific results

· Shun familiar wording, don't address the reviewer directly, and don't use slang, slang language, or superlatives

· Shun use of extra pictures - include only those figures essential to presenting results

Title Page:

Choose a revealing title. It should be short. It should not have non-standard acronyms or abbreviations. It should not exceed two printed lines. It should include the name(s) and address (es) of all authors.

Abstract:

The summary should be two hundred words or less. It should briefly and clearly explain the key findings reported in the manuscript--must have precise statistics. It should not have abnormal acronyms or abbreviations. It should be logical in itself. Shun citing references at this point.

An abstract is a brief distinct paragraph summary of finished work or work in development. In a minute or less a reviewer can be taught the foundation behind the study, common approach to the problem, relevant results, and significant conclusions or new questions.

Write your summary when your paper is completed because how can you write the summary of anything which is not yet written? Wealth of terminology is very essential in abstract. Yet, use comprehensive sentences and do not let go readability for briefness. You can maintain it succinct by phrasing sentences so that they provide more than lone rationale. The author can at this moment go straight to

shortening the outcome. Sum up the study, with the subsequent elements in any summary. Try to maintain the initial two items to no more than one ruling each.

- Reason of the study - theory, overall issue, purpose
- Fundamental goal
- To the point depiction of the research
- Consequences, including definite statistics - if the consequences are quantitative in nature, account quantitative data; results of any numerical analysis should be reported
- Significant conclusions or questions that track from the research(es)

Approach:

- Single section, and succinct
- As a outline of job done, it is always written in past tense
- A conceptual should situate on its own, and not submit to any other part of the paper such as a form or table
- Center on shortening results - bound background information to a verdict or two, if completely necessary
- What you account in an conceptual must be regular with what you reported in the manuscript
- Exact spelling, clearness of sentences and phrases, and appropriate reporting of quantities (proper units, important statistics) are just as significant in an abstract as they are anywhere else

Introduction:

The **Introduction** should "introduce" the manuscript. The reviewer should be presented with sufficient background information to be capable to comprehend and calculate the purpose of your study without having to submit to other works. The basis for the study should be offered. Give most important references but shun difficult to make a comprehensive appraisal of the topic. In the introduction, describe the problem visibly. If the problem is not acknowledged in a logical, reasonable way, the reviewer will have no attention in your result. Speak in common terms about techniques used to explain the problem, if needed, but do not present any particulars about the protocols here. Following approach can create a valuable beginning:

- Explain the value (significance) of the study
- Shield the model - why did you employ this particular system or method? What is its compensation? You strength remark on its appropriateness from a abstract point of vision as well as point out sensible reasons for using it.
- Present a justification. Status your particular theory (es) or aim(s), and describe the logic that led you to choose them.
- Very for a short time explain the tentative propose and how it skilled the declared objectives.

Approach:

- Use past tense except for when referring to recognized facts. After all, the manuscript will be submitted after the entire job is done.
- Sort out your thoughts; manufacture one key point with every section. If you make the four points listed above, you will need a least of four paragraphs.
- Present surroundings information only as desirable in order hold up a situation. The reviewer does not desire to read the whole thing you know about a topic.
- Shape the theory/purpose specifically - do not take a broad view.
- As always, give awareness to spelling, simplicity and correctness of sentences and phrases.

Procedures (Methods and Materials):

This part is supposed to be the easiest to carve if you have good skills. A sound written Procedures segment allows a capable scientist to replacement your results. Present precise information about your supplies. The suppliers and clarity of reagents can be helpful bits of information. Present methods in sequential order but linked methodologies can be grouped as a segment. Be concise when relating the protocols. Attempt for the least amount of information that would permit another capable scientist to spare your outcome but be cautious that vital information is integrated. The use of subheadings is suggested and ought to be synchronized with the results section. When a technique is used that has been well described in another object, mention the specific item describing a way but draw the basic

principle while stating the situation. The purpose is to text all particular resources and broad procedures, so that another person may use some or all of the methods in one more study or referee the scientific value of your work. It is not to be a step by step report of the whole thing you did, nor is a methods section a set of orders.

Materials:

- Explain materials individually only if the study is so complex that it saves liberty this way.
- Embrace particular materials, and any tools or provisions that are not frequently found in laboratories.
- Do not take in frequently found.
- If use of a definite type of tools.
- Materials may be reported in a part section or else they may be recognized along with your measures.

Methods:

- Report the method (not particulars of each process that engaged the same methodology)
- Describe the method entirely
- To be succinct, present methods under headings dedicated to specific dealings or groups of measures
- Simplify - details how procedures were completed not how they were exclusively performed on a particular day.
- If well known procedures were used, account the procedure by name, possibly with reference, and that's all.

Approach:

- It is embarrassed or not possible to use vigorous voice when documenting methods with no using first person, which would focus the reviewer's interest on the researcher rather than the job. As a result when script up the methods most authors use third person passive voice.
- Use standard style in this and in every other part of the paper - avoid familiar lists, and use full sentences.

What to keep away from

- Resources and methods are not a set of information.
- Skip all descriptive information and surroundings - save it for the argument.
- Leave out information that is immaterial to a third party.

Results:

The principle of a results segment is to present and demonstrate your conclusion. Create this part a entirely objective details of the outcome, and save all understanding for the discussion.

The page length of this segment is set by the sum and types of data to be reported. Carry on to be to the point, by means of statistics and tables, if suitable, to present consequences most efficiently.You must obviously differentiate material that would usually be incorporated in a study editorial from any unprocessed data or additional appendix matter that would not be available. In fact, such matter should not be submitted at all except requested by the instructor.

Content

- Sum up your conclusion in text and demonstrate them, if suitable, with figures and tables.
- In manuscript, explain each of your consequences, point the reader to remarks that are most appropriate.
- Present a background, such as by describing the question that was addressed by creation an exacting study.
- Explain results of control experiments and comprise remarks that are not accessible in a prescribed figure or table, if appropriate.
- Examine your data, then prepare the analyzed (transformed) data in the form of a figure (graph), table, or in manuscript form.

What to stay away from

- Do not discuss or infer your outcome, report surroundings information, or try to explain anything.
- Not at all, take in raw data or intermediate calculations in a research manuscript.

- Do not present the similar data more than once.
- Manuscript should complement any figures or tables, not duplicate the identical information.
- Never confuse figures with tables - there is a difference.

Approach

- As forever, use past tense when you submit to your results, and put the whole thing in a reasonable order.
- Put figures and tables, appropriately numbered, in order at the end of the report
- If you desire, you may place your figures and tables properly within the text of your results part.

Figures and tables

- If you put figures and tables at the end of the details, make certain that they are visibly distinguished from any attach appendix materials, such as raw facts
- Despite of position, each figure must be numbered one after the other and complete with subtitle
- In spite of position, each table must be titled, numbered one after the other and complete with heading
- All figure and table must be adequately complete that it could situate on its own, divide from text

Discussion:

The Discussion is expected the trickiest segment to write and describe. A lot of papers submitted for journal are discarded based on problems with the Discussion. There is no head of state for how long a argument should be. Position your understanding of the outcome visibly to lead the reviewer through your conclusions, and then finish the paper with a summing up of the implication of the study. The purpose here is to offer an understanding of your results and hold up for all of your conclusions, using facts from your research and generally accepted information, if suitable. The implication of result should be visibly described. Infer your data in the conversation in suitable depth. This means that when you clarify an observable fact you must explain mechanisms that may account for the observation. If your results vary from your prospect, make clear why that may have happened. If your results agree, then explain the theory that the proof supported. It is never suitable to just state that the data approved with prospect, and let it drop at that.

- Make a decision if each premise is supported, discarded, or if you cannot make a conclusion with assurance. Do not just dismiss a study or part of a study as "uncertain."
- Research papers are not acknowledged if the work is imperfect. Draw what conclusions you can based upon the results that you have, and take care of the study as a finished work
- You may propose future guidelines, such as how the experiment might be personalized to accomplish a new idea.
- Give details all of your remarks as much as possible, focus on mechanisms.
- Make a decision if the tentative design sufficiently addressed the theory, and whether or not it was correctly restricted.
- Try to present substitute explanations if sensible alternatives be present.
- One research will not counter an overall question, so maintain the large picture in mind, where do you go next? The best studies unlock new avenues of study. What questions remain?
- Recommendations for detailed papers will offer supplementary suggestions.

Approach:

- When you refer to information, differentiate data generated by your own studies from available information
- Submit to work done by specific persons (including you) in past tense.
- Submit to generally acknowledged facts and main beliefs in present tense.

Administration Rules Listed Before Submitting Your Research Paper to Global Journals Inc. (US)

Please carefully note down following rules and regulation before submitting your Research Paper to Global Journals Inc. (US):

Segment Draft and Final Research Paper: You have to strictly follow the template of research paper. If it is not done your paper may get rejected.

- The **major constraint** is that you must independently make all content, tables, graphs, and facts that are offered in the paper. You must write each part of the paper wholly on your own. The Peer-reviewers need to identify your own perceptive of the concepts in your own terms. NEVER extract straight from any foundation, and never rephrase someone else's analysis.

- Do not give permission to anyone else to "PROOFREAD" your manuscript.

- Methods to avoid Plagiarism is applied by us on every paper, if found guilty, you will be blacklisted by all of our collaborated research groups, your institution will be informed for this and strict legal actions will be taken immediately.)
- To guard yourself and others from possible illegal use please do not permit anyone right to use to your paper and files.

Criterion for Grading a Research Paper (Compilation) by Global Journals Inc. (US)

Please note that following table is only a Grading of "Paper Compilation" and not on "Performed/Stated Research" whose grading solely depends on Individual Assigned Peer Reviewer and Editorial Board Member. These can be available only on request and after decision of Paper. This report will be the property of Global Journals Inc. (US).

Topics	Grades		
	A-B	**C-D**	**E-F**
Abstract	Clear and concise with appropriate content, Correct format. 200 words or below	Unclear summary and no specific data, Incorrect form Above 200 words	No specific data with ambiguous information Above 250 words
Introduction	Containing all background details with clear goal and appropriate details, flow specification, no grammar and spelling mistake, well organized sentence and paragraph, reference cited	Unclear and confusing data, appropriate format, grammar and spelling errors with unorganized matter	Out of place depth and content, hazy format
Methods and Procedures	Clear and to the point with well arranged paragraph, precision and accuracy of facts and figures, well organized subheads	Difficult to comprehend with embarrassed text, too much explanation but completed	Incorrect and unorganized structure with hazy meaning
Result	Well organized, Clear and specific, Correct units with precision, correct data, well structuring of paragraph, no grammar and spelling mistake	Complete and embarrassed text, difficult to comprehend	Irregular format with wrong facts and figures
Discussion	Well organized, meaningful specification, sound conclusion, logical and concise explanation, highly structured paragraph reference cited	Wordy, unclear conclusion, spurious	Conclusion is not cited, unorganized, difficult to comprehend
References	Complete and correct format, well organized	Beside the point, Incomplete	Wrong format and structuring

INDEX

T

U

V

save our planet

Global Journal of Researches in Engineering

Visit us on the Web at www.GlobalJournals.org | www.EngineeringResearch.org
or email us at helpdesk@globaljournals.org

ISSN 9755861